"Internal characteristics, chemical compounds and spectroscopy of sapphire as single crystals"

Dissertation

zur Erlangung des Grades
„Doktor der Naturwissenschaften"

im Promotionsfach Mineralogie

am Fachbereich Chemie, Pharmazie und Geowissenschaften
der Johannes Gutenberg-Universität Mainz

Phan Thi Minh Diep

geb. in Dongnai, Vietnam

Mainz 2015

Dekan: ██████████████████

1. Berichterstatter: ████████████████████████████

2. Berichterstatter: █████████████

Tag der mündlichen Prüfung: 17.07.2015

ERKLÄRUNG

Hiermit bestätige ich, dass ich diese Arbeit selbständig verfasst und keine anderen als die angegebenen Quellen und Hilfsmittel verwendet habe.

Mainz, May 2015

Phan Thi Minh Diep

For my Family and my Love

❀ ♥ ♥ ❀

Table of contents

Abstract

In this study more than 450 natural sapphire samples (most of basaltic type) collected from 19 different areas were examined. They are from Dak Nong, Dak Lak, Quy Chau, two unknown sources from the north (Vietnam); Bo Ploi, Khao Ploi Waen (Thailand); Ban Huay Sai (Laos); Australia; Shandong (China); Andapa, Antsirabe, Nosibe (Madagascar); Ballapana (Sri Lanka); Brazil; Russia; Colombia; Tansania and Malawi.

The samples were studied on internal characteristics, chemical compositions, Raman-, luminescence-, Fourier transform infrared (FTIR)-, and ultraviolet-visible-near infrared (UV-Vis-NIR)- spectroscopy. The internal features of these sapphire samples were observed and identified by gemological microscope, con focal micro Raman and FTIR spectroscopy. The major and minor elements of the samples were determined by electron probe microanalysis (EPMA) and the trace elements by laser ablation inductively coupled plasma mass spectrometry (LA-ICP-MS).

The structural spectra of sapphire were investigated by con focal Raman spectroscopy. The FTIR spectroscopy was used to study the vibration modes of OH-groups and also to determine hydrous mineral inclusions in sapphire. The UV-Vis-NIR absorption spectroscopy was used to analyze the cause of sapphire color.

Natural sapphires contain many types of mineral inclusions. Typically, they are iron-containing inclusions like goethite, ilmenite, hematite, magnetite or silicate minerals commonly feldspar, and often observed in sapphires from Asia countries, like Dak Nong, Dak Lak in the south of Vietnam, Ban Huay Sai (Laos), Khao Ploi Waen and Bo Ploi (Thailand) or Shandong (China). Meanwhile, CO_2-diaspore inclusions are normally found in sapphires from Tansania, Colombia, or the north of Vietnam like Quy Chau.

Iron is the most dominant element in sapphire, up to 1.95 wt.% Fe_2O_3 measured by EPMA and it affects spectral characteristics of sapphire.

The Raman spectra of sapphire contain seven peaks ($2A_{1g} + 5E_g$). Two peaks at about 418.3 cm^{-1} and 577.7 cm^{-1} are influenced by high iron content. These two peaks shift towards smaller

1

wavenumbers corresponding to increasing iron content. This shift is showed by two equations $y(418.3) = 418.29 - 0.53x$ and $y(577.7) = 577.96 - 0.75x$, in which y is peak position (cm^{-1}) and x is Fe_2O_3 content (wt.%). By exploiting two these equations one can estimate the Fe_2O_3 contents of sapphire or corundum by identifying the respective Raman peak positions. Determining the Fe_2O_3 content in sapphire can help to distinguish sapphires from different origins, e.g. magmatic and metamorphic sapphire.

The luminescence of sapphire is characterized by two R-lines: R_1 at about 694 nm and R_2 at about 692 nm. This characteristic is also influenced by high iron content. The peak positions of two R-lines shift towards to smaller wavelengths corresponding to increasing of iron content. This correlation is showed by two equations $y(R_2) = 692.86 - 0.049x$ and $y(R_1) = 694.29 - 0.047x$, in which y is peak position (nm) of respective R-lines and x is Fe_2O_3 content (wt.%). Two these equations can be applied to estimate the Fe_2O_3 content of sapphire and help to separate sapphires from different origins. The luminescence is also applied for determination of the remnant pressure or stress around inclusions in Cr^{3+}-containing corundum by calibrating a 0-pressure position in experimental techniques.

The infrared spectra show the presence of vibrations originating from OH-groups and hydrous mineral inclusions in the range of 2500-4000 cm^{-1}. Iron has also an effect upon the main and strongest peak at about 3310 cm^{-1}. The 3310 cm^{-1} peak is shifted to higher wavenumber when iron content increases. This relationship is expressed by the equation $y(3310) = 0.92x + 3309.17$, in which y is peak position of the 3310 cm^{-1} and x is Fe_2O_3 content (wt.%). Similar to the obtained results in Raman and luminescence spectra, this expression can be used to estimate the Fe_2O_3 content and separate sapphires from different origins.

The UV-Vis-NIR absorption spectra point out the strong and sharp peaks at about 377, 387, and 450 nm related to dispersed Fe^{3+}, a broad band around 557 and 600 nm related to intervalence charge transfer (IVCT) Fe^{2+}/Ti^{4+}, and a broader band around 863 nm related to IVCT of Fe^{2+}/Fe^{3+}.

Generally, sapphires from different localities were completely investigated on internal features, chemical compounds, and solid spectral characteristics. The results in each part

contribute for identifying the iron content and separate sapphires from different localities order origins.

Zusammenfassung

Interne Eigenschaften, chemischen Untersuchung und Spektroskopie von Saphir als Einkristall

In dieser Arbeit wurden mehr als 450 natürlichen Saphire (die meisten von dem Basalt-Typ) aus 19 verschiedenen Geländen untersucht. Sie sind von Dak Nong, Dak Lak, Quy Chau, zwei unbekannten Geländen aus dem Norden (Vietnam); Bo Ploi, Khao Ploi Waen (Thailand); Ban Huay Sai (Laos); Australien; Shandong (China); Andapa, Antsirabe, Nosibe (Madagaskar); Ballapana (Sri Lanka); Brasilien; Russland; Kolumbien; Tansania und Malawi.

Die Saphiren wurden über innere Eigenschaften, chemische Zusammensetzungen, Raman-Lumineszenz-, Fourier-Transform-Infrarot (FTIR)- und Ultraviolet-Visible-Nah Infrared (UV-Vis-NIR)- Spektroskopie untersucht. Die inneren Eigenschaften dieser Saphirproben wurden beobachtet und durch mit Hilfe eines gemmologischen Mikroskops, einem konfokalen mikro-Raman und der FTIR-Spektroskopie identifiziert. Die Haupt- und Nebenelemente der Proben wurden mit der Elektronenstrahlmikroanalyse (ESMA), die Spurenelemente mit einer Laserablation-induktiv gekoppelter Plasma-Massenspektrometrie (LA-ICP-MS) bestimmt.

Die Strukturspektren von Saphir wurden von konfokaler Raman-Spektroskopie untersucht. Die FTIR-Spektroskopie wurde verwendet, um die Schwingungsmoden von OH-Gruppen zu studieren und auch wasserhaltigen Mineraleinschlüsse in Saphir zu identifizieren. Die UV-Vis-NIR-Absorptionsspektroskopie wurde verwendet, um die Ursache der Saphirfarbe zu bestimmen.

Natürlichen Saphiren enthalten viele Arten von mineralischen Einschlüssen. Typischerweise sind sie eisenhaltige Einschlüsse wie Goethit, Ilmenit, Hämatit, Magnetit oder Silicat-Minerale, häufig Feldspat, und werden sie oft in Saphiren aus asiatischen Ländern beobachtet, wie Dak Nong, Dak Lak im Süden von Vietnam, Ban Huay Sai (Laos), Khao Ploi Waen und Bo Ploi (Thailand) oder Shandong (China). Mittlerweile werden die CO_2-Diaspor Einschlüsse normalerweise in Saphiren aus Tansania, Kolumbien oder aus dem Norden von Vietnam wie Quy Chau gefunden.

Eisen ist das dominierende Element in Saphir, bis zu 1.95 Gew.-% Fe_2O_3 durch EPMA gemessen und es beeinflusst die spektralen Eigenschaften von Saphir.

Die Raman-Spektren von Saphir enthalten sieben Bänder ($2A_{1g} + 5E_g$). Zwei Peaks bei etwa 418.3 cm^{-1} und 577.7 cm^{-1} werden durch hohe Eisengehalte beeinflusst. Diese zwei Peaks verschieben sich zu kleineren Wellenzahlen, je höher der Eisengehalt ist. Diese Verschiebung wird durch folgende Gleichungen beschrieben: $y(418.3) = 418.29 - 0.53x$ und $y(577.7) = 577.96 - 0.75x$, wobei y die Peak-Position (cm^{-1}) und x der Fe_2O_3-Gehalt (Gew.%) ist. Durch die Nutzung dieser zwei Gleichungen können wir den Fe_2O_3-Gehalt von Saphir durch die Identifizierung der jeweiligen Raman-Peak-Positionen abschätzen. Die Bestimmung der Fe_2O_3-Gehalt kann helfen, Saphire unterschiedlicher Herkunft, wie zum Beispiel aus magmatischen oder metamorphen Entstehung, zu unterscheiden.

Die Lumineszenz von Saphir wird durch zwei R-Linien beeinfluss: R_2 bei etwa 692 nm und R_1 bei etwa 694 nm. Diese Eigenschaft wird auch von hohen Eisengehalt beeinflusst. Die Peak-Positionen von zwei R-Linien verschieben sich in Richtung zu kleineren Wellenlängen entsprechend der Erhöhung des Eisengehalts. Diese Korrelation wird durch zwei Gleichungen $y(R_2) = 692.86 - 0.049x$ und $y(R_1) = 694.29 - 0.047x$ definiert, wobei y Peak-Position (nm) nach R-Linien und x der Fe_2O_3-Gehalt (Gew.%) ist. Diese zwei Gleichungen können auch angewendet werden, um die Fe_2O_3-Gehalte in Saphiren abzuschätzen und Saphir von unterschiedlicher Herkunft zu trennen. Die Lumineszenz wird auch zur Bestimmung der Restdruck oder Spannung um Einschlüsse in Cr^{3+}-haltigen Korund durch Kalibrieren einer 0-Druckposition bei den experimentellen Techniken angewendet.

Die Infrarotspektren zeigen die Präsenz von Schwingungen von OH-Gruppen und wasserhaltigen Mineraleinschlüsse im Bereich von 2500-4000 cm^{-1}. Eisen hat auch einen Effekt auf den Haupt- und zugleich stärksten Peak bei etwa 3310 cm^{-1}. Der 3310 cm^{-1} Peak wird sich zu höheren Wellenzahlen bewegt, wenn der Eisengehalt sich erhöht. Diese Beziehung wird durch die Gleichung $y(3310) = 0.92x + 3309.17$ beschrieben, wobei y die Peak-Position bei 3310 cm^{-1} und x der Fe_2O_3-Gehalt (Gew.%) ist. Ähnlich wie in den Raman- und Lumineszenz-Spektren, kann dieser Ausdruck verwendet werden, um die Fe_2O_3-Gehalt in Saphir abzuschätzen und Stücke von unterschiedlicher Herkunft zu unterscheiden.

Die UV-VIS-NIR-Absorptionsspektren bestätigen starke und scharfe Peaks bei etwa 377, 387 und 450 nm, welche durch Fe^{3+} verbreitert werden, sowie ein breites Band zwischen rund 557 und 600 nm, welches auf einen Ladungsübertrag von Fe^{2+}/Ti^{4+} zurückzuführen ist, und ein breiteres Band um 863 nm, welches durch Ladungsübertragung zwischen Fe^{2+}/Fe^{3+} entsteht.

Im Allgemeinen wurden die Saphire aus verschiedenen Geländen vollständig auf interne Eigenschaften, chemischen Zusammenfassung und feste spektralen Eigenschaften untersucht. Die Ergebnisse in jedem Teil helfen bei der Identifizierung des Eisengehaltes und bei der Unterscheidung von Saphiren mit verschiedener Geländen oder Herkunft.

Figures and Tables

9

Chapter 1: Introduction

1.1. Objective of the thesis

Sapphire, a variety of corundum, in special cases is a precious gem which is traded with certificates of its origin. This certificate influences the value of the sapphire gems. However, distinguishing natural from synthetic sapphire or from various origins is difficult due to treatment, growing technologies or their occurrences. Furthermore, an overall study about sapphires such as internal features, chemical composition or spectroscopic characteristics has been reported.

With the advantage of a large number of natural sapphire samples, this study presents the internal features, chemical compounds and Raman, luminescence, FTIR, and UV-Vis-NIR absorption spectroscopy of more than 450 samples collected from 19 localities in the world.

The most important key in this study is the expressions as a useful tools for distinguish sapphires from different localities or origins by measuring the spectra and determining the iron content in the samples.

The achievements in this thesis contribute on identifying the stress in sapphire and found basement to evaluate sapphire or corundum in general.

1.2. Corundum in general

1.2.1. The corundum structure

Corundum is an aluminum oxide, α-Al_2O_3. Corundum is normally in its "pure" form colorless. If corundum contains chromium, it becomes rose to red, depending on the amount of the chromium content. The red variety is called ruby. If corundum is colorful, except red, it is called sapphire.

Corundum belongs to the corundum-ilmenite group together with hematite (Fe_2O_3) and ilmenite ($FeTiO_3$). This group crystallizes in the trigonal system with the point group $\bar{3}\,2/m$

and the space group R$\bar{3}$c. Pearson's Handbook (Villars 1991) of crystallographic data specifies that the lattice parameters of sapphire at room temperature to be a_o= b_o= 4.758 Å, c_o = 12.99 Å, $V_{unit\ cell}$ = 253.54 Å^3, Z=6 with the ratio of a/c=1:2.73, the values of the angles are $\alpha = \beta = 90^o$ and $\gamma = 120^o$. The number of formula per unit cell, Z=6 means that there are 12 aluminum atoms and 18 oxygen atoms per one unit cell.

Figure 1.2.1.1 shows corundum structure sketch with red balls (O^{-2}) and blue balls (Al^{3+}) in unit cell. In Figure 1.2.1.1, this structure sketch is observed in the projection in plane (xy) and direction (z). Each Al^{3+} ion is bonded to 6 oxygen ions in an octahedron [AlO6]$^{-9}$, and only 2/3 of the octahedra are filled by aluminum cations (Figure 1.2.1.2).
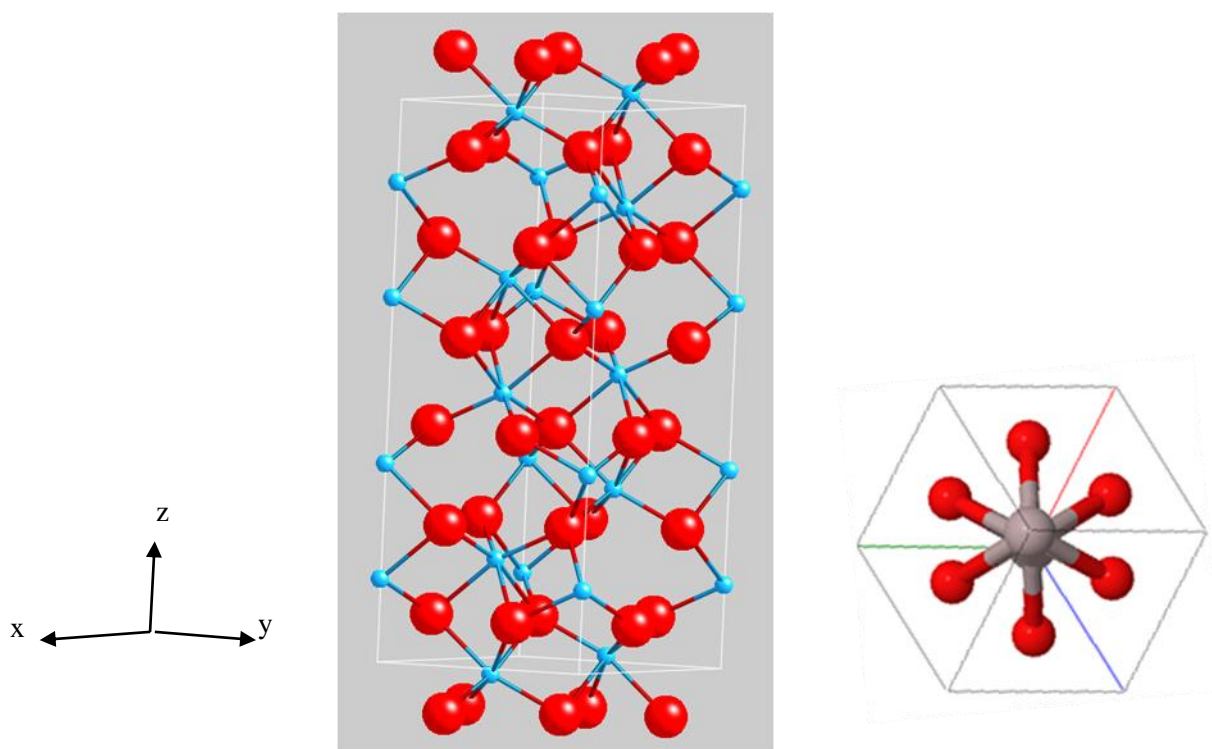
Figure 1.2.1.1: Crystal structure of corundum is observed in the projection in plane (xy) and direction (z). Red balls: O^{-2}, blue balls: Al^{3+}. The crystal structure sketch was made with the CrystalMaker version 2.5 and Manual User (Palmer 1995).
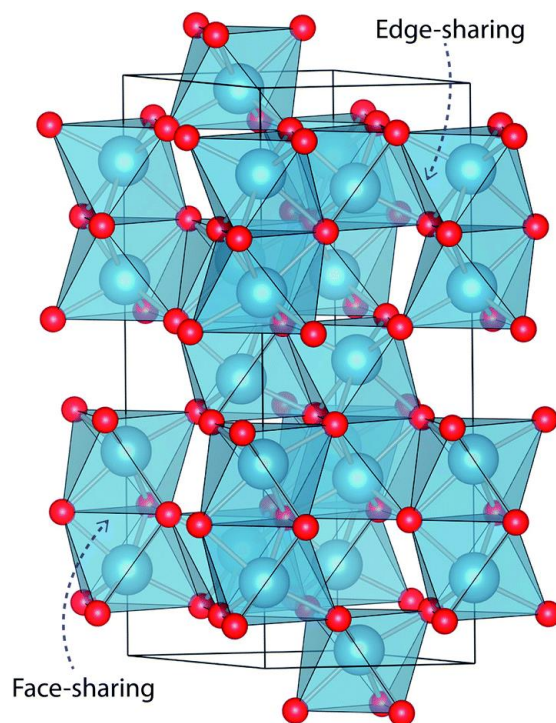
Figure 1.2.1.2: Corundum contains repeating units of the octahedron $[AlO_6]^{-9}$, and 2/3 of the octahedron are filled by aluminum cations (Bristow et al. 2014).

The replacement of Al^{3+} ions by other elements can cause changes in the lattice structure, as e.g. distortion. Due to the larger ionic radius (Shannon 1976) and heavier atomic mass of Fe^{3+} (0.645 Å and 55.845 g/mol) and Cr^{3+} (0.615 Å and 51.996 g/mol) in comparison to Al^{3+} (0.535 Å and 26.982 g/mol), the replacement by Fe^{3+} and Cr^{3+} ions widens the crystal structure locally and the lattice parameters can be increased. This leads to a local distortion of the octahedral sites.

The various colors of corundum originate from different mechanisms. The red color of ruby is due to electronic transitions of dispersed Cr^{3+} ions in the octahedral coordination (Nassau 1983, Fritsch and Rossman 1987). The blue sapphire originates from intervalence charge transfer (IVCT) between Fe^{2+} and Ti^{4+} ions (Ferguson and Fielding 1971, 1972, Fritsch and Rossman 1987, 1988 (Part 2 and Part 3)). Figure 1.2.1.3 illustrates two adjacent octahedral sites containing Fe^{2+} and Ti^{4+} which replace Al^{3+} in the corundum structure of the blue sapphire (Nassau, 1983).
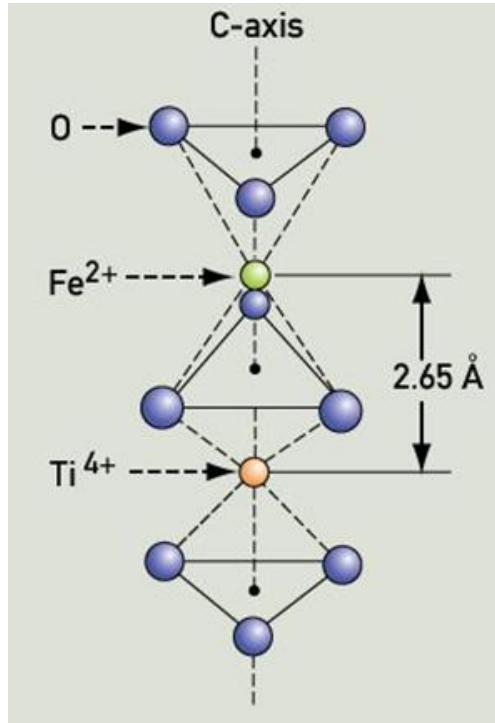
Figure 1.2.1.3: Two adjacent octahedral sites containing Fe^{2+} and Ti^{4+} in blue sapphire (Nassau, 1983).

1.2.2. Properties of corundum

Corundum is an anisotropic crystal which has properties such as thermal expansion and thermal conductivity, which vary significantly by the crystal orientation.

Hardness

Corundum has Moh's hardness of 9. It scratches other minerals which are softer than like quartz or feldspar. Table 1.2.3.1 shows the Knoop scale of some synthetic corundum crystals (Hughes 1997).

Table 1.2.2.1: Hardness in Knoop scale of synthetic corundum crystals (Kg/mm^{-2}) (Hughes 1997).

Material	Orientation of Diamond point	Before heat treatment	After heat treatment
Colorless corundum (melt grown)	$\perp$ c axis	2720	2720
	// c axis	2350	2150
Colorless corundum (Verneuil)	$\perp$ c axis	2280	2370
	// c axis	2350	2450
Ruby (Verneuil)	$\perp$ c axis	2750	2750
	// c axis	2900	2730

Cleavage and parting

Because of the hardness of corundum, the identification of the cleavage is difficult. However, Belyaev (1980) showed that a cleavage exists in colorless corundum. It was found along the rhomboheron $\{10\bar{1}1\}$ and also prismatic $\{11\bar{2}0\}$ faces. A property which is likely similar to cleavage is parting. While cleavage is found in the basic structure, parting is an effect of structural defects. Parting causes fractures and tends to separate planes. In this study, some samples with parting were observed from Tansania and Ballapana (Madagascar) areas and in a Russian crystal sapphire along rhomboheron $\{10\bar{1}1\}$ as shown in Figure 1.2.3.1.

Figure 1.2.2.1: Parting along the rhomboheron $\{10\bar{1}1\}$ in a Russian sapphire in this study. This sapphire is opaque blue and 20 mm in diameter.

Specific gravity

Corundum has a specific gravity from 3.95 to 4.1 (Pratt 1906). Colorless corundum show a specific gravity of 3.989 and ruby and sapphire show a value of 3.997 (Webster 1983). The specific gravities of corundum enriched in Fe or Cr are higher, approximately 4.06 (Hughes 1997).

Optical properties

Colorless corundum has refractive index with ordinary-ray (o-ray) index of n_o=1.7687 and extraordinary-ray (e-ray) n_e=1.7606 (Webster 1983). Generally, the o-ray has values between 1.766 and 1.780 and the e-ray between 1.758 and 1.772 (Hughes 1997). The birefringence of corundum defined by $\triangle n = n_e - n_o$ of 0.008 (Buschow et al. 2001).

Thermal properties

Belyaev (1980) reported the melting point of corundum to be at 2030^oC and the boiling point at 3500^oC. Hughes (1997) published the boiling point at 3500^oC, the melting point between 2030^oC and 2050^oC, and the softening point at 1800^oC.

Hughes (1997) measured thermal expansion of corundum parallel to the c axis of 6.66×10^{-6} at 20-50°C and 9.03×10^{-6} at 20-1000°C, and perpendicular to the c axis 5×10^{-6} at 50°C. Other sources reported thermal expansions at 300 K of $4.5 \times 10^{-6} K^{-1}$ ($\perp$ c-axis), $5.3 \times 10^{-6} K^{-1}$ (// c-axis) (Buschow et al. 2001) and $5.1 \times 10^{-6} K^{-1}$ ($\perp$ c-axis), $5.74 \times 10^{-6} K^{-1}$ (// c-axis) (Yates et al. 1972).

Electrical properties

Colorless sapphire is known to be one of the best electric insulators. They are used as insulating substrate in high power, high frequency integrated circuits. Buschow et al. (2001) reported a dielectric constant of 1.768 $\perp$ to the *c*-axis and 10.6 // to the *c*-axis at 300K and 1 MHz.

Chemical properties

According to Hughes (1997), the solubility of corundum in 100 g of water at 29^oC is 9.8×10^{-5} g. Corundum dissolves slowly in boiling nitric acid in orthophosphoric acid at 300^oC, and in potassium bisulfate between 400 and 600^oC. It dissolves well in borax between 800 and 1000^oC.

Chapter 2: Research Materials and Methods

2.1. Research materials

More than 450 natural sapphires collected from 19 localities were examined, including Dak Nong province and Krong Nang, in Dak Lak province from the south of Vietnam, Quy Chau in Nghe An province and two unknown sources from the north of Vietnam; Bo Ploi in Kanchanaburi province and Khao Ploi Waen in Chanthaburi province, Thailand; Ban Huay Sai in Bokeo province, Laos; Australia; Changle in Shandong province, China; Andapa in Antsiranana province, Antsirabe in the Antananarivo province, and Nosibe in Ambohitra province, Madagascar; Ballapana in the Sabaragamuwa province, Sri Lanka; Brazil; Russia; Colombia; Tansania and Malawi. Most all sapphire samples are dark blue fragments. Some of them are medium blue, green, brown, yellow, light pink and grey fragments. A few are idiomorphic with hexagonal pyramid prisms, or barrel shaped. In addition they were observed by microscopy to determine inclusions and other internal features.

The samples were cut and polished on one side or few sides to observe the internal features as well as to determine the inclusions under the transparent or reflection light. About 200 samples, in which the c-axes were observed, were cut and polished in plane-parallel slices, approximate 1 mm in thickness for spectral measurements. The main and minor elements of these samples were determined EPMA, in which about 150 samples were measured with LA-ICP-MS technique to determine trace elements. The samples after cutting and polishing were cleaned in an ultrasonic device for 15-20 minutes.

2.1.1. Sapphire from Vietnam

2.1.1.1. Sapphire from Dak Nong and Krong Nang-Dak Lak from the south of Vietnam

Since the 1980s the blue to bluish green gem sapphire is in the south of Vietnam recovered from secondary deposits, mainly alluvium placers in alkali basalts (Smith et al. 1995). In the Dak Nong area, sapphire is found in weathered residual soils lying above alkali basalt flows and also in placer deposits in the rivers or streams (Long et al. 2004).

Sapphire from Dak Nong in this study was found in alluvium placers. They are angular to partly rounded eroded fragments. Some of them are idiomorphic with hexagonal pyramid prisms, or barrel shapes. They are mostly dark blue. Some of them are medium blue, bluish green, brown, yellow, grey and colorless. The fragments vary from 3 mm to 8 mm whereas the prisms or barrel shaped samples vary from about 3 to 14 mm in diameter and from 5 to15 mm in length. Sapphire is found together with red zircon crystals. These zircon crystals occur as isolated crystals and also solid mineral inclusions in Dak Nong sapphire.

Figure 2.1.1.1: Sapphires from Dak Nong, Vietnam are partly rounded eroded fragments.

Sapphire from Dak Lak was collected at Krong Nang district, Dak Lak provinve, Vietnam. Most of them appear as angular to partly round eroded fragments. They were found in placer deposits in Quaternary sediments which lie in a terrain of depressions and valley terraces (Khoi et al. 2014). The samples which were chosen for this study are mostly bluish green, greenish blue or blue. Figure 2.1.1.2 shows Dak Lak sapphire which is more green color.

Figure 2.1.1.2: Sapphires from Dak Lak, Vietnam.

2.1.1.2. Sapphire from Quy Chau and two unknown sources from the north of Vietnam

In the north of Vietnam, the gem corundum is found in metamorphic rocks, typically marbles and also gneisses, schists, and the placer deposits (Smith et al. 1995, Long et al. 2004).

Quy Chau sapphire

According to Long et al. (2004), corundum from Quy Chau has metamorphic origin. They are very rare rubies disseminated in marbles associated with pyrite and graphite, and in the placers, and there is very rare blue sapphire.

Corundum from Quy Chau for this study is sapphire which is combined as bulk rock with the host rock as shown in Figure 2.1.1.2.1. The density of sapphire crystals in this bulk rock is dense and it is difficult to separate them out of the bulk rock.

Figure 2.1.1.2.1: Sapphire crystals in a host rock from Quy Chau in the north of Vietnam.

Crystal bulk rock from an unknown source in the north of Vietnam (Unknown-Northern Vietnam)

This crystal bulk rock in this study was grown in polycrystalline host rock of feldspar, an aggregate of many crystals or grains. They are easy to separate from the host rock and opaque with whitish light blue color.

Figure 2.1.1.2.2: Sapphire crystals in polycrystalline of feldspar from an unknown source in northern Vietnam.

Trapiche crystal sapphire from an unknown source in the north of Vietnam (Trapiche-Northern Vietnam)

The sample is partly rounded eroded and broken. It has trapiche pattern and color zoning. The sample has a diameter of 25 mm. It has a core in ivory-white color, dark blue and milky adjacent hexagonal rings and an ivory-white large outer ring.

Figure 2.1.1.2.3: Crystal sapphire with trapiche and color zoning from an unknown source in the north of Vietnam.

2.1.2. Sapphire from Ban Huay Sai in Bokeo, Laos

Sapphire from the Ban Huay Sai alluvial gem field, Laos, derive from local Cenozoic basalts (Sutherland et al. 2002, Hughes 2011) and commonly occur as well-formed crystals or broken fragments of crystals (Sutherland et al. 2002). In this study, there are 11 samples of Ban Huay Sai sapphires were examined. They are broken or eroded fragments as shown in Figure 2.1.2. Their colors range from light blue to greenish blue, from transparent to opaque.
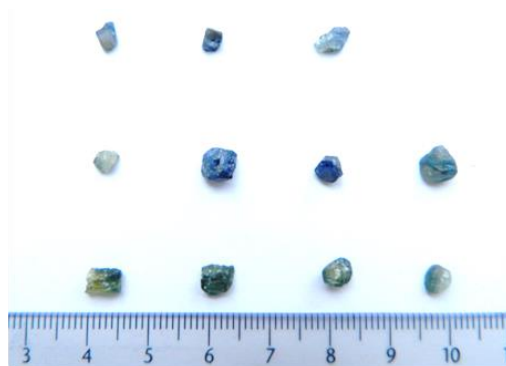
Figure 2.1.2: Sapphires from Ban Huay Sai, BoKeo, Laos.

2.1.3. Sapphire from Khao Ploi Waen in Chanthaburi and Bo Ploi in Kanchanaburi, Thailand

Sapphire from Thailand in general and Khao Ploi Waen and Bo Ploi derives from mafic volcanic rocks, in particular alkaline basaltic deposits (Vichit 1975, Keller 1982, Levinson and Cook 1994). In Khao Ploi Waen and Bo Ploi, sapphires were found in residual basaltic soil, eluvium and alluvium placers (Coenraads et al. 1995) or as rarely metacrysts in Bo Ploi (Arnond et al. 2005).

Sapphire samples from Khao Ploi Waen and Bo Ploi in this study were found in alluvium placers and weathered residual soils. They are fragments of crystals and some of them show the orientation of the crystal. Their colors vary from dark blue to greenish blue, grey and colorless.

Figure 2.1.3: Sapphires from Bo Ploi, Kanchanaburi, Thailand.

2.1.4. Sapphire from Australia

Like gem corundum from Southeast Asia, corundum from Australia is known as gems associated with alkali basalt (Vichit 1975, Levinson and Cook 1994).

The Australian sample for this study is a dark blue sapphire from an unknown source. This sample was separated into two parts for measurements.

Figure 2.1.4: A dark blue sapphire from Australia.

2.1.5. Sapphire from Changle in Shandong, China

According to Guo et al. (1992b) and Hu et al. (2007), Changle sapphires in Shandong have alkali basalt environment. Sapphires from this area were found with relatively large size, average of 5-20 mm and ranged from dark blue to yellow, and were sometimes zoned.

In this study, sapphires were collected from Changle, Shandong and have basaltic origin. The samples are round eroded fragments and are from dark blue to yellowish green or large crystals with size up to 23 mm (Figure 2.1.5). They are barrel-shaped prisms and dark blue colored. Trapiche patterns were also observed with plane-parallel slices similar to those described from Dak Nong (Vietnam) sapphires.
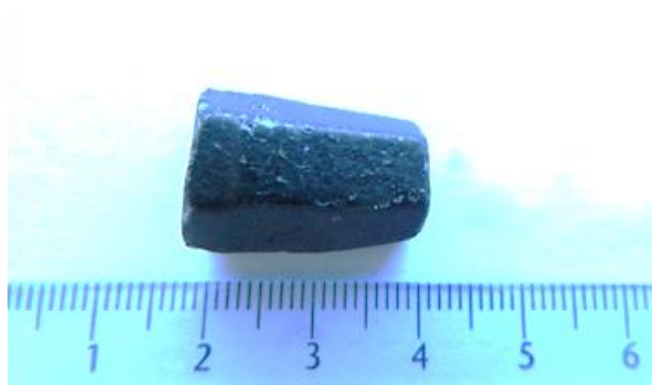
Figure 2.1.5: A barrel-shaped prism sapphire crystal from Changle, Shandong, China.

2.1.6. Sapphire from Andapa, Antsirabe and Nosibe, Madagascar

Sapphire from Nosibe was found in the north of Madagascar characterized by basaltic deposit. The samples were blue, green and yellow sapphires and mainly found in the alluvium of small creeks by local villagers (Rhamdhor and Milisenda 2004, Rakotondrazafy et al. 2008).

Antsirabe locates nearly in the middle of Madagascar. Corundum from here was found as ruby in alkali basalts or corundum was derived from alluvial corundum deposits (Rakotondrazafy et al. 2008).

Andapa deposit locates in Antsiranana province in the north of Madagascar and the information of corundum from this area has not reported. However, sapphires from a deposit which is situated about 70 km south of Antsiranana, in Antsiranana province were recovered from alluvial deposits from basaltic rocks (Schwarz et al. 2000). Corundum from Nosibe was basaltic sapphire type deposit (Schwarz et al. 2000, Rhamdhor and Milisenda 2004).

Corundum from Andapa, Antsirabe and Nosibe in Madagascar in this study is eroded fragments of sapphires approximately 3-4 mm and normally show their orientation. Almost all of them are from dark blue to light blue.

2.1.7. Sapphire from Ballapana, Sri Lanka

Sri Lanka is famous for gem corundum which occurs with other gemstones in alluvial, eluvial and residual gravels on granulite fancies rocks of the Highland Series, for example in Kataragama, Embilimpitya or Ratnapura areas (De Maesschalck, Oen 1989). They are described to be transparent, well-formed crystals, (Katagagama), transparent to translucent, not well-formed crystals (Embilimpitiya, Ratnapura) and show parting (Kataragama, Ratnapura). In another literature, Ratnapura sapphires were extracted from alluvial gravels and colluvium with yellow, pale blue, blue and pink color (Waltham 2011). A new discovery of high-quality blue sapphires at Thammannawa primary deposit near Kataragama have well-formed crystals, good transparency and pure color (Dharmaratne et al. 2012).

Investigated sapphires crystals from Ballapana, Sri Lanka occur as hexagonal prism. They have not been described in any literature. They show parting along (0001) and cracks which are

healed by dark brown material. The maximum size is approximately 20 mm in length, and 9 mm in diameter.

Figure 2.1.7: Sapphires crystals with hexagonal prism of from Ballapana, Madagascar.

2.1.8. Sapphire from Brazil

Gem-quality sapphire from Brazil was known to be blue, fancy-color and color-change sapphires from Creek region of Minas Gerais (Epstein et al. 1994). They were explored from alluvium in recent gravels or colluvium on local hillsides.

In this study, a pale blue Brazil sapphire from an unknown source was investigated. This sample has a size of 4 x 2 mm and the *c*-axis could be identified.

2.1.9. Sapphire from Russia

Corundum from Russia has been known to be gem-quality corundum, mainly sapphires from alluvial placer deposit at Nezametnoye, Primorye region, Far East Russia (Khanchuk et al. 2003, Graham et al. 2008). The corundum is from pale to dark blue, greyish blue, greenish blue, brownish green, brown and grey.

The Russian crystal sapphire in this study shows parting parallel to the rhombohedron $\{10\bar{1}1\}$. It has an opaque blue color and has a size of 20 mm in diameter.
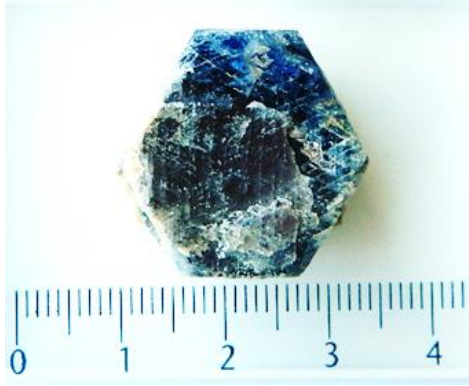
Figure 2.1.9: A sapphire crystal from Russia with hexagonal prism.

2.1.10. Sapphire from Colombia

Gem-quality sapphires of Colombia were recovered from stream beds and terrace gravels near the Colombian village of Mercaderes (Keller et al. 1985, Duroc-Danner 2002). They are simple hexagonal prism, occur in a wide variety of colors and are commonly rounded due to extensive transport.

Colombian sapphire in this study occurs as corroded fragments, some of them as hexagonal prisms. The samples are pale blue, greenish blue, blueish green and light pink. These light pink colored sapphires were only observed in this area.

Figure 2.1.10: Sapphires from Colombia.

29

2.1.11. Sapphire from Tansania

Rubies and sapphires from Winza, Tansania have been mined from both eluvial and primary deposits (Schwarz 2008). The gem-quality corundums are classified into two types: prismatic-tabular-rhombohedral and dipyramidal, and generally medium red and dark red. Top-quality rubies are often rhombohedral. Additionally to that samples from Tunduru district of Tansania (Chitty 2009) have been investigated and all of the sapphires are from alluvial and ellluvial deposits. Tansanian sapphires in this study come from an unknown source. They show hexagonal prism, and are pale light blue with mixed brown cracks perpendicular to the c-axes.

Figure 2.1.11: Sapphires with hexagonal prism from Tansania.

2.1.12. Sapphire from Malawi

Malawi sapphires occur as hexagonal prism. They are mixed pale light green and brown colored.

Figure 2.1.12: Hexagonal prism sapphires from Malawi.

2.2. Experimental methods

2.2.1. Gemological microscope

The gemological microscope is a useful tool to study internal characteristics of gem stones and pieces of jewelry that contain them. This is an important task and contributes a general view of internal properties of objects such as cracks, fissures, position and shape of inclusions, color and their phases.

2.2.2. Confocal micro Raman and luminescence spectroscopy

Raman spectroscopy is an analytical method based on the interaction between laser light and the lattice or molecules vibrations. This method has been applied to determine the mineralogy of minerals and gems. One of the most powerful advantages of Raman spectroscopy in gemology is the potential of the confocal mode coupling to a microscope to observe and identify inclusions of gems without preparation or destruction of the samples.

In this study, confocal Raman microscopy is used to collect Raman spectra of corundum and inclusions in corundum on the micro scale. The micro-Raman spectra of the samples were collected by using a LabRAM 800 high resolution spectroscope which was coupled to an Olympus-BX41 optical microscope, with a Si-based CCD detector and an automated x-y-z stage. The laser source was a frequency-doubled Nd-YAG laser (532.21 nm) with a spot size of 2 x 2 μm. The Raman spectrometer was calibrated by using the 520.7 cm^{-1} peak of a silicon wafer (Kuebler et al. 2006, Frost et al. 2011). The spectra were recorded by the program LabSpec v.4.02 (Horiba Jobin Yvon) in the spectral range from 120 cm^{-1} to 1200 cm^{-1} with 20 seconds exposure time, 2 accumulation, a 400 μm con-focal pinhole, 100 μm slit width, 50x magnification, and a grating with 1800 grooves/mm at room temperature. The spectral resolution is ~0.5 cm^{-1}.

The process when a stone absorbs a shorter wavelength (higher energy) and emits a longer wavelength (lower energy) in the visible light region is called luminescence. One origin of luminescence in sapphires is the chromium. The luminescence of sapphire which is excited by a laser light is called photoluminescence or laser induced luminescence (LIL). The advantage of this method is, that is highly sensitive, quick and non-destructive, and therefore it is used to detect chromium contents in sapphire. The luminescence spectra of sapphires in

this study were measured with the same acquisition conditions as for Raman spectroscopy, however the spectra collection time was one second. The wavelength calibration was done by using three lines (671.70, 692.95 and 702.41 nm) of a Neon light source nearest to the R_1 and R_2 lines with a spectral resolution of 0.01 nm.

After subtracting the background, the Raman and luminescence spectra were fitted by using an additional peak fitting module of the program Origin-lab 7.5 professional version. The Voigt function was used to fit the Raman and luminescence spectra to determine the Raman and R-lines peak positions. 98% of the used laser light was polarized. Almost all of the measurements were carried out with the *c*-axis perpendicular to the electric vector *E* of the laser light.

2.2.3. FTIR absorption spectroscopy

Due to its high sensitivity concerning the polar O-H bonds, FT-IR absorption spectroscopy is used to detect hydrogen in the structure of materials. In this study, IR spectroscopy was used to determine OH-groups, water or hydrous mineral inclusions in sapphire.

The FT-IR spectra of the background and the sample were recorded at room temperature by using a Thermo Scientific Nicolet 6700 FT-IR spectrometer equipped with an optimized beam condenser. The spectrometer was attached with a highly sensitive MCT-A (Mercury Cadimium Telluride) detector which was cooled by liquid nitrogen. The spectra were taken in the range of 600-6000 cm^{-1} with transmission mode. Each measurement was performed within 64 scans and with a spectral resolution of 4 cm^{-1}. The Voigt function was used to determine the peak positions of OH-groups after subtracting a linear background.

2.2.4. UV-Vis-NIR absorption spectroscopy

Since the color of sapphire originates from the transition of electrons in energy levels, the UV-Vis-NIR spectroscopy was used to examine the causes of the sapphire. The UV-Vis-NIR spectra were measured with a Zeiss Axiolmager A2m microscope, which was equipped with two spectrometers from the J&M Company (Germany). The first diode array spectrometer (TIDAS S-CCD) works in the region from 200-980 nm with a spectral resolution of 0.75 nm and the second one (TIDAS S900 with an InGaAs-detector) works in the region 900-1600 nm with a resolution of 2.8 nm. The spectra were recorded with 20 scans. All spectra were taken with polarized light.

2.2.5. Electron Probe Micro-Analysis (EPMA)

EPMA is a chemical analytical tool to determine the chemical compositions of very small volumes on the surface of polished thin section of rocks or minerals. In this study, EPMA was used to determine major and minor elements Al_2O_3, TiO_2, V_2O_3, Ga_2O_3, Fe_2O_3, SiO_2, Cr_2O_3, Mn_2O_3 and MgO in the sapphire samples.

The samples are polished on the surface and mounted in epoxy plugs (Figure 2.2.5). After that, they are coated with a thin film of carbon to increase the conductivity. Carbon and not gold was used to reduce the interference between the electron beam and emitted X-rays because of the thinness and lightness of carbon. After this preparation, the samples are loaded into the high vacuum sample chamber to perform the measurements.

Figure 2.2.5: The samples are mounted in epoxy plugs.

The measurements are performed using a JEOL JXA 8900RL which is equipped with 5 wavelength dispersive spectrometers. The experiments were run using 20 kV acceleration voltages and 20nA filament current. A corundum reference material is selected to analyze the chemical composition of Al_2O_3, TiO_2, V_2O_3, Ga_2O_3, Fe_2O_3, SiO_2, Cr_2O_3, Mn_2O_3 and MgO oxides. Each sample was analyzed at 5 different points, and an averaged value was calculated. The detection limit varies for each element and depends on the analysis condition, calculating program, reference material and sample. The detection limit of measurements is 0.01 wt.%.

2.2.6. Laser Ablation-Inductively Coupled Plasma-Mass Spectrometry (LA-ICP-MS)

LA-ICP-MS is a highly sensitive technique for trace element determination due to its low detection limits. It can detect major and trace elements which are not detectable by non-destructive methods, like EPMA.

The analyses were performed by using an Agilent 7500 ce quadrupole Technologies coupled to a New Wave UP213 Nd:YAG 213 nm laser ablation system. Helium was used to transport the ablated particles from the ablation cell into the plasma. The laser ablation used a pulse repetition rate of 10 Hz, an energy density of 6 J cm^{-2} and the ablation time was 60 seconds. The laser beam of 100 μm diameter was focused on 50 μm on the sample surface. The Standard Reference Material NIST-612 glass was used for drift correction and NIST-610 glass and BCR was measured as an unknown samples. Aluminum was used as internal standard element for each analysis, with the aluminum mass fraction determined by EPMA. Data reduction was carried out by the software GLITTER 4.0. Each analysis took 120 seconds to detect the beginning background (30 s), the sample (60 s) and the ending background signals (30 s).

The elements measured by the LA-ICP-MS were Li, Be, Na, Mg, Si, P, K, Ca, Sc, Ti, V, Cr, Mn, Co, Ni, Zn, Ga, Rb, Sr, Y, Zr, Nb, Mo, Cs, Ba, Ta, W, Pb and Bi. The detection limits are different for differing spot sizes and each element. The detection limits were generally below 1 ppm (0.0001 μg g^{-1}).

Chapter 3: Internal Characteristics of Sapphire

Microscopic investigations and Raman measurements showed plentiful internal characteristics of sapphire in this study. These characteristics include trapiche patterns, color zoning, twinning, fingerprint or healed fissures, solid-, fluid- and gas inclusions. The inclusions can be single or multi-phase, and occur as isolated crystals or in clusters. These characteristics may help to distinguish sapphire among areas.

3.1. Trapiche patterns

Trapiche patterns are commonly found in sapphire from Dak Nong (Vietnam) and less in samples from Shandong (China). They are categorized as trapiche sapphire with star-like patterns, showing hexagonal core, six trapezoidal arms, and six triangular sectors. The trapiche characteristics of these samples are similar to those described for Colombian emeralds (McKague 1964, Nassau and Jackson 1970, O'Donoghue 1971) and trapiche rubies from Mong Hsu, Myanmar (Schmetzer 1996). The same results are briefly mentioned in gem news (Koivula et al. 1994) for a purple-pink trapiche sapphire from Vietnam, for trapiche corundum from Myanmar (Henn and Bank 1996) and trapiche sapphire from the south of Vietnam (Kanyarat Khotchanin et al. 2010).

The trapiche sapphire in this study show dark brown or grey cores, yellow or lighter brown or grey arms and blue or transparent sectors when viewed parallel to the *c* axis. The brown cores and the arms show many black or brown solid inclusions. Figure 3.1.1(a) shows a typical trapiche sapphire slice cut perpendicular to the *c*-axis from Dak Nong (Vietnam). This slice is approximately 10 mm in diameter and has a huge dark brown core. The six trapezoidal arms show extremely sharp and narrow alternating zones of yellow-brown color. The six triangular sectors are blue and transparent. Figure 3.1.1 (b) shows a trapiche pattern from Shandong (China). It is about 4 mm in diameter, and the core is more than 1 mm in diameter. It has a grey core, yellowish brown to grey arms and a blue sector.

<div align="center">(a)   (b)</div>
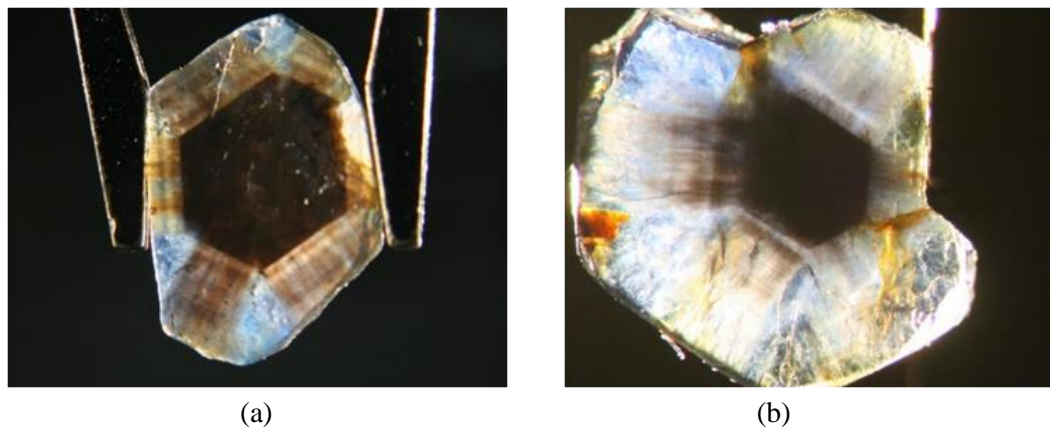
Figure 3.1.1: Trapiche sapphire: (a) A trapiche pattern from Dak Nong (Vietnam), (b) A trapiche pattern from Shandong (China).

The other type of trapiche in this study shows a less intensive colored core and arms. Figure 3.1.2 (a) shows a sample from Dak Nong (Vietnam) with a yellowish blue core with some tiny black ore mineral inclusions. The rim shows as whitish tube-like structures, radiating from the core. Another sample, also from Dak Nong (Vietnam), shows a trapiche pattern with a grey hexagonal core, whitish arms and extremely sharp hexagonal blue zones, as shown in Figure 3.1.2 (b).

<div align="center">(a)   (b)</div>
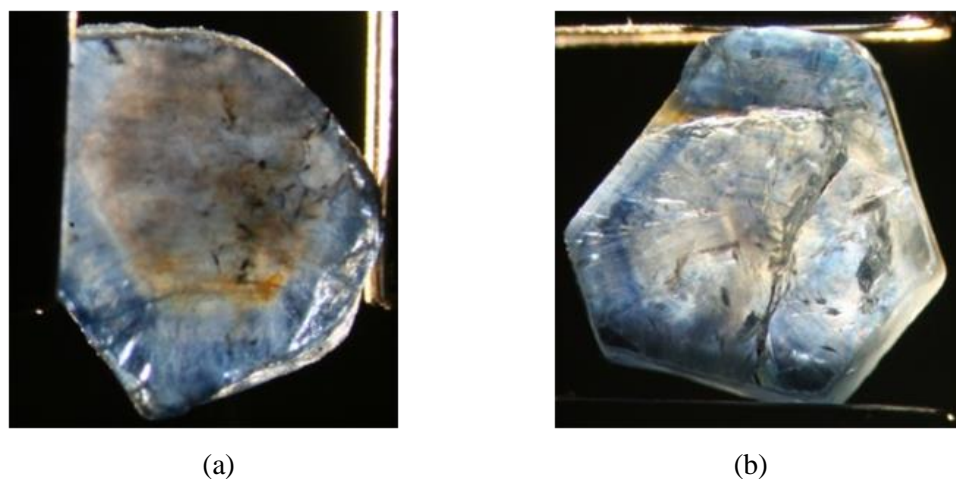
Figure 3.1.2: Trapiche sapphire: (a) Hexagonal core and tube-like structures in the rim (Dak Nong, Vietnam), (b) Trapiche patterns and hexagonal blue zone (Dak Nong, Vietnam).

3.2. Color zoning

Color zoning in a crystal shows distinctive growth and color zones as results of various chemical composition changes during the growth of the crystal. They are commonly hexagonal patterns when viewed parallel to the *c*-axis. The growth lines are always straight and found to be parallel to the crystal faces, along which they are formed. The color zones vary in size from extremely sharp and narrow to broad and diffuse. Some color zonings are introduced in Figure 3.2. Color zoning shows growth zoning, with extremely sharp brown and lighter brown zones in a sample from Khao Ploi Waen (Thailand) (Figure 3.2 a). For the sample observed parallel to the c axis, color zoning shows sharp or broad brownish hexagonal bands (Figure 3.2 b and Figure 3.2 c), extremely sharp or broad blue bands (Figure 3.2 d), or alternately extremely sharp blue and brown bands (Figure 3.2 e). A special sample showed two parallel rows of triangular blue zones when this sample was cut parallel to the *c*-axis (Figure 3.2 f).

| (a) | (b) | (c) |

| (d) | (e) | (f) |
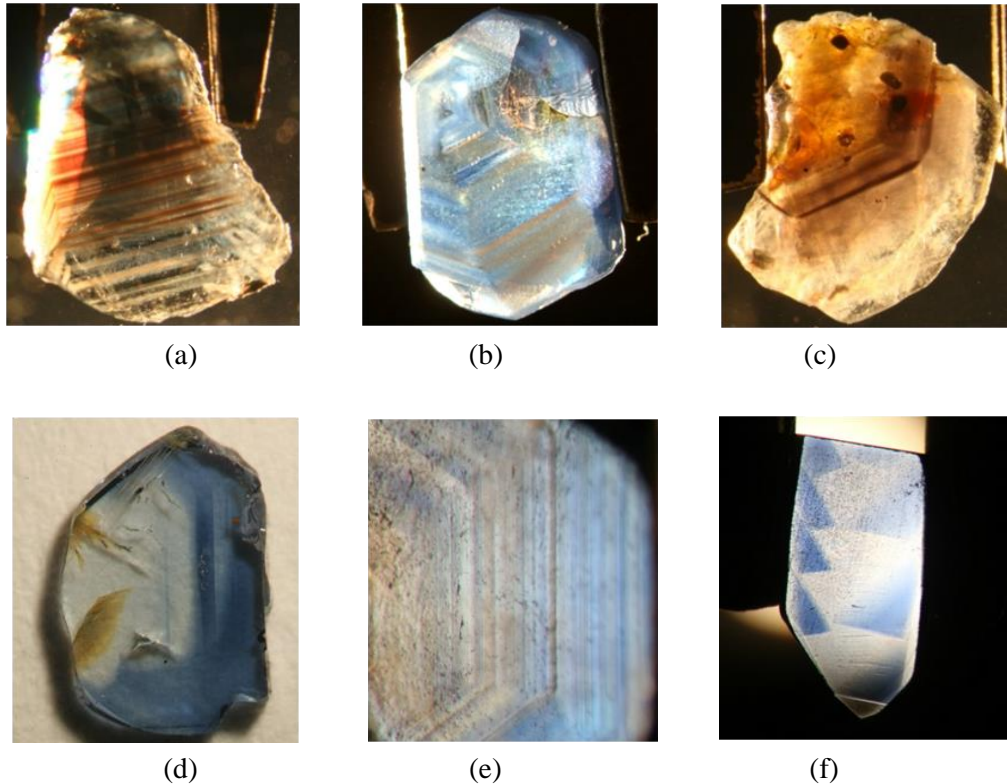
Figure 3.2: Color zoning observed in the samples: (a) Khao Ploi Waen (Thailand), (b) Shandong (China), (c) Bo Ploi (Thailand), (d) Nosibe (Madagascar), (e) Dak Nong (Vietnam), (f) Andapa (Madagascar).

3.3. Twinning

Twinning occurs when the distinctive crystals grow individually but they share some lattice points or planes together. Polysynthetic glide or lamellar twining is a common feature in the investigated samples.

Figure 3.3 (a) shows an intersecting lamella and a polysynthetic glide twinning together with growth structure in a blue sample from Dak Nong (Vietnam). A dark blue sample from Australia shows a polysynthetic twinning in polarized light (Figure 3.3 b). Polysynthetic twinning is repeated over a distance in the trapiche sample from an unknown location in the north of Vietnam (Figure 3.3 c). Obvious lamella twinning, shown as varying colors, is repeated over a distance in a sample from Quy Chau (Vietnam) (Figure 3.3 d). Twinning shows lamella twins intersecting at approximately 60° when observed parallel to the c-axis (Figure 3.3 e), or angular twinning created by three polysynthetic twins orientated in different directions (Figure 3.4 f).

(a)	(b)	(c)
(d)	(e)	(f)
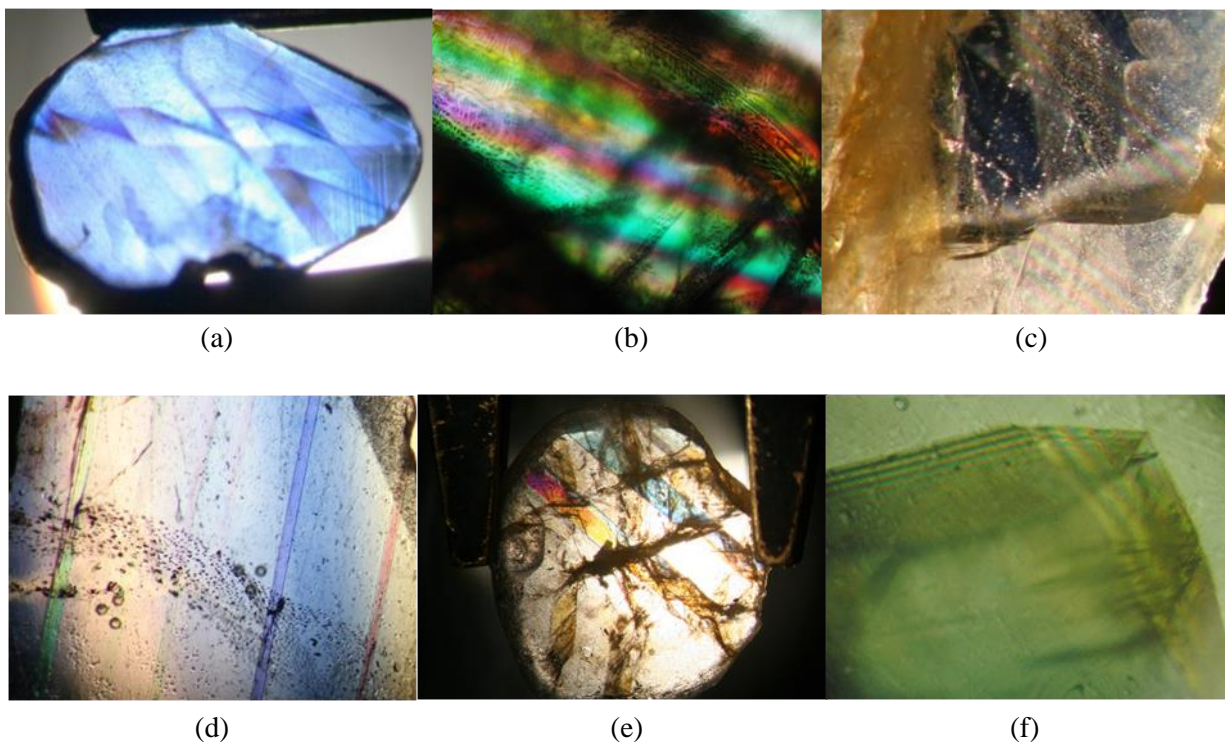
Figure 3.3: Twinning: (a) Dak Nong (Vietnam), (b) Australia, (c) Unknown 2-North Vietnam, (d) Quy Chau (Vietnam), (e) Colombia, (f) Bo Ploi (Thailand).

3.4. Healed fissures

The host crystal usually contains fissures. Growth fluids may enter and heal these fissures. The fluids left behind are trapped in tiny cavities and fingerprints or healed inclusions result. According to Hughes (1997), the fissures may be healed by solely liquid, liquid and gas, liquid and solid, or liquid, gas and solid.

(a)   (b)

(c)   (d)
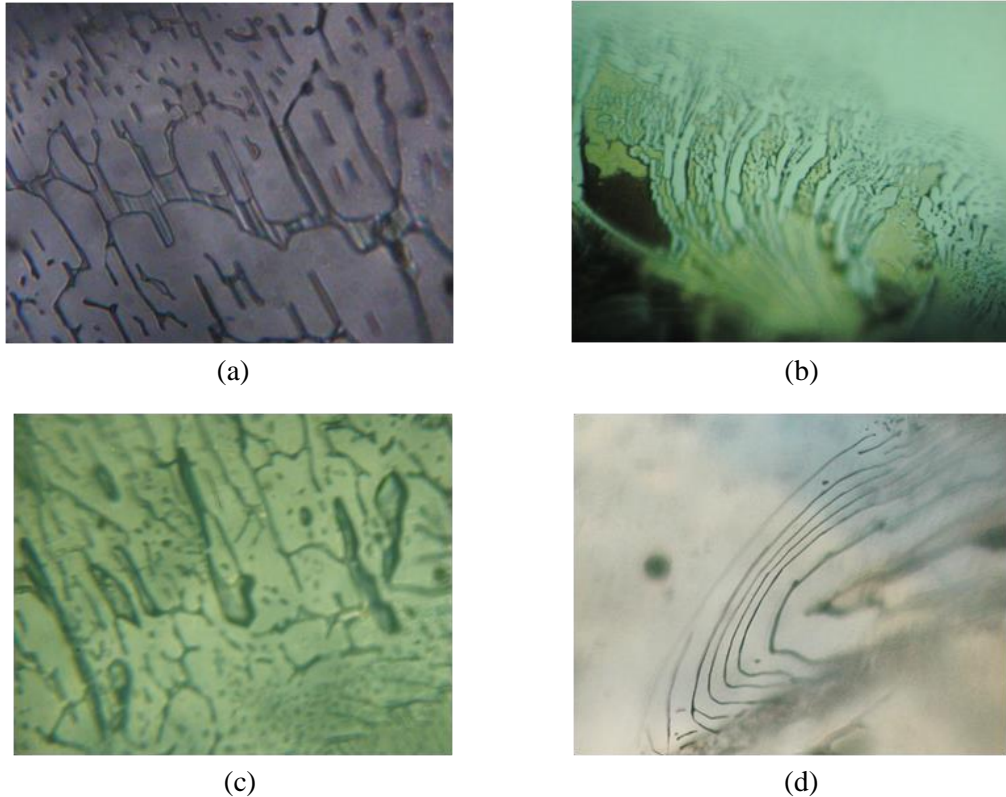
Figure 3.4.1: Healed fissures: (a) Tansania, (b) Bo Ploi (Thailand), (c) Ban Huay Sai (Laos), (d) Andapa (Madagascar).

Figure 3.4.1 (a) and (b) show healed fissures filled by fluid material observed in a Tansania and a Bo Ploi (Thailand) sample, respectively. They show elongated, curved cracks forming a network in the samples. Healed fissures by fluids and tiny solids are more common. Fingerprint inclusions created by fluids and tiny brown particles look like leaf patterns with veins (Figure

3.4.1 c). In other cases, fingerprint inclusions filled by fluids and tiny black solids show concentric curves (Figure 3.4.1 d).

When illuminated at the proper angle, well-healed fissures show dark areas while the residual fluids are reflective, causing iridescent open areas as shown in Figure 3.4.2. In Figure 3.4.2 (a), dark areas show angular patterns and interleaved iridescent areas. Another case is presented in Figure 3.4.2 (b) where healed fractures appear as separately "island" with small round or angular dark areas and large iridescent areas.

(a)   (b)
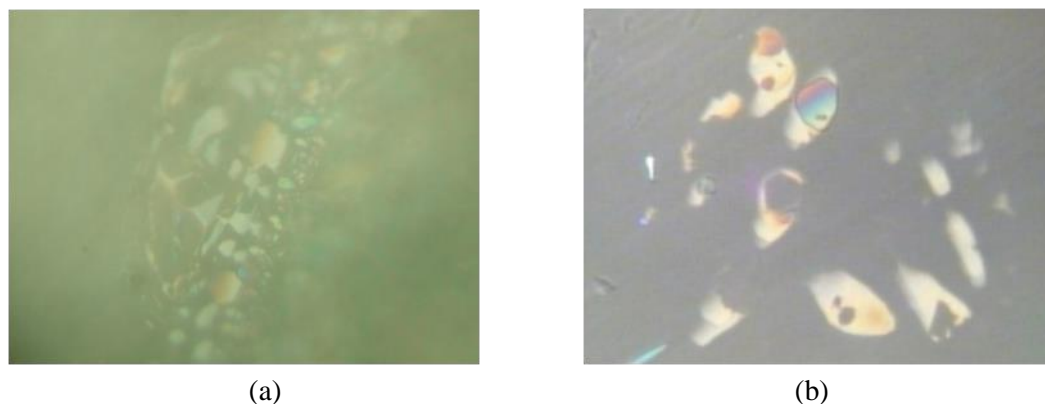
Figure 3.4.2: Healed fissures iridescent reflective consist of angular grains in two different Dak Nong samples.

3.5. Fluid inclusions

Fluid inclusions are secondary inclusions and are located along the healed fissures. They are made of fluid, like water and gas bubbles (Izokh et al. 2010). Figure 3.5.1 (a), (b) and (e) show fluid inclusions in negative crystals with gas bubbles. In Fig 3.5.1 (e), fluid inclusions occur also with a large number of needle-like brown to dark inclusions. The observations also show that the volume ratios of aqueous inclusions and gas bubbles are different. Fluid inclusions can be elongated, as in Figure 3.5.1 (c) and (d), or angular, as in Fig 3.5.1 (f). Raman spectra show that the gas bubbles to be CO_2 and the fluid to be H_2O (Figure 3.5.2 and Figure 3.5.3).
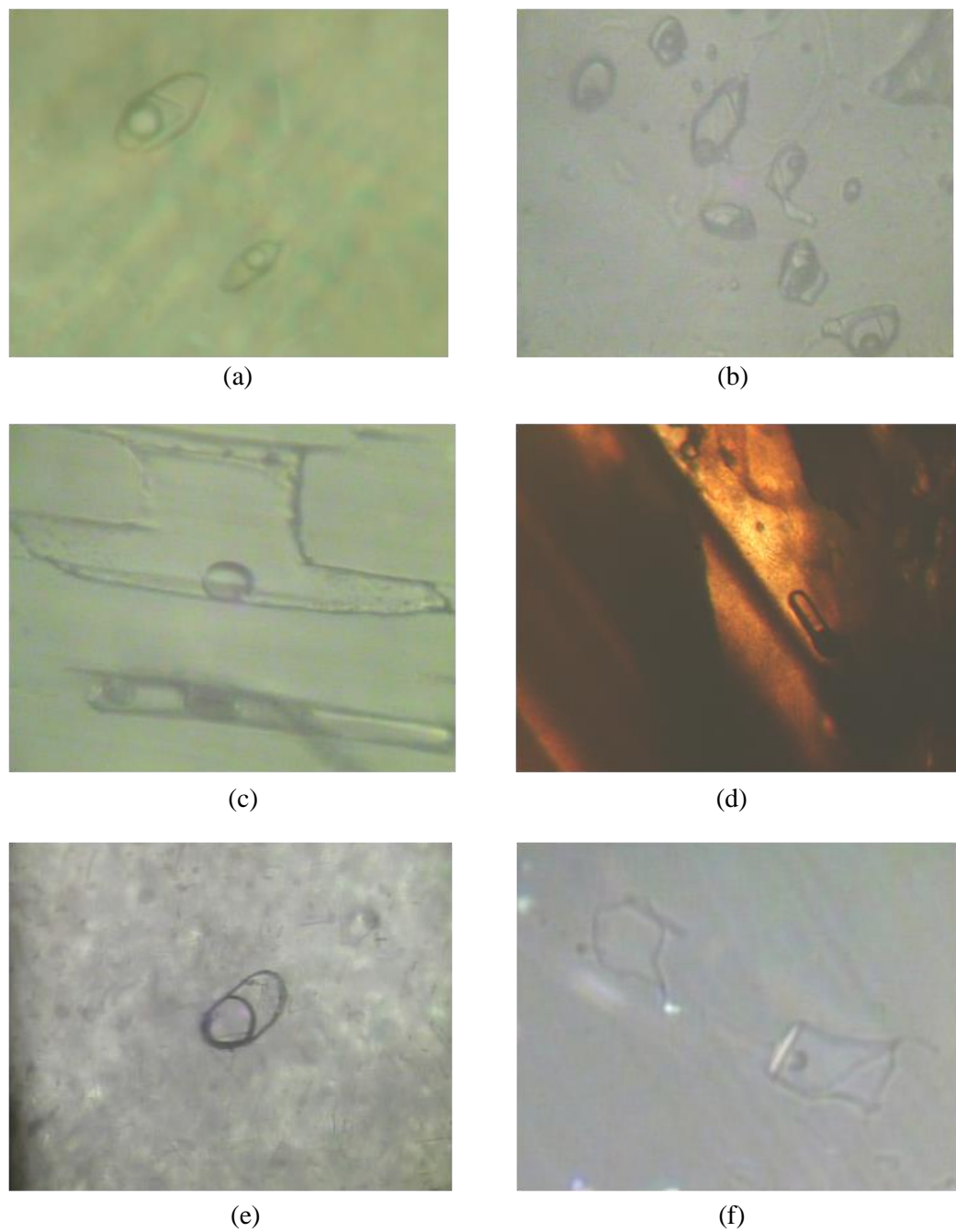
Figure 3.5.1: Fluid inclusions made of aqueous inclusions and gas bubbles observed in (a) Dak Nong (Vietnam), (b) Bo Ploi (Thailand), (c, d) Ban Huay Sai (Laos), (e) Khao Ploi (Thailand), and (f) Dak Nong (Vietnam).
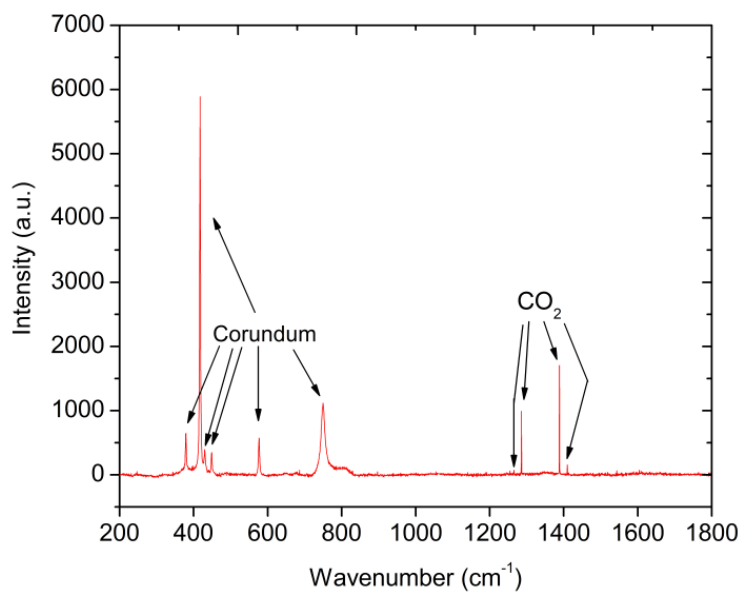
Figure 3.5.2: The Raman spectra of the CO$_2$ gas bubble in fluid inclusion shown in Figure 3.5.1 (a).
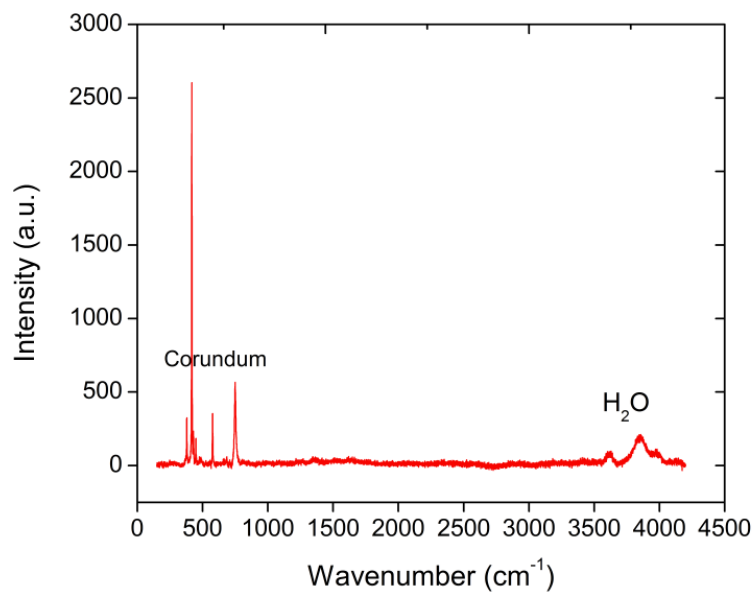
Figure 3.5.3: The Raman spectra of the fluid inclusion shown in Figure 3.5.1 (c).

3.6. Iron oxide inclusions

A large number of brown to black micro inclusions were observed in the core and the arm of the trapiche sapphire from Dak Nong (Vietnam) (Figure 3.6.1. They are round or needle-like inclusions. They could be mangano-ilmenite ($FeTiO_3$), ilmenorutile ($Ti_{0.7}Nb_{0.2}Fe^{2+}_{0.2}O_2$), ulvöspinel (Fe-Ti spinel), hematite (Fe_2O_3), and mangano-hercynite (Fe-spinel) inclusions, according to those described from Kanyarat Khotchanin et al. (2010).
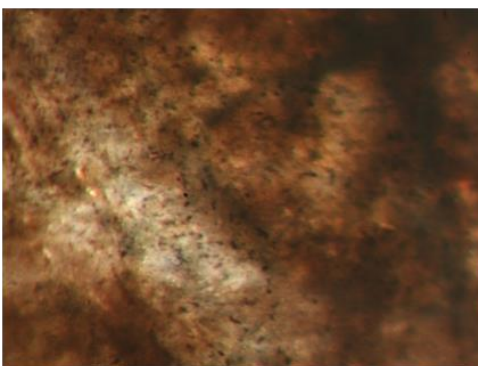
Figure 3.6.1: A large number of brown to black micro inclusions observed at the core of a trapiche sapphire from Dak Nong (Vietnam).

Short needle-like inclusions were often observed in samples from Dak Nong, Dak Lak (Vietnam), Andapa (Madagascar) and Khao Ploi Waen (Thailand). Few of these needles were identified as ilmenite and hematite by EPMA (Nguyen Ngoc Khoi et al. 2014). Figure 2.6.2 shows needle-like inclusions in a sample from Dak Lak.
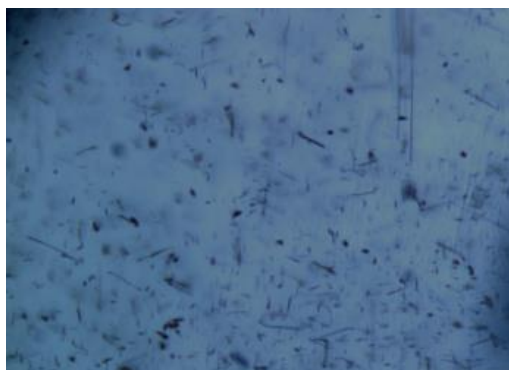
Figure 3.6.2: Needle-like inclusions as hematite or ilmenite according to EPMA analyses in a sample from Dak Lak (Vietnam).

Ilmenite and goethite inclusions were also found as isolated crystals and were identified by Raman laser measurements. Figure 3.6.3 shows two goethite inclusions in two sapphire samples from Dak Nong (Vietnam). The left goethite inclusion shows twining and the right one contains a black inclusion, which was determined to be graphite. The Raman spectra of the left one are shown in Figure 3.6.4.

(a)   (b)

Figure 3.6.3: Goethite inclusions from Dak Nong (Vietnam) under reflection light: (a) A goethite crystal inclusion with twinning structures, (b) Goethite as inclusion containing a black graphite inclusion.
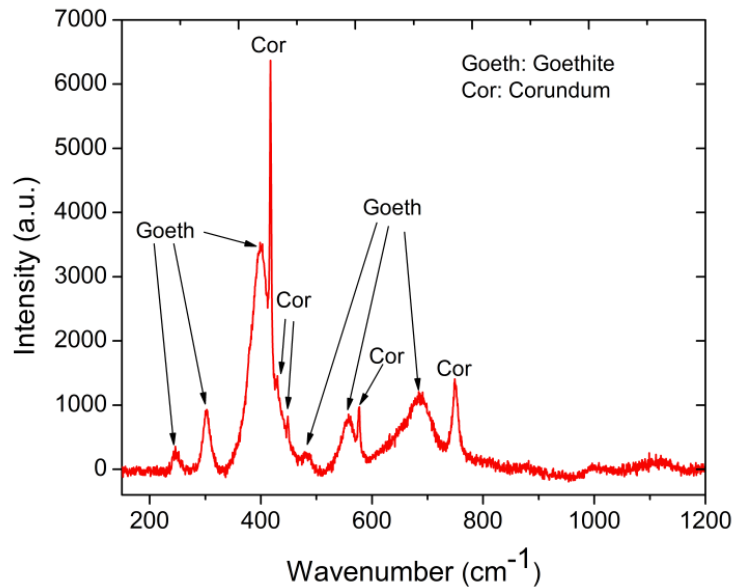
Figure 3.6.4: The Raman spectra of the goethite inclusion shown in Figure 3.6.3 (a).

Figure 3.6.5 shows several ilmenite inclusions. They occur separately as orange-pink crystals which are cut on the surface of a sample from Dak Nong (Vietnam) (Figure 3.6.5 a) or three brown crystals in a sample from Bo Ploi (Thailand) (Figure 3.6.5 b). They occur also as clusters which are distributed within the whole sample, as observed in a sample from Andapa (Madagascar) (Figure 3.6.5 c) or in another one from Ban Huay Sai (Laos) (Figure 3.6.5 d). They are brown to black grains. They can have more angular regular shapes, as in a sample from Andapa (Madagascar), or show rounded droplet like shapes in a sample from Ban Huay Sai (Laos). Figure 3.6.6 presents the Raman spectra of the orange-pink ilmenite inclusion which is shown in Figure 3.6.5 (a).
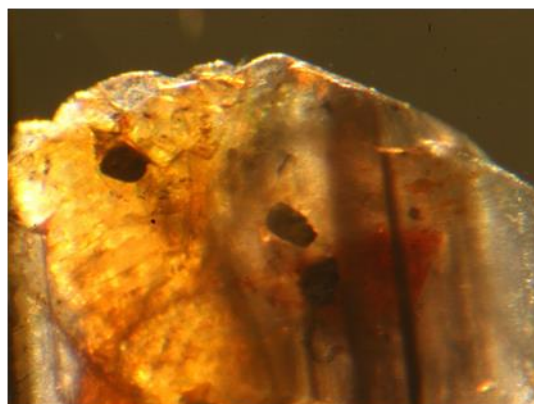
(a)　　　　　　　　　　　　　　　　(b)
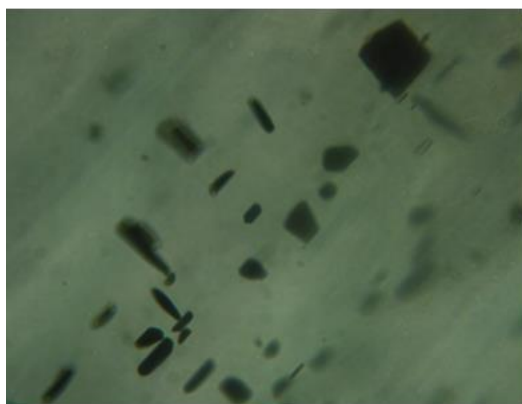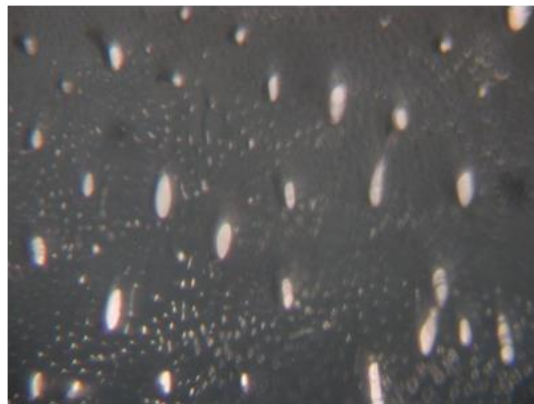
(c)　　　　　　　　　　　　　　　　(d)

Figure 3.6.5: Some ilmenite inclusions observed in this study: (a) Dak Nong (Vietnam), (b) Bo Ploi (Thailand), (c) Andapa (Madagascar), (d) Ban Huay Sai (Laos).
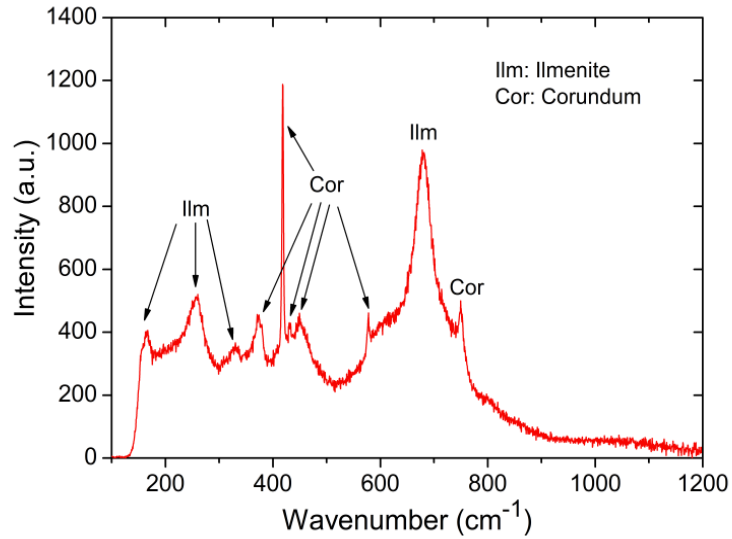
Figure 3.6.6: The Raman spectra of the orange-pink ilmenite inclusion in Figure 6.6.5.

Hematite inclusions commonly occur as black hematite platelets in hexagonal shape as shown in Figure 3.6.7. Only one magnetite inclusion was found in a Dak Nong sample. It is has cubic crystal form and a metallic black luster. This magnetite inclusion and its Raman spectra are given in Figure 3.6.8.
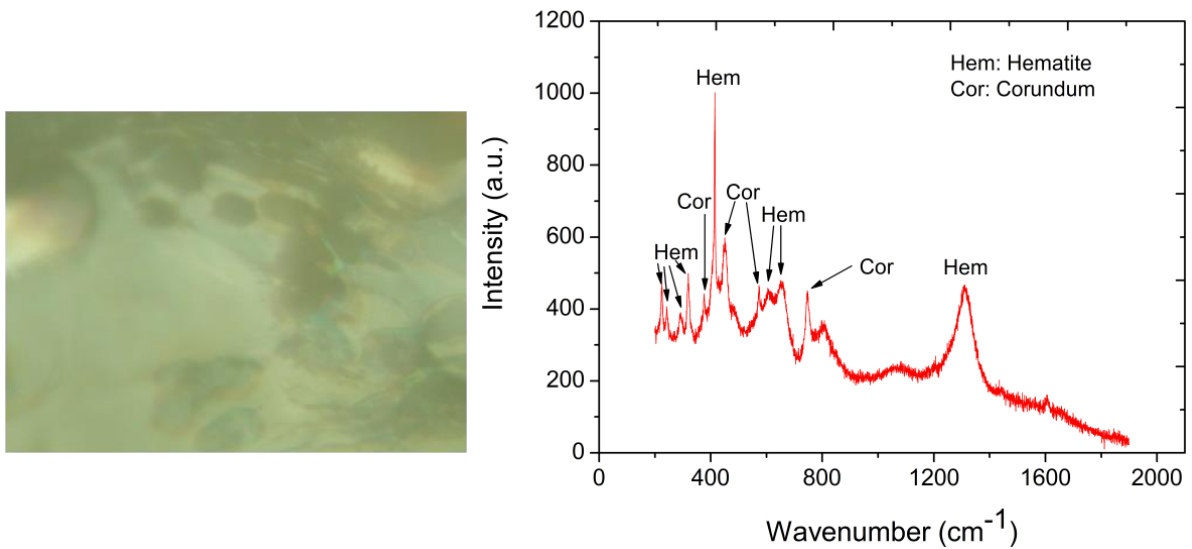
Figure 3.6.7: Black hematite platelets in hexagonal forms in a sample from Dak Nong (Vietnam) and the according Raman spectra.
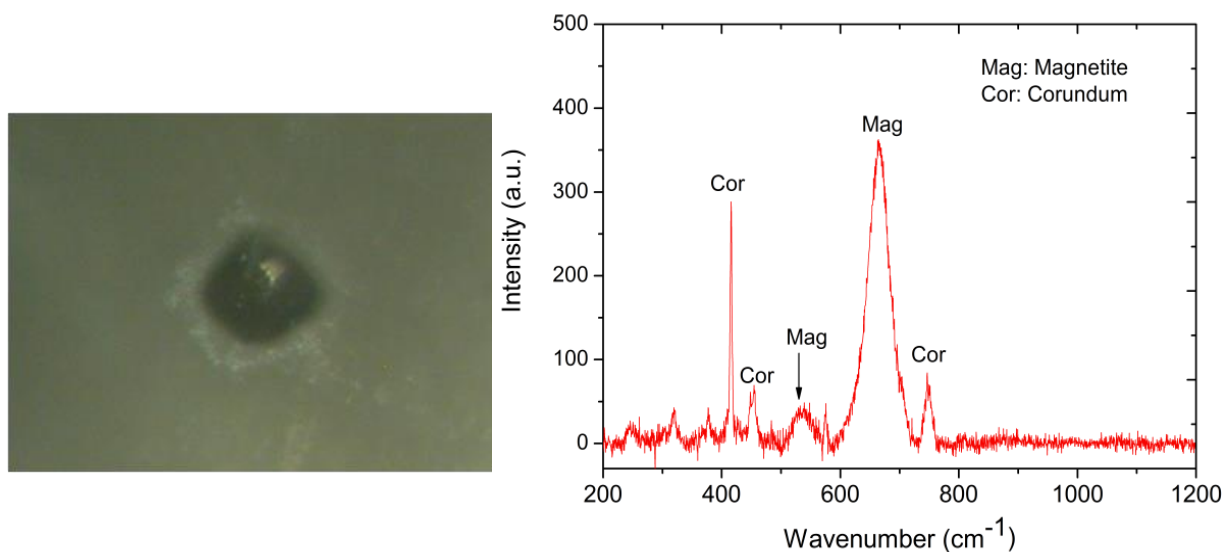
Figure 3.6.8: A black isometric magnetite inclusion in a sample from Dak Nong (Vietnam) and the according Raman spectra.

3.7. Needle or whitish tubes

(a)   (b)
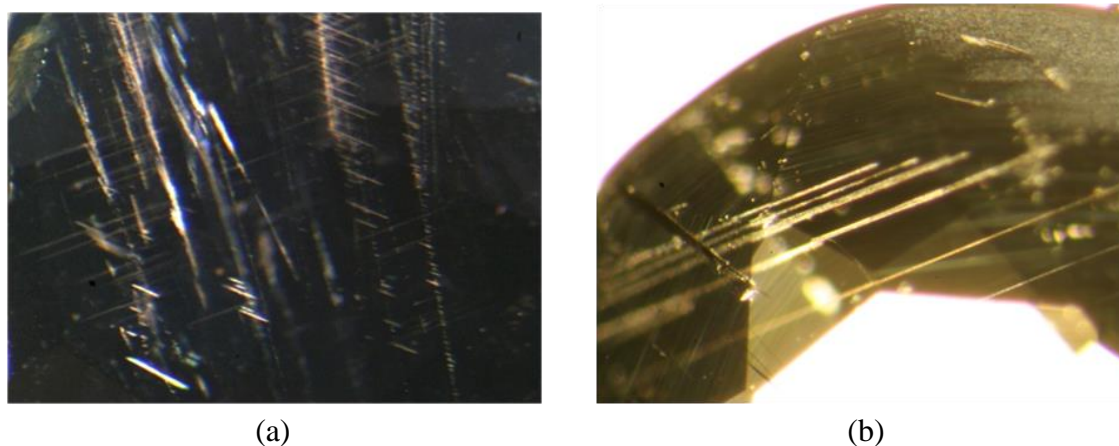
Figure 3.7: Needles or whitish tubes were observed in a samples from Ban Huay Sai (Laos (a) and in a sample from Bo Ploi (Thailand (b).

Long and thin needles or whitish tubes were often observed in the samples. However they could not be determined by Raman spectrometry due to small particle size. They were assumed

to be rutile (TiO_2) needles or whitish tubes filled up by boehmite (β-AlO(OH)) or diaspore (α-AlO(OH)) (Hughes 1997, Gübelin and Koivula 2008 and Chitty 2009). Within corundum host, rutile unmixes in the basal plane, parallel to the faces of the second-order hexagonal prism {1120} (Hughes 1997). Appearance of rutile is very important for origin determination of corundum because oriented rutile inclusions develop through exsolution (Gübelin and Koivula 2008).

3.8. Boehmite, diaspore, kaolinite and OH-groups

Hydrous inclusion boehmite, diaspore and kaolinite were detected by FTIR spectroscopy because of its high sensitivity to the polar O-H bonds. Only diaspore was observed by microscope and determined by both FTIR and Raman spectroscopy.

The peak in the range of 3100-3400 cm^{-1} characterizes structural bonded OH-groups (Volynets et al. 1969 and 1972, Beran 1991, Moon and Phillips 1991 and 1994, Häger 1996, Beran and Rossman 2006, Schwarz et al. 2008). Figure 3.8.1 shows the FTIR spectra of boehmite, diaspore, kaolinite and OH-groups.
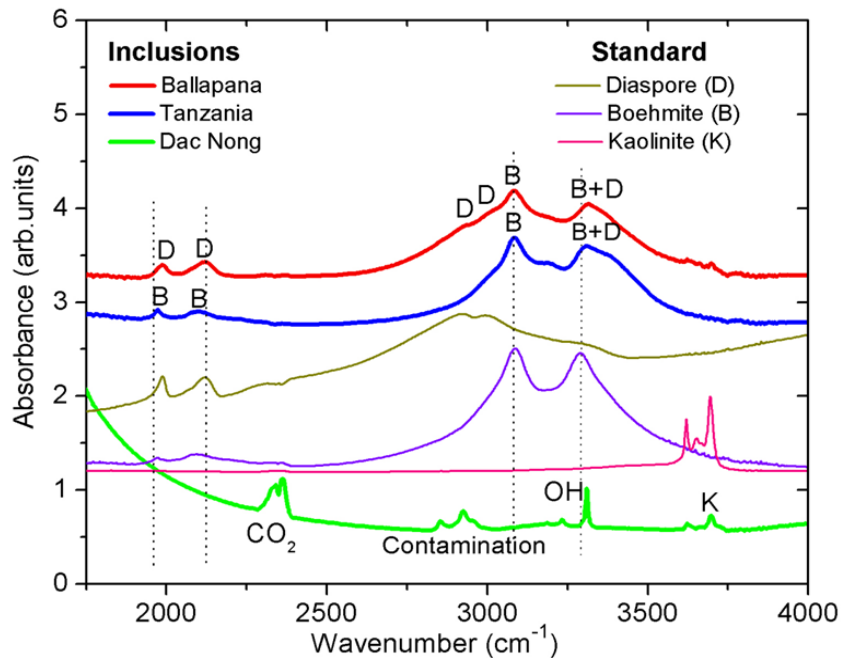
Figure 3.8.1: Boehmite, diaspore, kaolinite inclusions and structural bonded OH-groups in sapphire were determined by FTIR spectroscopy.

CO_2-diaspore inclusions were observed in almost all of the samples from Tansania, Malawi, Ballapana (Sri Lanka), and from the north of Vietnam. Several of CO_2-diaspore inclusions were also found in a sample from Andapa (Madagascar). They are products of retrograde metamorphism. These multi-phase inclusions gather into planar groups with elongated tubes (Figure 3.8.2 a) or as separately cavities (Figure 3.8.2 b). They are angular shaped negative tubes or cavities filled with diaspore and CO_2 gas, which could be determined by Raman spectrometry (Figure 3.8.3), and tiny black particles or flaky substances which could not be identified by Raman spectrometry. This can be explained due to the size of particles or flakes smaller as the spot size of laser beam of 2x2 (µm).

This type of CO_2-diaspore inclusion is similar to those observed for metamorphic sapphire from Tansania (Gübelin and Koivula 2008, Chitty 2009), from Sri Lanka (Hughes 1997, Gübelin and Koivula 2008), from Chimwadzulu, Malawi (Rankin 2002). These black daughter inclusions were confirmed to be calcite by Laser Raman micro-spectrometer (Rankin 2002).

(a)   (b)
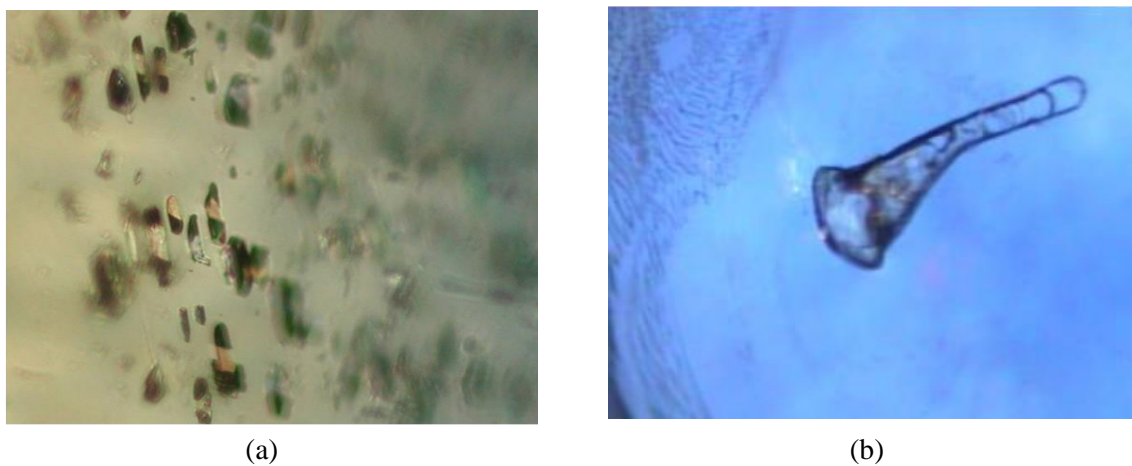
Figure 3.8.2: CO₂-diaspore inclusions and tiny black inclusions: (a) Planar groups of cavities in a sample from Quy Chau (Vietnam), (b) A tube with broad tail together with healed fissures in an Andapa (Madagascar) sample.
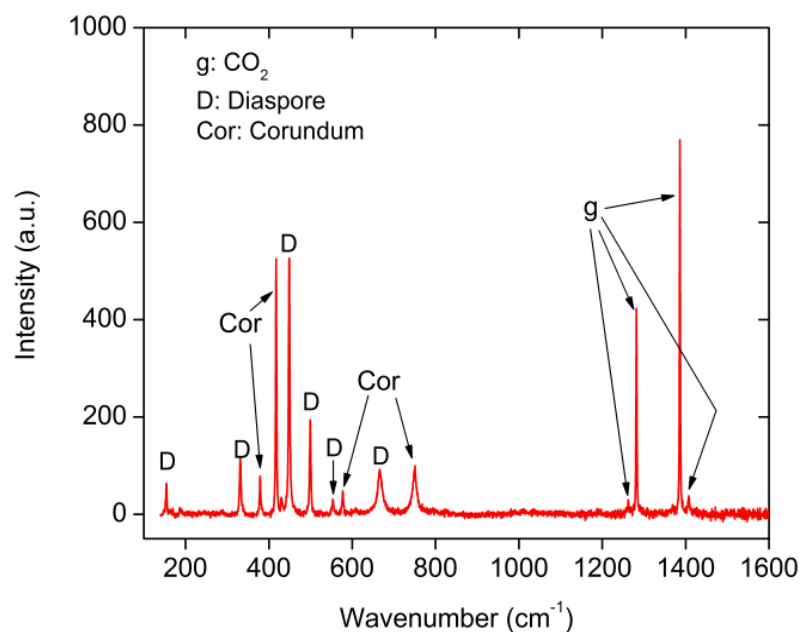
Figure 3.8.3: The Raman spectra of sapphire and CO_2-diaspore inclusion in a sample from Quy Chau (Vietnam).

In this study, the sapphires containing CO_2-diaspore inclusions were heat up to 1750^oC. In the heat-treated sapphires, CO_2-diaspore inclusions were not observed, instead of the planar of the dark or empty cavities. The Raman spectra showed only the peaks of sapphire. This was interpreted that diaspore AlO(OH) were dehydrated and became corundum Al_2O_3.

$$2AlO(OH) = Al_2O_3 + H_2O \qquad (3.8)$$
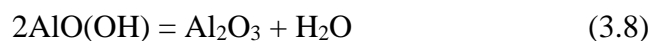
3.9. Spinel inclusion

Spinel ($MgAl_2O_4$) inclusion was observed in a sample from Dak Nong (Vietnam). Figure 3.9 shows this spinel inclusion and its Raman spectra.
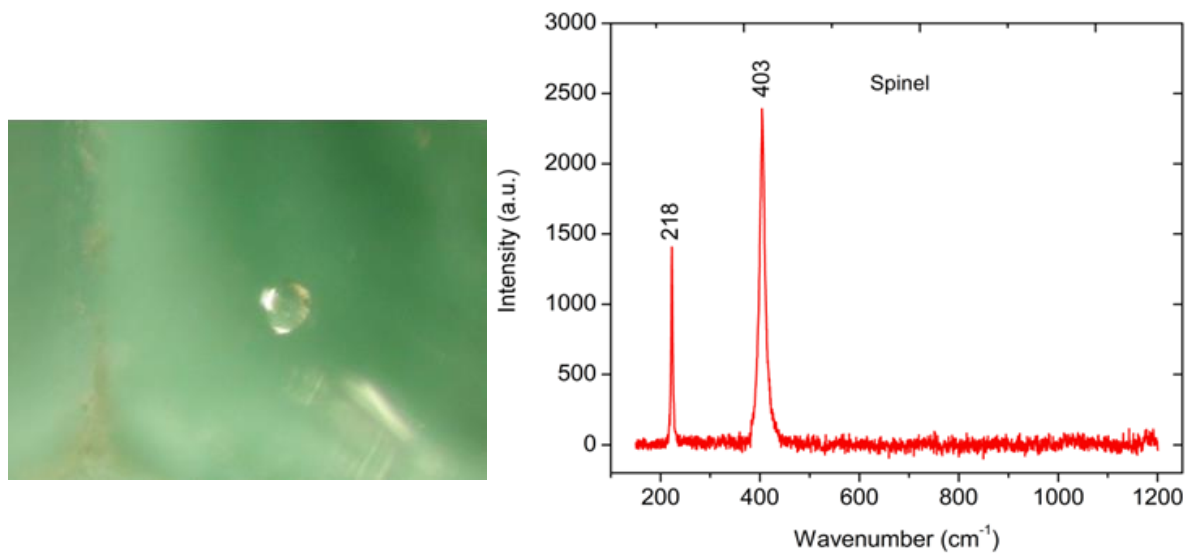
Figure 3.9: Spinel inclusion in a sample from Dak Nong (Vietnam) and its Raman spectra.

3.10. Feldspar inclusions

Feldspar can also occur with corundum in igneous rocks which are silica deficient (Hurlbut et al. 1998). Plagioclase feldspar (Na, Al, Si / K, Ca) is often found in basaltic sapphire (Smith 1995) or sodium plagioclase (albite and oligioclase) and alkali feldspar in corundum from basaltic terrains (Guo et al. 1996). In this study, almost all of the samples have basaltic origin relative to extrusive igneous rock and feldspar inclusions were often observed, especially in the samples from Dak Nong, Dak Lak in the south of Vietnam and Ban Huay Sai in Laos. They appeared as transparent or nontransparent crystals in a variety of forms including prismatic, tabular or slab. Several feldspar inclusions observed by microscope are shown in Figure 3.10.1 and its according Raman spectra are given in Figure 3.10.2.
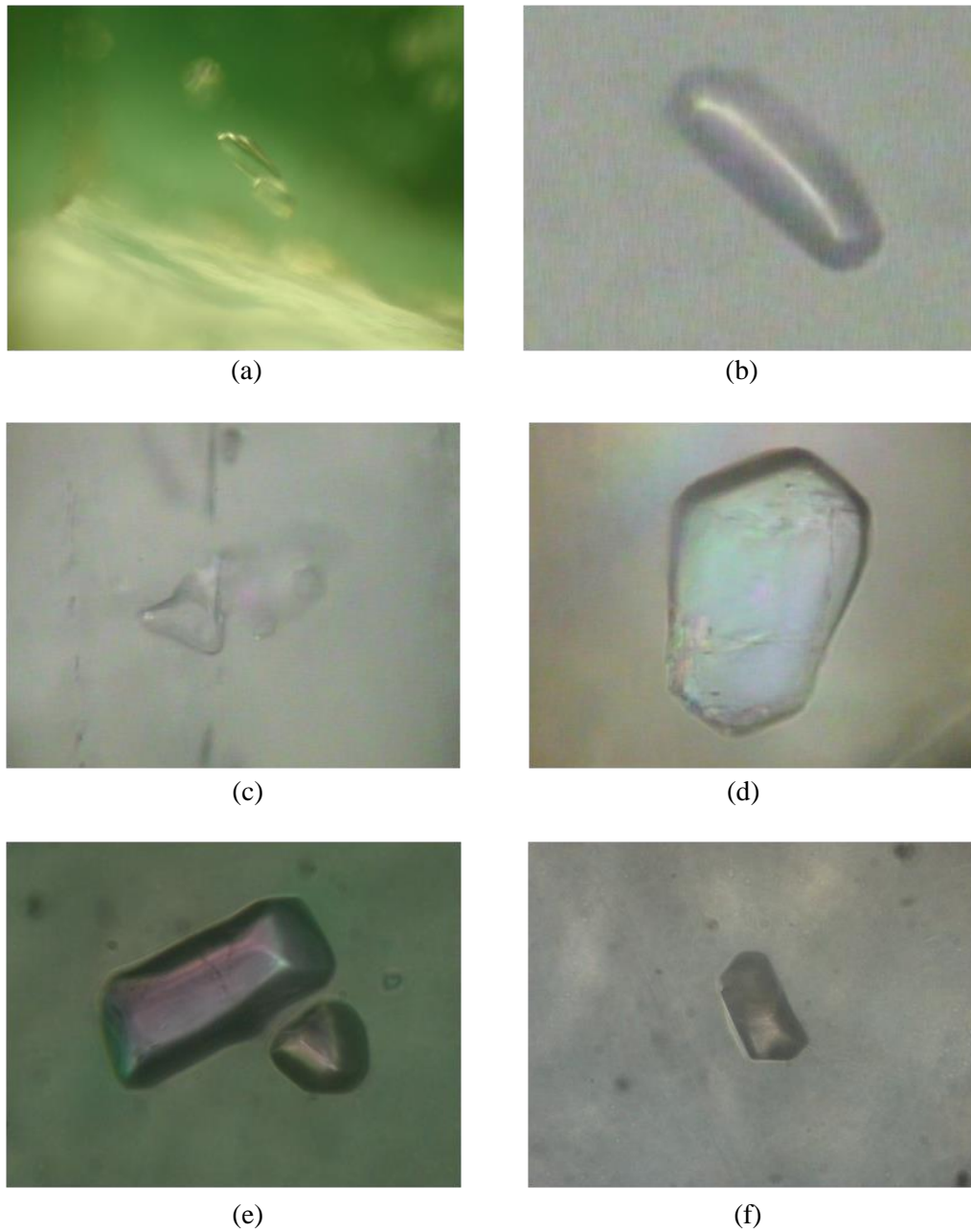
Figure 3.10.1: Feldspar inclusions are commonly found in sapphire.

(a) Two transparent feldspar inclusions in a sample from Dak Nong (Vietnam).

(b) A long and prismatic feldspar inclusion in a sample from Brazil.

(c) A slab of feldspar inclusions in a sample from Quy Chau (Vietnam).

(d) A feldspar inclusions in Russian sample.

(e) Two adjacent inclusions in a sample from Ban Huay Sai (Laos).

(f) A feldspar inclusion in a sample from Dak Lak (Vietnam).
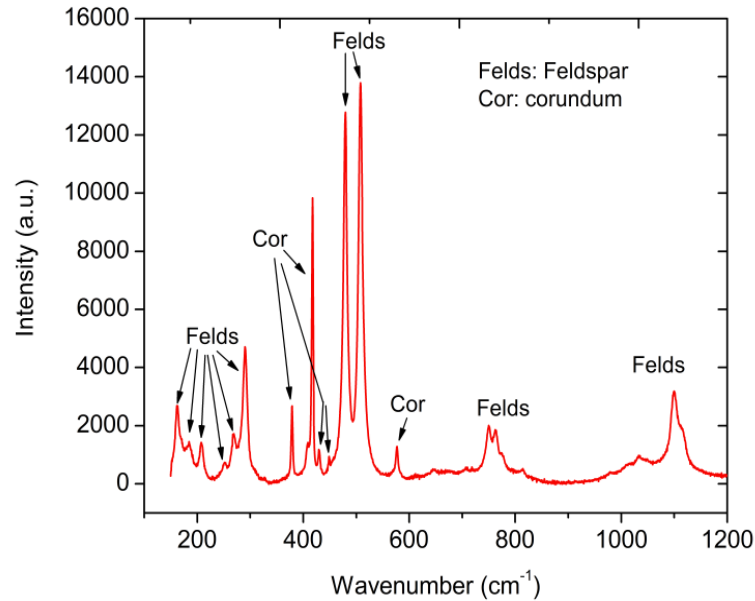
Figure 3.10.2: Raman spectra of a feldspar inclusion in the Russian sample shown in Figure 3.10.

3.11. Zircon inclusions

Zircon ($ZrSiO_4$) is a syngenetic silicate mineral and is found both in magmatic and metamorphic sapphire (Gübelin and Koivula, 1986 and Garnier et al. 2005). They are found in placers and also as inclusions in corundum, which suggests their genetic relationship. In this study, zircon inclusions were found in the samples from Malawi, Tansania, Colombia, Dak Nong (Vietnam), Andapa (Madagascar), Ban Huay Sai (Laos), Shandong (China), and Ballapana (Sri Lanka) as well-formed crystals. Most of them show dipyramidal prismatic crystal habit. Besides, they also occur often as clusters in the samples from Malawi, Colombia and Tansania. Individual crystals in these clusters are also well-formed dipyramidal prismatic and randomly orientated. Isolated zircon inclusions are shown in Figure 3.11.1 and zircon clusters in Figure 3.11.2. Furthermore, zircon inclusions also occur as tabular forms as two transparent zircon crystal inclusions observed in a Tansanian sample and another observed in a Ban Huay Sai sample in Figure 3.11.3.
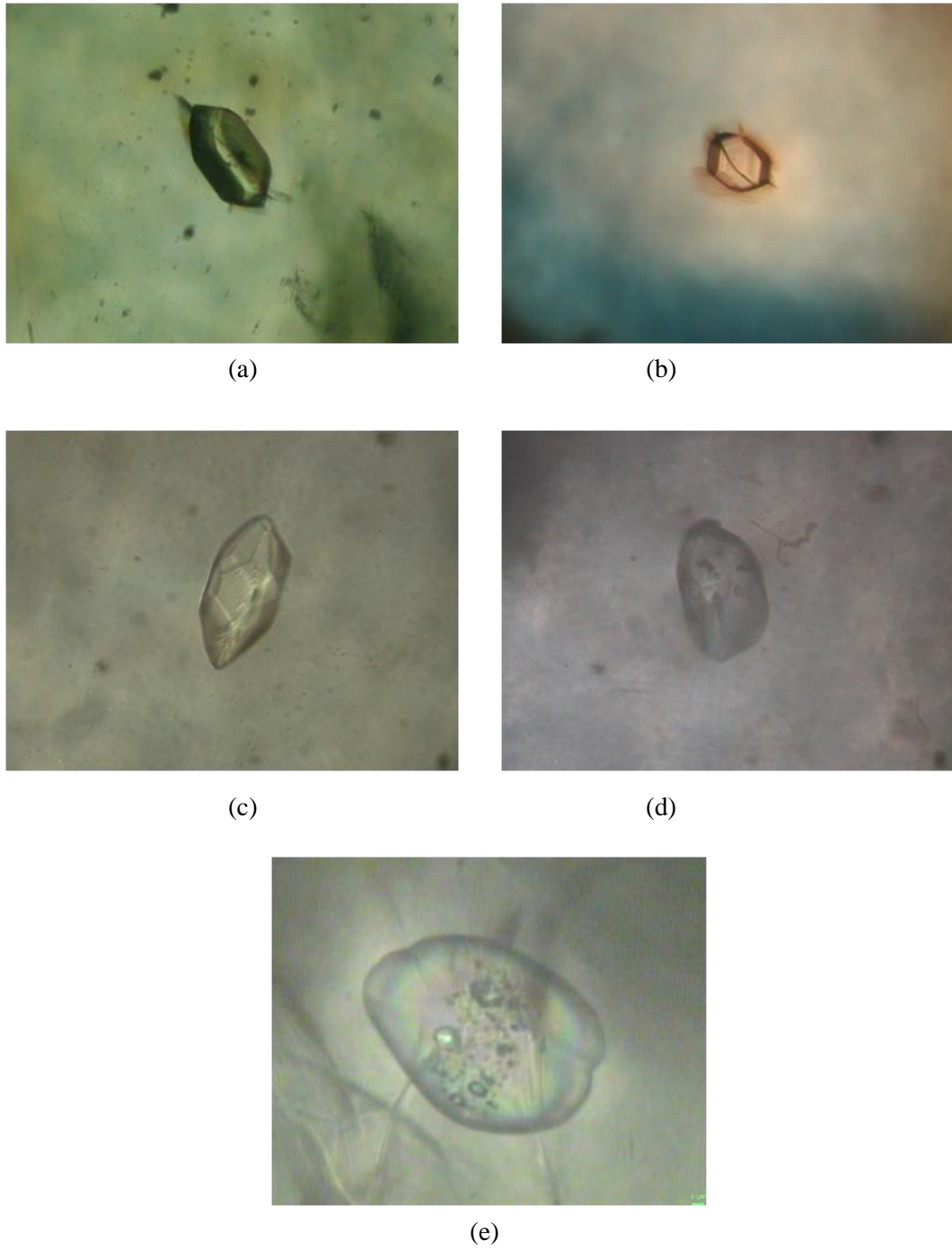
Figure 3.11.1: Zircon inclusions in well-formed dipyramidal prismatic in (a) Dak Nong (Vietnam), (b) Shandong (China), (c) Andapa (Madagascar), (d) Ballapana (Sri Lanka), and (e) Malawi.
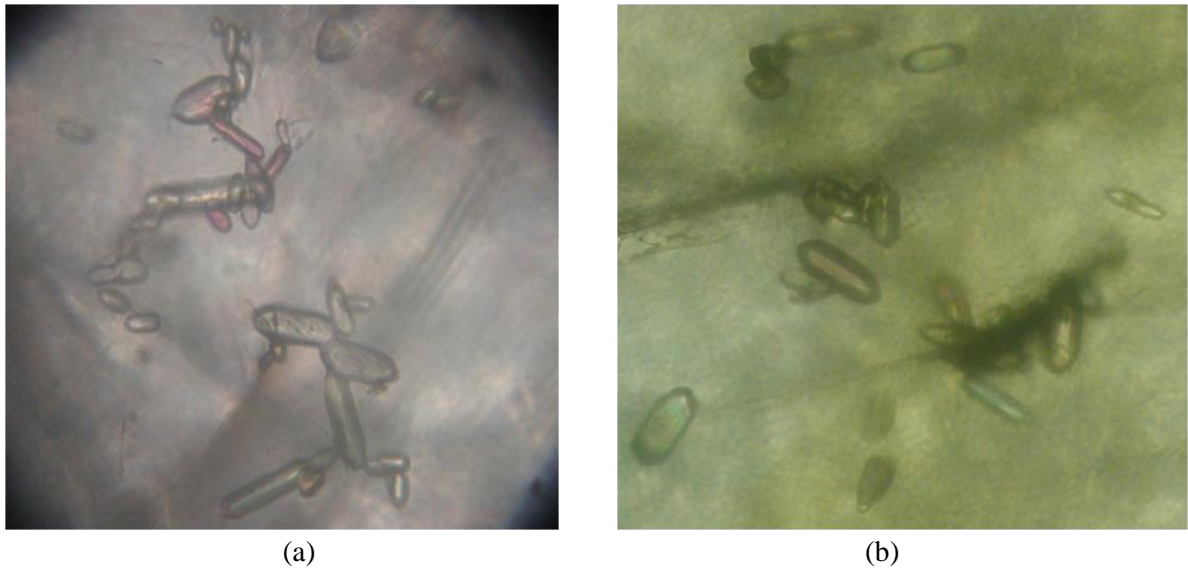
Figure 3.11.2: Clusters of zircon crystals are observed in samples from Tansania (a) and Comlombia (b).
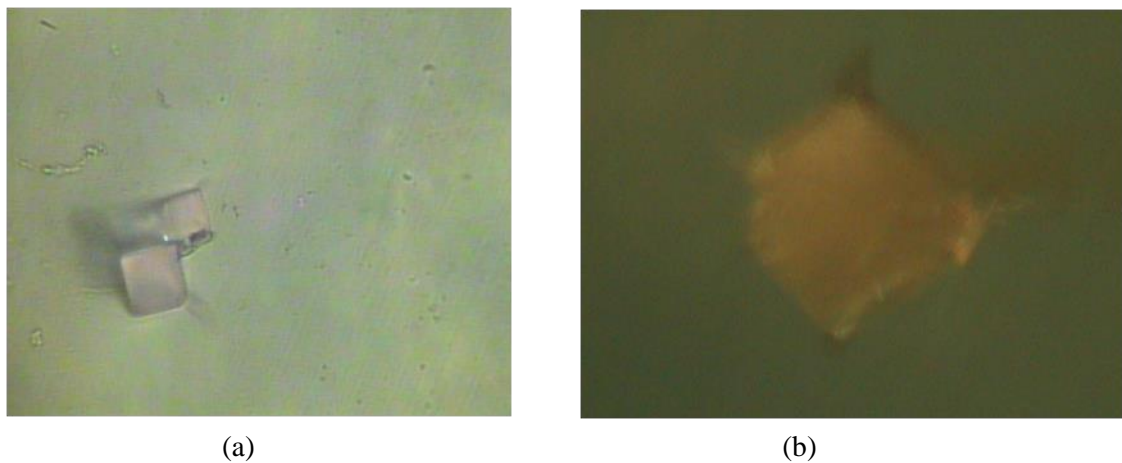
Figure 3.11.3: Zircon inclusions in tabular forms: (a) Two transparent zircon crystal inclusions in a Tansanian sample, (b) A gray zircon inclusion in a Ban Huay Sai (Laos).

Zircon commonly contains radioactive elements as uranium and thorium. Radioactive decay damages the structure of zircon, resulting in the process called the metamictization. Zhang et al. (2000) and Woodhead et al (1991) show that zircon could have high U and Th content, the

metamictization increases and the crystal structure of zircon gradually becomes to be amorphous. Wanthanachaisaeng et al. (2006) reported zircon influenced by strong metamictization closer to be amorphous than crystalline. Investigating zircon inclusions in corundum reveals the degree of metamictization of the zircon inclusion and its influence to corundum host. Determination of *U* and *Th* content in zircon inclusion provides information about the formation and the age of the corundum.

The microscopic study on zircon inclusions in sapphire shows eroded holes on the surface of zircon inclusions like corroded surface. This reflects that zircon inclusions were affected by the metamictization. Raman spectra show that the zircon inclusions have more carvings on the surface, their Raman peak positions are shifted to longer wavenumbers. The Raman spectra of zircon inclusions in the samples from Dak Nong (Vietnam), Colombia and Tansania, which are shown in Figure 3.11.1, are given in Figure 3.11.4. It can be seen from this figure that the metamictization in zircon inclusions from Tansania is higher than those in Dak Nong and Colombia, corresponding in a broadening and a shift of the peak maxima to higher wavenumbers.
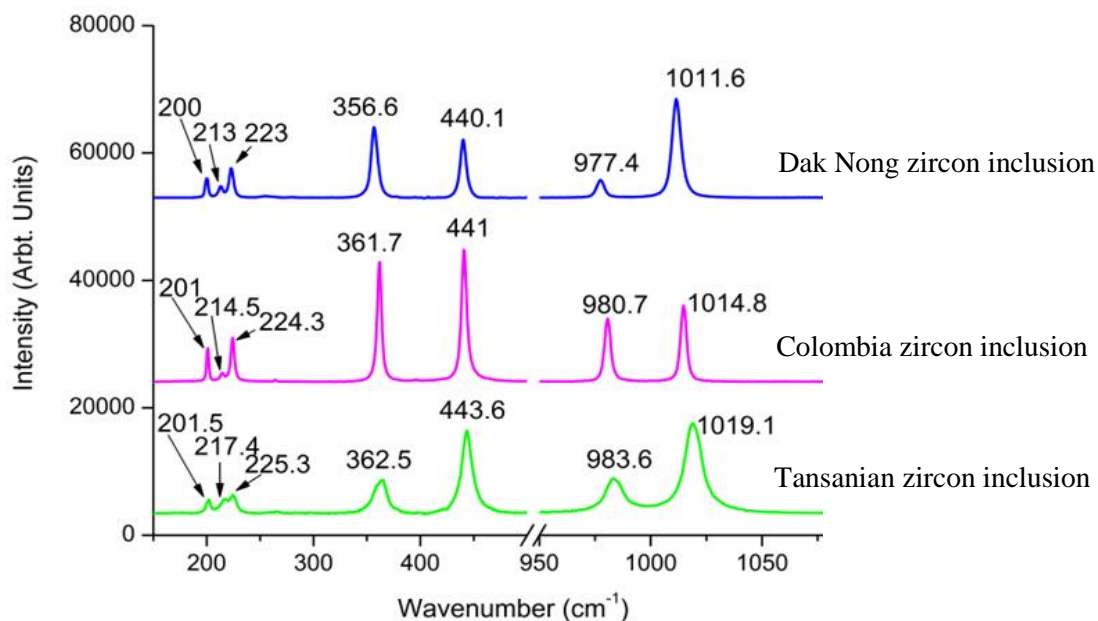
Figure 3.11.4: Raman spectra of zircon inclusions (shown in Figure 3.11.1) from Dak Nong (Vietnam), Colombian and Tansanian samples.

3.12. Mica inclusions

Muscovite, a typical mineral of mica group was found in sapphire from Quy Chau-Nghe An and Luc Yen-Yen Bai in the north of Vietnam (Pham et al. 2004). In this study, a muscovite inclusion as hexagonal platelet shape was observed in a Bo Ploi sample. The muscovite inclusion and its Raman spectra are shown in Figure 3.12.
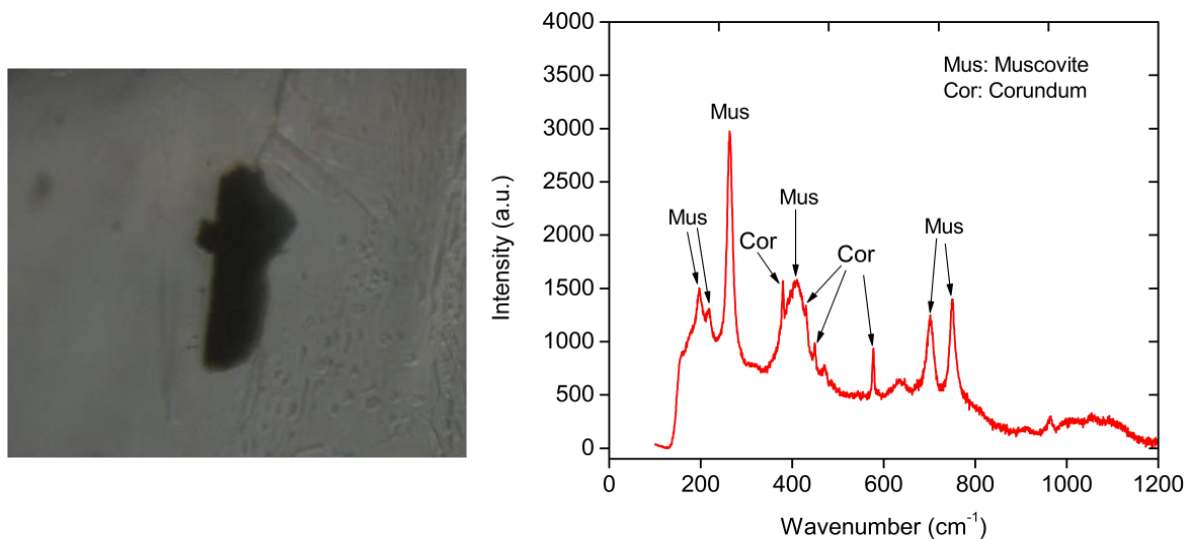
Figure 3.12: A platelet of muscovite inclusion in a sample from Bo Ploi (Thailand) and the according Raman spectra.

3.13. Cordierite inclusion

Cordierite or iolite is a magnesium iron aluminum ring silicate with 6-member ring. Figure 3.40 presents a cordierite inclusion in orthorhombic pyramidal form in a Dak Nong (Vietnam) sample and the according Raman spectra.
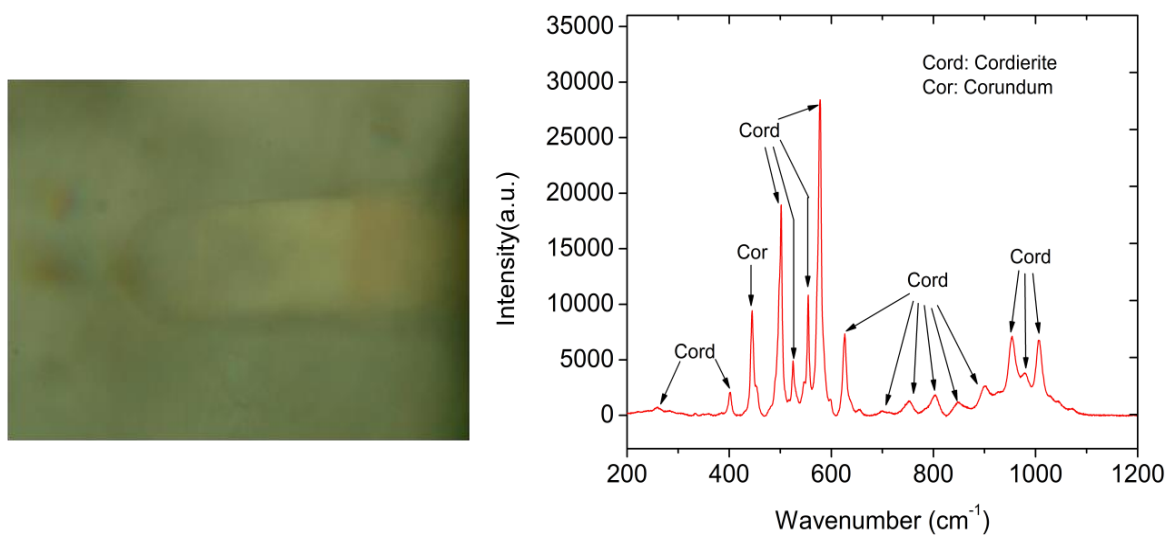
Figure 3.13: Cordierite inclusion in a sample from Dak Nong (Vietnam) and the according Raman spectra.

3.14. Tantalite inclusions

Tantalite is mineral group with formula $(Fe,Mn)(Ta,Nb)_2O_6$. It is normally called columbite-tantalite or Coltan due to tantalum (Ta) and niobium (Nb) and has dull black metallic color. In this study, the tantalite inclusions were often observed in the samples from Bo Ploi (Thailand), Andapa (Madagascar), Ban Huay Sai (Laos) and Dak Lak (Vietnam). They occur in black or black metallic color and commonly appear together with the healed fissures as shown in Figure 3.14.1.

(a)

(b)

(c)
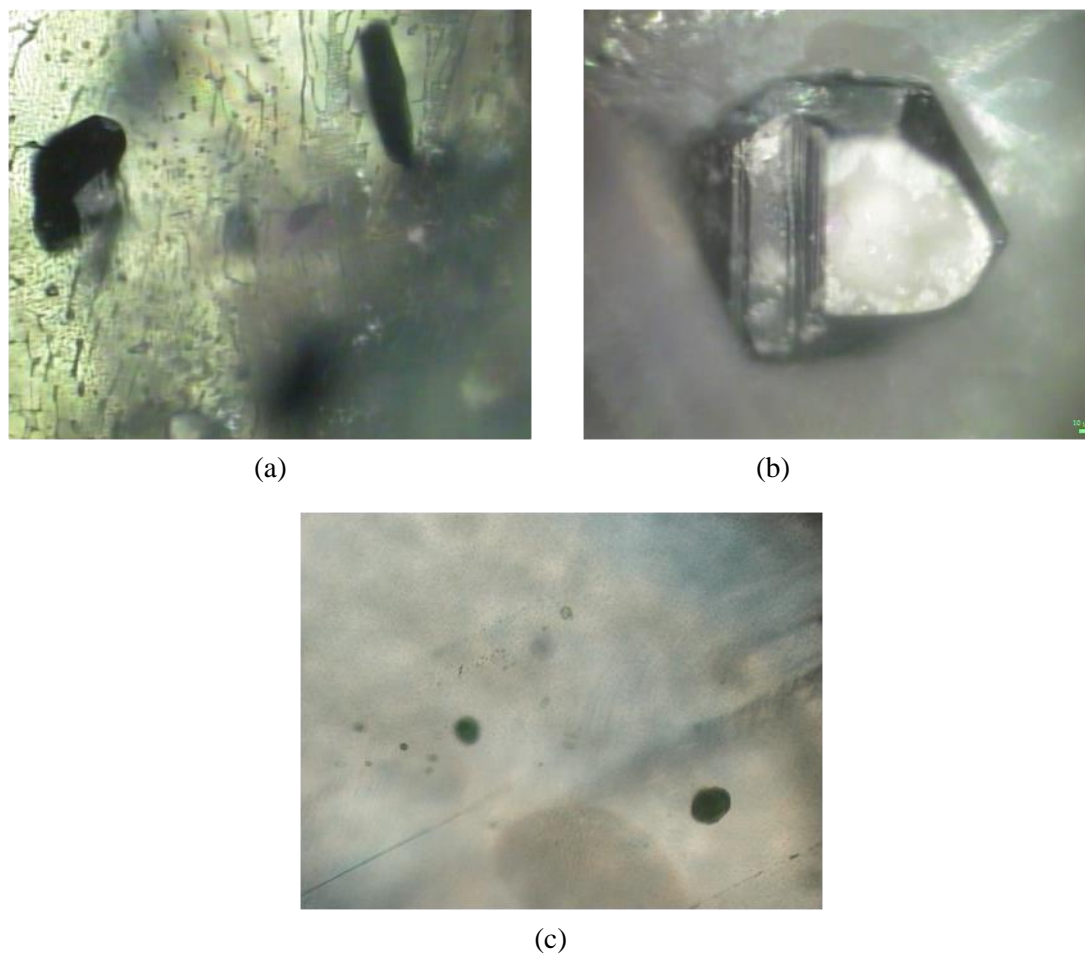
Figure 3.14.1: Dull black metallic columbite-tantalite inclusions: (a) Dak Lak (Vietnam), (b) Bo Ploi (Thailand), (c) Andapa (Madagascar).

Tantalite which is Mn-rich and Fe-poor is called mangano-tantalite and is colored red (Grice et al. 1976, Bermanec et al. 2009). Several mangano-tantalite inclusions were observed in a Ban Huay Sai sample with typical dark red color and well-formed crystal structure. Figure 3.14.2 shows two mangano-tantalite inclusions in two different orthorhombic shapes from this Ban Huay Sai sample. The left one is truncated rhombic pyramid shape, and the right one shows rhombic prism pyramid shape.

Figure 3.14.3 shows the Raman spectra of the mangano-tantalite inclusion in Figure 3.14.2 (the left one).
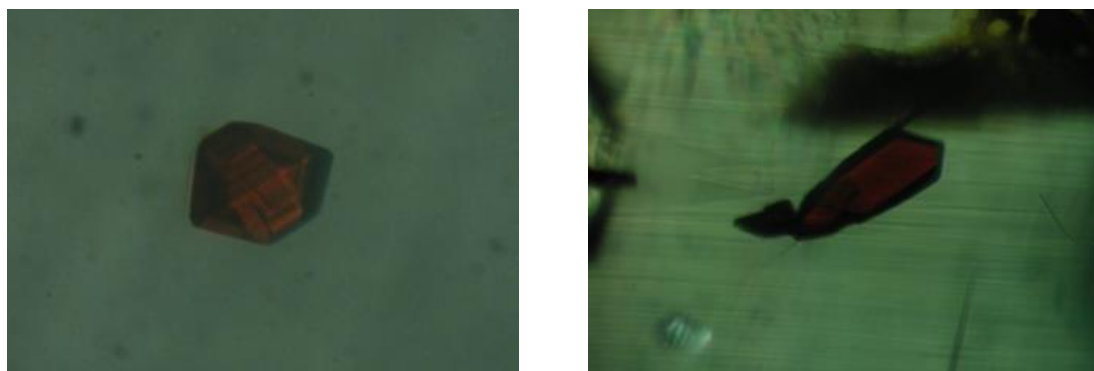
Figure 3.14.2: Two dark red mangano-tantalite inclusions in two different crystal forms in a Ban Huay Sai sample.
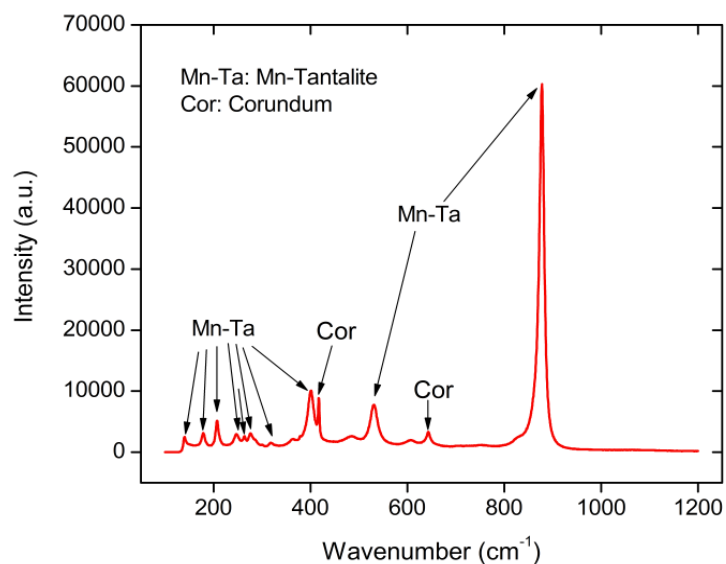
Figure 3.14.3: Raman spectra of mangano-tantalite inclusion which was shown in Figure 3.14.2 (the left one) in a Ban Huay Sai sample.

All internal features of sapphire in this study are listed in Table 3.1. In general, sapphire in this study, including the samples from Dak Nong, Dak Lak in the south of Vietnam, Bo Ploi, Khao Ploi Waen in Thailand, Ban Huay Sai in Laos, Andapa, Antsirabe, Nosibe in Madagascar are characterized by iron-containing inclusions like ilmenite, goethite, hematite or magnetite or Si-high relatively inclusions like feldspar or zircon. Zircon inclusions appear commonly in

Tansania, Colombia and Malawi samples as clusters of orientated single zircon crystals. CO_2-diaspore inclusions were much observed in the sample from Tansania, Malawi and two unknown sources in the north of Vietnam.

Table 3.1: The internal features of sapphire from different localities in this study.

1: Dak Nong, 2: Dak Lak, 3: Quy Chau, 4: Unknown northern Vietnam, 5: Trapiche unknown northern Vietnam, 6: Ban Huay Sai, 7: Bo Ploi, 8: Khao Ploi Waen, 9: Australia, 10: Shandong, 11: Brazil, 12: Colombia, 13: Andapa, 14: Antsirabe, 15: Nosibe, 16: Tansania, 17: Ballapana, 18: Russia, 19: Malawi

Country	Vietnam					Laos	Thailand		Australia	China	Brazil	Colombia	Madagascar			Tansania	Sri Lanka	Russian	Malawi
	1	2	3	4	5	6	7	8	9	10	11	12	13	14	15	16	17	18	19
Trapiche	+++			+						++									
Color zoning	++	++	+	+		+	+	+		++		+		+	+				
Twinning	+	+							+			+						+	
Healed fissures	++	++	+		+	++	+		+	+		+	+					+	
Fluid inclusion	+	+				+	+												
Hematite	++	++																	
Magnetite	+																		
Ilmenite	++	++					+		+	+				++					
Goethite	++						++												
Graphite	+																		
Needles/Tubes	+					+	+	+					+	+					

Table 3.1: The internal features of sapphire from different localities in this study (be continued).

1: Dak Nong, 2: Dak Lak, 3: Quy Chau, 4: Unknown northern Vietnam, 5: Trapiche unknown northern Vietnam, 6: Ban Huay Sai, 7: Bo Ploi, 8: Khao Ploi Waen, 9: Australia, 10: Shandong, 11: Brazil, 12: Colombia, 13: Andapa, 14: Antsirabe, 15: Nosibe, 16: Tansania, 17: Ballapana, 18: Russia, 19: Malawi

Country	Vietnam					Laos	Thailand		Australia	China	Brazil	Colombia	Madagascar			Tansania	Sri Lanka	Russian	Malawi
	1	2	3	4	5	6	7	8	9	10	11	12	13	14	15	16	17	18	19
Boehmite																+	+		
Kaolinite	+									+									
CO_2-diaspore			+++	+++	+++								+			+++	+++		+++
Spinel	+																		
Feldspar	+					+				+								+	
Zircon	+					+				+	+	+++	+			+++	+++		+
Muscovite							+												
Cordierite	+																		
Tantalite						+													
Coltan		+				+	+						+						
Mn-tantalite						+													

Chapter 4: Chemical Compounds of Sapphire

In corundum (α-Al_2O_3), aluminum can be replaced by trace elements like iron, titanium, chromium, and vanadium in the octahedral sites (Volynets and Sidorova 1971, Ferfuson and Fielding 1972, Fritsch and Rossman 1987, 1988 (Part 2 and Part 3)). In this part, the measured oxides include Al_2O_3, TiO_2, V_2O_3, Ga_2O_3, Fe_2O_3, SiO_2, Cr_2O_3, Mn_2O_3 and MgO in wt.% by EPMA. The LA-ICP-MS analyses are applied to determine elements with define content in ppm. They are Li, Be, Na, Mg, Si, P, K, Ca, Sc, Ti, V, Cr, Mn, Co, Ni, Zn, Ga, Rb, Sr, Y, Zr, Nb, Mo, Cs, Ba, Ta, W, Pb and Bi.

4.1. Chemistry of sapphire by EPMA

Table 4.1 presents the chemical compositions of sapphire samples in this study in wt.% oxides by EPMA measurements with minimum, maximum and standard deviation value. Chemical analyses by EPMA show that Iron is the most dominant minor element in the studied sapphire samples. The samples characterized by high Iron content (>0.3 wt.% Fe_2O_3) are from Dak Nong, Dak Lak from the south of Vietnam, Shandong, Australia, Ban Buay Sai, Khao Ploi Waen, Bo Ploi, Andapa, Antsirabe, Nosibe, Tansania, Ballapana, Brazil, Russia and Colombia. The samples from the north of Vietnam have low Iron content (<0.3 wt.% Fe_2O_3), and in several cases, it is even below detection limit ("bdl" <0.01 wt.% Fe_2O_3). The brown cores and the arms of trapiche samples from Dak Nong (Vietnam) and Shandong (China) have very high iron content, from 1.17 to 1.947 wt.% Fe_2O_3. An amount of 1.947 wt.% Fe_2O_3 is detected in the core of a Shandong sample.

After iron, gallium and silicon is present in almost all samples. The highest gallium content detected in a sample from Shandong (China) is 0.1 wt.% of Ga_2O_3 and the highest silicon content, also reported in this sample is 0.17 wt.% of SiO_2. Titanium is very low to "bdl" of the EPMA. The highest titanium content found in a Nosibe sample is 0.243 wt.% of TiO_2. Vanadium, chromium, manganese and magnesium are typically "bdl".

Table 4.1: Chemical composition measured by EPMA of the studied sapphire samples in wt.% with minimum, maximum and standard deviation values. The number in the bracket is amounts of the samples.

Origins	Al_2O_3	TiO_2	V_2O_3	Ga_2O_3	Fe_2O_3	SiO_2	Cr_2O_3	Mn_2O_3	MgO	Total
Dak Lak (10)	97.457-99.633 0.567	0.010-0.042 0.011	"bdl"	0.021-0.038 0.005	0.508-1.662 0.349	0.025-0.033 0.003	"bdl"	"bdl"-0.010	"bdl"-0.010	98.922-100.282 0.383
Dak Nong (58)	94.623-100.168 0.896	"bdl" -0.157	"bdl" -0.152	0.018-0.051 0.006	0.242-1.880 0.327	"bdl" -0.115	"bdl" -0.026	"bdl" -0.011	"bdl" -0.025	96.306-100.857 0.773
Quy Chau (3)	97.557-97.683 0.443	0.023-0.035 0.006	"bdl"-0.010	"bdl"-0.017	0.255-0.305 0.028	0.016-0.024 0.004	0.010-0.025 0.007	"bdl" -0.01	"bdl"	97.894-98.053 0.430
Trapiche (North VN) (2)	97.603-97.970 0.259	0.173-0.174 0.259	"bdl"	"bdl"	"bdl"-0.010	0.029-0.030 0.001	"bdl"-0.01	"bdl" -0.01	0.010-0.011 0.005	97.847-98.211 0.257
Unknown, (North VN) (2)	97.943-98.153 0.584	0.055-0.095 0.064	0.009-0.011 0.005	0.012-0.013 0.009	0.104-0.143 0.045	0.018-0.023 0.007	"bdl"	"bdl"	0.02-0.026 0.013	98.166-98.462 0.618

Table 4.1: Chemical composition measured by EPMA of the studied sapphire samples in wt.% with minimum, maximum and standard deviation values (be continued).

Origins	Al_2O_3	TiO_2	V_2O_3	Ga_2O_3	Fe_2O_3	SiO_2	Cr_2O_3	Mn_2O_3	MgO	Total
Khao Ploi Waen (6)	97.943-99.166 0.432	"bdl"-0.012	"bdl"-0.01	0.011-0.027 0.006	1.470-1.778 0.109	0.025-0.042 0.006	"bdl"	0.01-0.012 0.003	"bdl"	99.662-100.812 0.433
Bo Ploi (16)	99.38-99.81 0.363	"bdl"-0.016	"bdl" -0.011	"bdl"-0.037	0.377-0.557 0.068	0.023-0.045 0.011	"bdl"-0.013	"bdl"-0.01	"bdl" -0.01	98.866-100.305 0.359
Ban Huay Sai (7)	98.200-100.016 0.696	"bdl"-0.194	"bdl" -0.007	0.023-0.055 0.013	0.368-1.367 0.428	0.014-0.029 0.006	"bdl"	"bdl" -0.010	"bdl" -0.003	99.575-100.636 0.327
Australia (2)	97.307-98.687 0.976	0.055-0.132 0.054	"bdl" -0.003	0.026-0.027 0.001	0.963-1.023 0.042	0.020-0.026 0.005	"bdl"	0.007-0.009 0.002	"bdl"	98.522-99.767 0.880
Shandong (35)	96.220-99.880 0.622	"bdl"-0.143	"bdl"-0.010	0.024-0.105 0.019	0.860-1.947 0.226	0.015-0.171 0.031	"bdl" -0.011	"bdl"-0.013	"bdl" -0.022	97.647-101.059 0.590
Colombia (9)	98.147-99.994 0.586	"bdl"-0.092	"bdl" -0.010	"bdl"-0.019 0.005	0.448-0.999 0.207	0.023-0.053 0.012	"bdl"-0.076	"bdl"-0.013	"bdl"-0.014	98.722-100.751 0.608

Table 4.1: Chemical composition of the studied sapphire samples in wt.% of oxides with minimum, maximum and standard deviation values by EPMA measurements (be continued).

Origins	Al_2O_3	TiO_2	V_2O_3	Ga_2O_3	Fe_2O_3	SiO_2	Cr_2O_3	Mn_2O_3	MgO	Total
Antsirabe **(9)**	97.837-99.088 0.365	0.012-0.229 0.066	"bdl" -0.01	0.032-0.067 0.011	0.884-1.318 0.162	0.017-0.064 0.018	"bdl" -0.010	"bdl"-0.010	"bdl"	99.089-100.375 0.381
Andapa **(6)**	98.358-99.808 0.545	0.005-0.171 0.064	"bdl"-0.006 "bdl"	0.008-0.031 0.010	0.696-1.576 0.328	0.020-0.028 0.004	"bdl" -0.016	"bdl" -0.01	"bdl"	100.026-100.843 0.304
Nosibe **(10)**	97.787-99.810 0.778	0.006-0.243 0.087	"bdl" -0.010	0.014-0.064 0.016	0.835-1.366 0.155	0.023-0.055 0.011	"bdl" -0.006	"bdl" -0.01	"bdl" -0.01	99.074-100.811 0.749
Russia **(1)**	98.250-98.780 0.282	"bdl" -0.010	"bdl" -0.010	0.019-0.033 0.008	0.433-0.449 0.009	0.024-0.030 0.003	"bdl"	"bdl" -0.014	"bdl"	98.749-99.288 0.289
Brazil **(1)**	98.640-99.290 0.256	0.047-0.078 0.0136	"bdl" -0.017	"bdl"-0.019	0.814-0.834 0.009	0.013-0.019 0.003	"bdl"	"bdl"-0.013	"bdl"	99.566-100.212 0.253
Tansania **(5)**	97.403-97.900 5.782	"bdl"-0.01	"bdl" -0.01	0.006-0.011 0.003	0.768-0.908 0.055	0.021-0.038 0.009	"bdl"-0.019	"bdl"-0.017	"bdl"	98.249-98.782 5.795
Ballapana **(5)**	97.617-98.423 0.342	"bdl"	"bdl" -0.01	0.017-0.034 0.007	0.940-1.040 0.048	0.014-0.036 0.009	"bdl" -0.003	"bdl" -0.010	"bdl" -0.01	98.735-99.475 0.320

Due to the fact that, the Fe_2O_3 is the most dominant content in the examined studies, Figure 4.1.1-4.1.7 shows correlation diagrams of the oxides detected by EPMA versus the basis of Fe_2O_3 content.
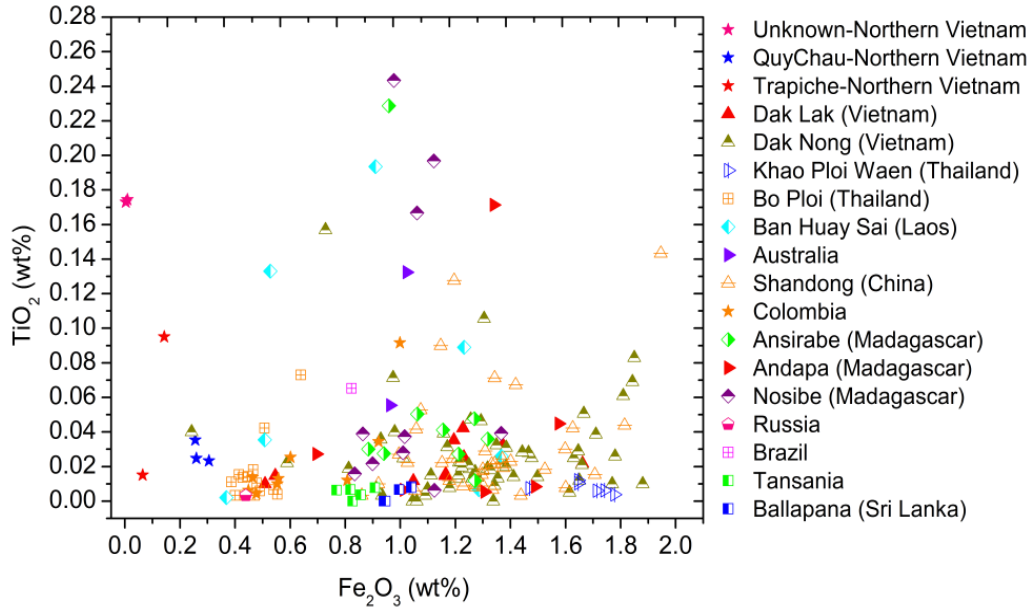
Figure 4.1.1: Correlation diagram of the TiO_2 and Fe_2O_3 content in the samples.
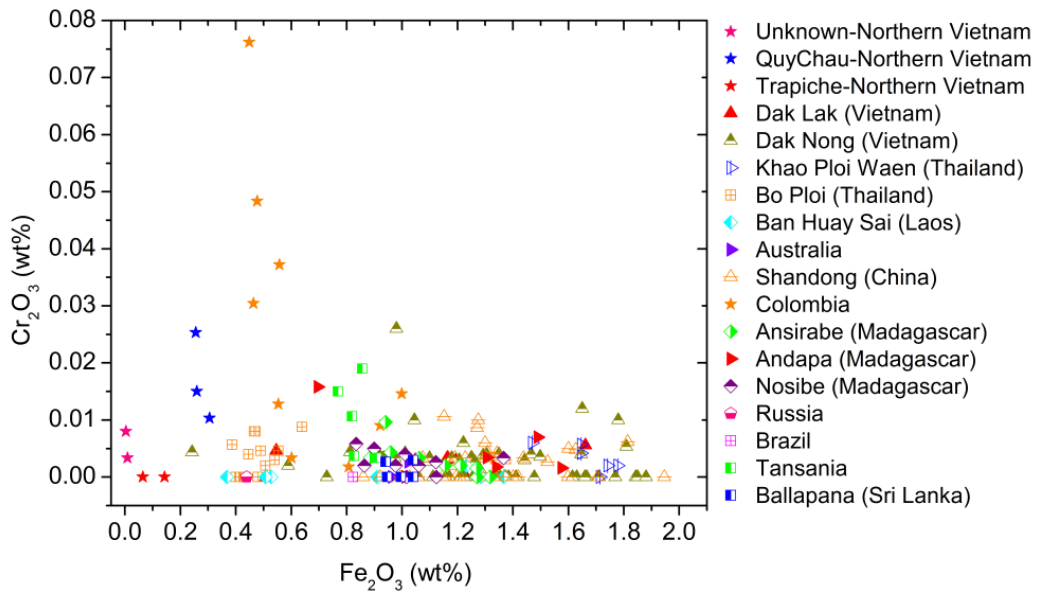
Figure 4.1.2: Correlation diagram of the Cr_2O_3 and Fe_2O_3 content in the samples.
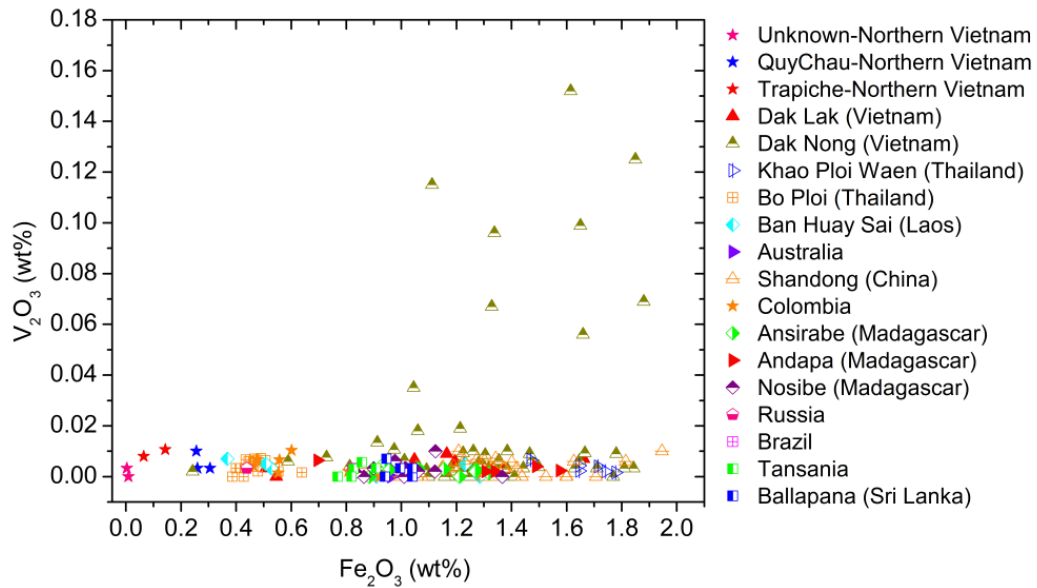
Figure 4.1.3: Correlation diagram of the V₂O₃ and Fe₂O₃ content in the samples.
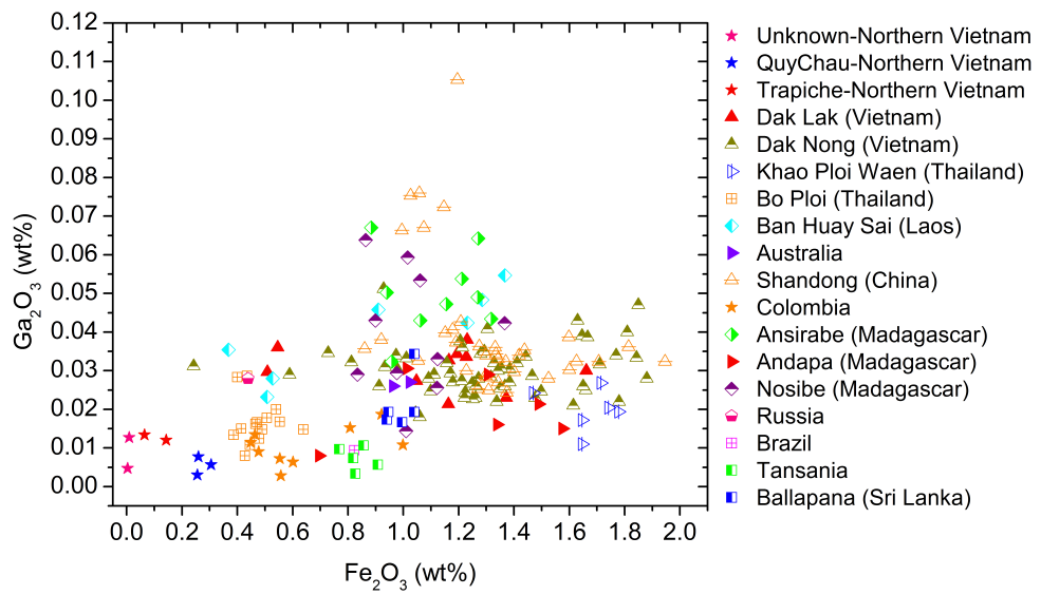
Figure 4.1.4: Correlation diagram of the Ga₂O₃ and Fe₂O₃ content in the samples.
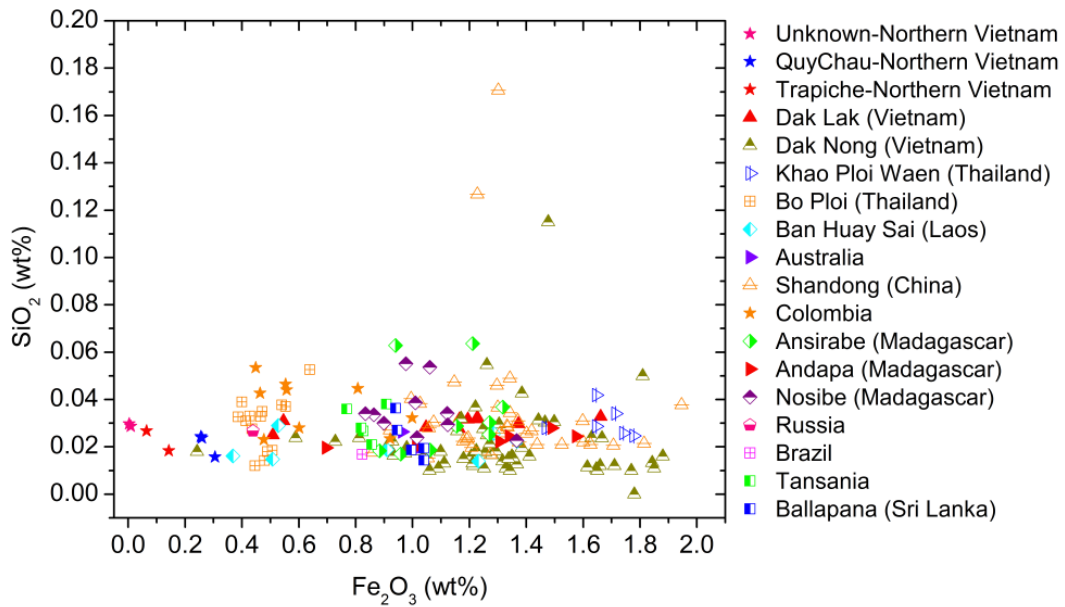
Figure 4.1.5: Correlation diagram of the SiO₂ and Fe₂O₃ content in the samples.
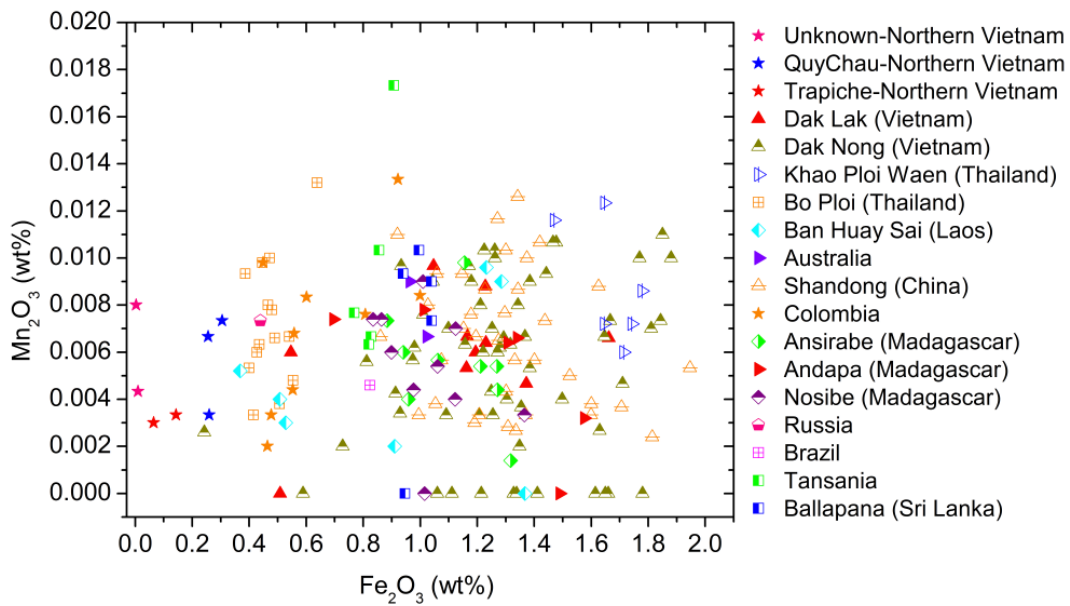
Figure 4.1.6: Correlation diagram of the Mn₂O₃ and Fe₂O₃ content in the samples.
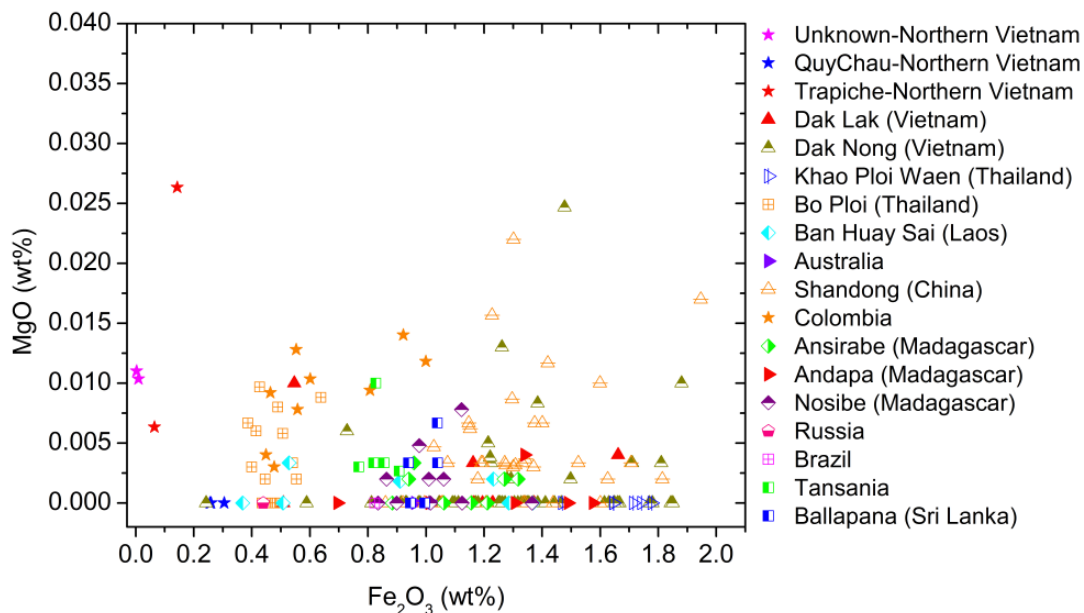
Figure 4.1.7: Correlation diagram of the MgO and Fe₂O₃ content in the samples.

4.2. The ratio of Cr₂O₃/Ga₂O₃ and Fe₂O₃

Due to geological characteristics, chemical compositions of corundum may be used to distinguish corundum from different origins, and to differentiate natural and synthetic corundum (Stern and Hänni 1982, Tang et al. 1988, 1989, Muhlmeister et al. 1998, Sutherland et al. 1998b, Joseph et al. 2000, Saminpanya et al. 2003). Sutherland et al. (1998b) and Sutherland and Schwarz (2001) used the ratio of Cr_2O_3/Ga_2O_3 by EPMA to separate basaltic from metamorphic corundum. According to these results, corundum characterized by the ratio of Cr_2O_3/Ga_2O_3 below 1 is typical for basaltic origins, and that of Cr_2O_3/Ga_2O_3 higher than 1 is typical for metamorphic origins. This is only phenomenology, but it gives a good fingerprint.

The ratio of Cr_2O_3/Ga_2O_3 vs the Fe_2O_3 content of sapphire is shown in Figure 4.2.1. Figure 4.2.2 shows a close-up view of the Cr_2O_3/Ga_2O_3 lower than 1. Almost all of the samples having high Iron content and the ratio of Cr_2O_3/Ga_2O_3 lower than 1 show their basaltic origins like reported in some experiments (Sutherland et al. 1998b, Sutherland and Schwarz 2001). Some samples from Tansania and Colombia have the ratio of Cr_2O_3/Ga_2O_3 higher than 1, and their

71

iron content is high. All samples from the north of Vietnam have low iron content (<0.3 wt.% Fe_2O_3), and all samples from Quy Chau (Vietnam) have this ratio higher than 1.
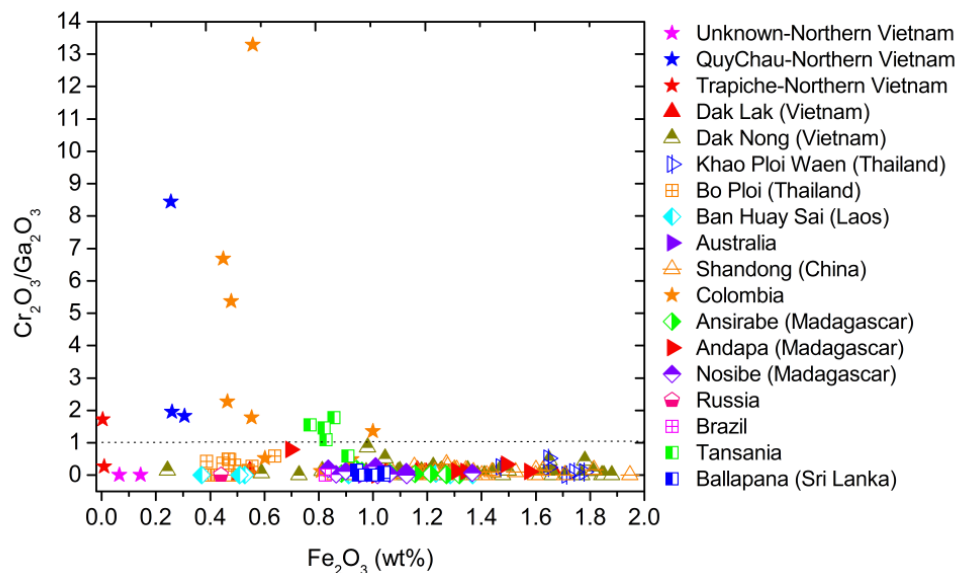
Figure 4.2.1: Ratio of Cr_2O_3/Ga_2O_3 vs. Fe_2O_3 of the examined samples from all localities.
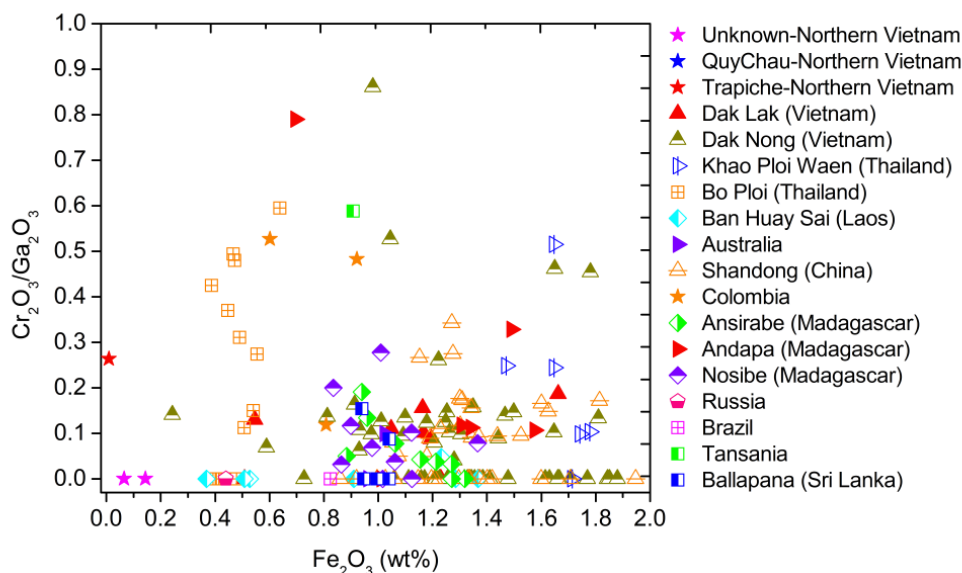
Figure 4.2.2: A close view from 0 to 1 of the ratio of Cr_2O_3/Ga_2O_3 vs. Fe_2O_3.

A note in Table 4.1 that, the total chemical compositions of the samples from Tansania, Quy Chau, trapiche pattern and an unknown source from North Vietnam are around from 97-98% of α-Al$_2$O$_3$ content. This can be explained that, the samples from these areas contain hydrous inclusions (boehmite, diaspore), and this decreases the total composition of α-Al$_2$O$_3$. These diaspore inclusions distribute wholly in these samples, and are determined by Raman and FTIR measurements. Boehmite inclusions are also reported in this study but less often, and determined by FTIR (see the content in the inclusions and FTIR sections). Diaspore, α-AlO(OH) and boehmite, γ-AlO(OH) are aluminium oxide hydroxide mineral. They are morphous and occur as alteration products of corundum.

4.3. Chemical analyses by LA-ICP-MS

As seen in Table 4.3 the traces of Si, Ti, V, Cr, Ga, Mg and Mn which are low and normally below detection limit of the EPMA, are sensitive with LA-ICP-MS. The concentrations of silicon vary from 500-2000 ppm and are much more in Ballapana and unknown-source North Vietnam samples. The concentrations of gallium are variable around 200-500 ppm in Nosibe, Shandong and Ban Huay Sai samples, and around 20-200 in the remained samples. The concentrations of titanium are more variable, from 10-760 ppm and much more in the samples related to blue color like Nosibe, Ansirabe, and Dak Nong samples. The concentrations of magnesium are less, varying from 20-260 ppm. The concentrations of chromium and vanadium are less compared to those of titanium and magnesium. The concentrations of chromium change from around 1-70 ppm and up to 260 ppm in light pink Colombian samples, while those of vanadium are from 10-30 ppm. The concentrations of manganese are generally too low, from "bdl" to 4 ppm. There are only one sample from Dak Nong with 24 ppm manganese and one Antsirabe sample with 12 ppm manganese detected.

Figure 4.3.1 shows the percentages of important trace elements in sapphire by ternary diagrams. In these diagrams, if the data points close to 1 (or 100%), the percentage of according trace element in the samples is more dominant than two remained elements.

In Table 4.3, Unk = "unknown" and NVN = North Vietnam.

Table 4.3: Chemical composition of the samples by LA-ICP-MS analyses in ppm. The number in the bracket is the sample amounts.

Element	Dak Lak (7)	Dak Nong (18)	Shandong (27)	Australia (2)	Ban Huay Sai (4)	Bo Ploi (8)	Khao Ploi Waen (2)	Russia (1)	Colombia (5)
Li	"bdl"	"bdl"	"bdl"-0.29	"bdl"-0.08	"bdl"-0.64	"bdl"-0.66	"bdl"	"bdl"	"bdl"-0.15
Be	"bdl"-0.46	"bdl"	"bdl"	0.07-0.34 0.19	0.49-31.14 12.62	"bdl"-0.33	"bdl"-0.10	"bdl"	"bdl"-0.06
Na	4.15-7.84 1.36	"bdl"	"bdl"	4.68-8.93 3.01	3.99-68.71 31.90	"bdl"-10.75	9.65-10.47 0.58	5.92	"bdl"-94.53
Mg	5.81-22.48 5.52	5.25-33.34 9.44	6.06-71.98 13.25	2.54-3.12 0.41	0.74-9.84 4.49	9.92-49.59 13.76	10.87-12.15 0.91	1.79	23.92-82.06 21.86
Si	770.97-911.99 48.05	628.77-1614.39 218.54	641.37-1448.72 186.50	680.82-788.83 76.38	549.22-825.53 127.71	593.96-891.31 87.30	751.41-837.57 60.92	835.88	572.58-730.18 59.35
P	12.53-17.25 1.47	11.03-843.14 267.91	"bdl"	14.02-17.53 2.48	13.95-15.46 0.69	9.11-18.69 3.31	13.72-14.04 0.23	13.80	10.93-16.35 2.04
K	2.55-3.78 0.94	"bdl"	"bdl"	"bdl"	"bdl"-42.75	"bdl"-19.65	"bdl"-5.42	"bdl"	"bdl"-1.99
Ca	6.11-52.86 20.85	"bdl"	"bdl"	"bdl"	"bdl"	"bdl"-116.21	"bdl"-15.25	12.47	"bdl"-9.85
Sc	"bdl"-0.20	"bdl"	"bdl"	"bdl"-0.06	"bdl"-0.26	"bdl"-0.16	"bdl"-0.10	"bdl"	"bdl"-0.13
Ti	33.37-180.48 48.59	102.53-530.58 113.94	23.41-816.55 178.19	248.53-295.93 33.51	51.31-420.35 173.45	17.42-203.12 63.12	45.84-46.89 0.74	7.69	35.21-209.98 69.21
V	2.64-21.53 6.45	13.86-215.50 51.89	2.09-34.84 10.33	5.48-6.41 0.66	0.41-1.62 0.54	5.62-15.82 3.98	1.02-2.29 0.90	12.22	6.23-25.82 7.37
Cr	1.69-5.70 1.53	1.42-22.69 7.59	1.17-40.23 10.94	1.62-1.69 0.04	1.50-3.98 1.17	1.69-35.12 12.66	1.79-2.52 0.51	7.04	20.99-256.67 98.69
Mn	0.21-0.78 0.19	0.26-24.22 6.17	0.29-4.22 1.02	0.22-1.23 0.71	0.21-1.74 0.70	0.33-8.02 2.85	0.94-1.17 0.16	0.24	"bdl"-0.18
Co	"bdl"-0.07	"bdl"	"bdl"	"bdl"	"bdl"-0.38	"bdl"-13.29	"bdl"-0.04	"bdl"	"bdl"-0.30
Ni	"bdl"-0.25	"bdl"	"bdl"	"bdl"-0.08	"bdl"-0.37	"bdl"-1.94	"bdl"-0.13	"bdl"	"bdl"-0.28

Table 4.3: Chemical composition of the samples by LA-ICP-MS analyses in ppm (be continued).

Element	Dak Lak (7)	Dak Nong (18)	Shandong (27)	Australia (2)	Ban Huay Sai (4)	Bo Ploi (8)	Khao Ploi Waen (2)	Russia (1)	Colombia (5)
Zn	1.73-3.52 0.63	1.68-12443.04 3792.00	0.77-13.16 3.17	1.91-5.51 2.55	1.15-9.27 3.68	0.59-10.33 3.65	1.62-2.45 0.59	3.33	0.73-4.86 1.67
Ga	178.17-242.85 23.51	1.53-325.76 91.47	167.48-876.98 179.24	192.55-207.11 10.30	176.46-423.78 121.97	93.28-195.21 38.91	132.34-149.89 12.41	224.07	36.66-77.37 16.02
Rb	"bdl"	"bdl"	"bdl"	"bdl"	"bdl"	"bdl"	"bdl"	"bdl"	"bdl"-0.44
Sr	"bdl"-0.01	"bdl"	"bdl"	0.01-0.02 0.01	"bdl"-0.05	"bdl"-0.07	"bdl"	"bdl"	"bdl"-0.06
Y	"bdl"-0.01	"bdl"	"bdl"	"bdl"	"bdl"-0.07	"bdl"-0.03	"bdl"	"bdl"	"bdl"-0.01
Zr	"bdl"-0.01	"bdl"	"bdl"	"bdl"-0.06	0.08-3.13 1.32	"bdl"-0.34	"bdl"	"bdl"	"bdl"-0.03
Nb	"bdl"-1.47	"bdl"	"bdl"	0.05-2.44 1.69	0.79-327.60 136.62	"bdl"-0.82	"bdl"-0.07	"bdl"	"bdl"-0.03
Mo	"bdl"-0.08	"bdl"	"bdl"	"bdl"	"bdl"	"bdl"-0.29	"bdl"	"bdl"	"bdl"-0.08
Cs	"bdl"-0.02	"bdl"	"bdl"	"bdl"	"bdl"-0.20	"bdl"-0.04	"bdl"	"bdl"	"bdl"
Ba	"bdl"-0.04	"bdl"	"bdl"	"bdl"-0.03	"bdl"	"bdl"-0.99	"bdl"	"bdl"	"bdl"-0.05
Ta	0.02-7.15 3.01	"bdl"	"bdl"	0.21-10.44 7.23	6.62-1100.13 481.97	"bdl"-2.37	"bdl"-0.01	"bdl"-0.01	"bdl"-0.02
W	"bdl"-0.01	"bdl"	"bdl"	"bdl"	"bdl"-2.37	"bdl"-0.18	"bdl"-0.02	"bdl"	"bdl"-0.12
Pb	0.02-0.07 0.02	"bdl"	"bdl"	0.04-0.08 0.02	0.02-3.49 1.72	"bdl"-0.64	"bdl"-0.04	"bdl"-0.05	0.04-0.12 0.03
Bi	"bdl"-0.03	"bdl"	"bdl"	"bdl"	"bdl"	"bdl"-0.07	"bdl"-0.01	"bdl"	"bdl"

Table 4.3: Chemical composition of the samples by LA-ICP-MS analyses in ppm (be continued).

Element	Unk-NVN (2)	Quy Chau (3)	Trapiche-NVN (2)	Nosibe(4)	Antsirabe (3)	Andapa (2)	Tansania (5)	Ballapana (5)
Li	0.13-0.37 0.17	"bdl"-0.06	0.24-0.36 0.08	"bdl"-0.10	"bdl"-1.51	bdl	"bdl"	0.15-5.53 2.19
Be	0.07-0.36 0.20	"bdl"	"bdl"-0.11	"bdl"-0.08	0.07-8.34 4.55	"bdl"	0.08-1.00 0.39	0.06-0.13 0.03
Na	6.34-13.43 5.01	"bdl"-6.73	9.36-45.08 25.25	"bdl"-121.33	5.10-527.05 281.88	"bdl"-3.61	3.02-9.46 2.49	5.37-12.60 2.70
Mg	63.33-261.48 140.12	2.89-4.62 1.22	47.39-50.66 2.31	3.58-10.24 2.91	1.03-22.87 10.94	"bdl"-12.72	19.69-34.78 6.95	25.22-64.35 15.22
Si	939.36-1832.99 631.89	713.22-733.94 14.65	748.51-1027.38 197.19	657.03-699.48 23.68	684.59-2260.81 845.64	719.26-741.96 16.05	545.80-683.59 57.20	788.90-1896.27 509.67
P	12.20-16.05 2.72	12.79-15.77 2.11	12.97-34.27 15.06	12.07-16.50 1.99	13.86-20.60 3.43	12.81-15.85 2.15	11.49-16.88 2.26	12.61-15.43 1.09
K	115.46-143.49 19.82	"bdl"-1.90	"bdl"-5.20	"bdl"	3.66-357.63 195.80	Bld	"bdl"-38.07	5.67-18.36 5.54
Ca	18.22-33.55 10.84	15.82-27.00 7.91	11.86-23.88 8.50	"bdl"-17.79	"bdl"-511.90	"bdl"-16.05	"bdl"-15.18	9.11-23.37 6.46
Sc	0.08-0.17 0.07	"bdl"-0.14	"bdl"-0.40	"bdl"-0.11	0.07-0.11 0.02	"bld"	"bdl"-0.09	0.12-0.17 0.02
Ti	172.38-714.04 383.01	108.63-147.91	677.10-760.84 59.21	37.08-169.29 63.43	155.74-860.05 370.70	35.26-52.18 11.96	22.55-35.51 5.37	16.81-48.62 13.19
V	37.15-38.29 0.81	27.78 1.80	5.91-6.57 0.46	10.28-27.68 8.34	2.94-13.20 5.14	5.73-6.17 0.31	12.71-17.08 1.74	10.49-14.83 1.92
Cr	1.36-2.08 0.51	70.46-74.16 2.62	18.57-68.37 35.21	1.00-1.76 0.31	1.40-1.52 0.07	"bdl"-4.72	49.87-123.98 28.08	4.84-8.16 1.19
Mn	"bdl"-2.73	"bdl"-1.55	0.13-0.29 0.11	0.35-0.57 0.09	0.53-41.51 23.15	0.37-0.41 0.03	0.20-1.16 0.41	0.38-1.94 0.64
Co	0.04-0.15 0.08	"bdl"	"bdl"-0.27	"bdl"-0.17	"bdl"-0.07	"bdl"-0.04	"bdl"-0.06	0.02-0.18 0.06

Table 4.3: Chemical composition of the samples by LA-ICP-MS analyses in ppm (be continued).

Element	Unk.-NVN (2)	Quy Chau (3)	Trapiche-NVN (2)	Nosibe(4)	Antsirabe (3)	Andapa (4)	Tansania (5)	Ballapana (5)
Ni	0.47-0.82 0.25	"bdl"-0.21	0.26-1.11 0.60	"bdl"-0.16	"bdl"-0.13	"bdl"	"bdl"-0.26	0.09-0.32 0.08
Zn	1.30-39.69 27.15	0.24-1.00 0.54	2.16-7.98 4.11	2.47-6.66 1.84	2.15-7.62 2.91	"bdl"-1.53	1.54-5.60 1.45	1.42-16.03 6.00
Ga	73.86-85.68 8.36	29.28-33.86 3.24	50.20-52.45 1.59	298.07-416.02 53.21	216.91-455.79 120.15	203.05-219.69 11.77	41.27-62.90 8.90	161.68-180.47 7.37
Rb	0.91-1.24 0.23	"bdl"	"bdl"	"bdl"-0.05	"bdl"-2.07	bld	"bdl"-0.56	"bdl"-0.27
Sr	0.30-0.35 0.03	"bdl"-0.05	0.42-0.46 0.03	"bdl"-0.02	0.01-4.01 2.31	"bdl"	0.01-0.37 0.15	0.01-0.09 0.03
Y	0.01-0.05 0.03	"bdl"-0.11	0.03-0.06 0.02	"bdl"-0.01	"bdl"-0.06	"bdl"-0.01	"bdl"-0.02	0.09-0.56 0.19
Zr	0.02-2.15 1.51	"bdl"-0.01	"bdl"-0.06	"bdl"-0.02	"bdl"-0.33	"bdl"-0.01	"bdl"-0.62	0.03-0.06 0.01
Nb	0.01-4.17 2.94	0.00-0.04 0.03	0.01-0.11 0.07	"bdl"-0.06	0.01-320.70 181.04	"bdl"-0.08	"bdl"-0.01	0.15-1.30 0.45
Mo	"bdl"-0.04	"bdl"-0.03	"bdl"-0.15	"bdl"-0.07	"bdl"-4.09	bld	"bdl"-0.18	"bdl"-0.05
Cs	0.26-0.36 0.07	"bdl"-0.04	"bdl"	"bdl"-3.73	"bdl"-0.02	bld	"bdl"-0.56	"bdl"-0.04
Ba	0.93-5.02 2.89	0.04-0.07 0.02	0.07-0.63 0.39	"bdl"-0.06	0.06-3.08 1.71	bld	"bdl"-10.01	0.11-2.02 0.70
Ta	0.44-4.25 2.70	0.03-1.16 0.79	0.06-0.67 0.43	"bdl"-0.21	0.02-62.33 31.89	"bdl"-0.02	"bdl"-0.01	"bdl"-0.01
W	0.03-1.32 0.91	"bdl"-0.02	"bdl"-0.04	"bdl"-0.03	"bdl"-0.31	bld	"bdl"-0.74	0.02-0.05 0.01
Pb	0.05-1.40 0.96	"bdl"-0.52	0.16-2.41 1.59	0.02-0.16 0.06	0.05-0.60 0.30	"bdl"-0.04	0.05-0.21	0.12-4.29 1.71
Bi	"bdl"-0.02	"bdl"-0.01	0.02-0.15 0.09	"bdl"	0.02-0.13 0.06	bld	"bdl"-0.40	"bdl"-0.01
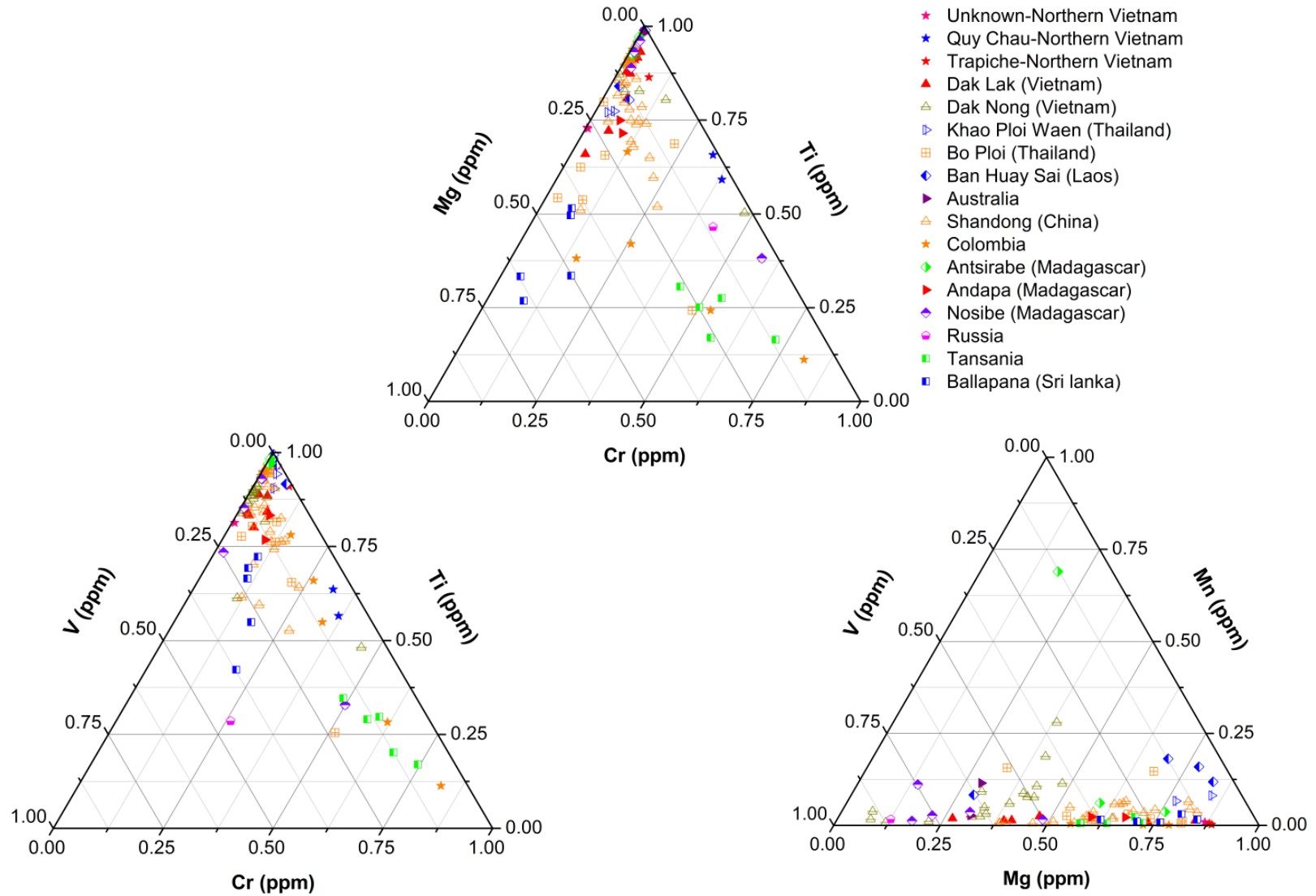
Figure 4.3.1: Ternary diagram shows percentages of important trace elements.

Chapter 5: Raman Spectroscopy of Sapphire and the Influence of the Fe_2O_3 Content on the Spectra

5.1. Overview on Raman spectroscopy of corundum

Raman spectra of corundum were first studied by Hibben (1932) using the excitation wavelength of 435.8 nm of Hg. This experiment showed the existence of four Raman lines at 536, 728, 931 and 1191 cm^{-1}. However, this result was contradictory to those of later research. Deutschbein (1932b) detected only one single Raman line at 415 cm^{-1} with the radiation of the two lines of a mercury arc, at 404.6 and 435.8 nm. Also with these Hg sources, Mani (1942) collected the Raman spectra of corundum with two lines, one peak at 415 cm^{-1} and an additional peak at 376 cm^{-1}.

Based on group theoretical analysis, Bhagavantam and Venkatarayudu (1939) expected seven Raman active frequencies. After that, these active modes ($2A_{1g}+5E_g$) have been observed by Krishnan (1947) and Porto and Krishnan (1967). The work of Krishnan (1947) presented that the Raman spectra of corundum exhibited seven vibration modes. These are at 375, 417, 432, 450, 578, 642 and 751 cm^{-1} in which the 450, 578 and 751 cm^{-1} vibrations are polarized. Porto and Krishnan (1967) reported seven Raman active phonon modes at 378, 418, 432, 451, 578, 645, and 751 cm^{-1} of corundum in different orientations. Ashkin et al. (1968) studied the Raman spectra of corundum at different temperatures in which corundum showed seven lines at 378 (±5), 416.7, 429.4, 448.1, 677.1, 644.8 and 746.6 cm^{-1} at 300 K.

Xu et al. (1995) reported seven corundum Raman modes at atmospheric pressure, centered at 377.9, 416.6, 429.5, 451.2, 575.9, 644.4, and 749.9 cm^{-1}. Kadleikova et al. (2001) also reported seven Raman frequencies of the mineral at 376, 414, 428, 440, 573, 642 and 748 cm^{-1} as shown in Figure 5.1.1 and two more frequencies at 176.3 and 724.6 cm^{-1} at a distance of 1 cm from the center of the sample. Munisso et al. (2009) investigated sapphire single crystals at different crystallographic planes and detected seven vibration bands centered at about 378, 418, 432, 451, 578, 645, and 751 cm^{-1}. The Raman peak positions of corundum in the literature are summarized in Table 5.1.1.
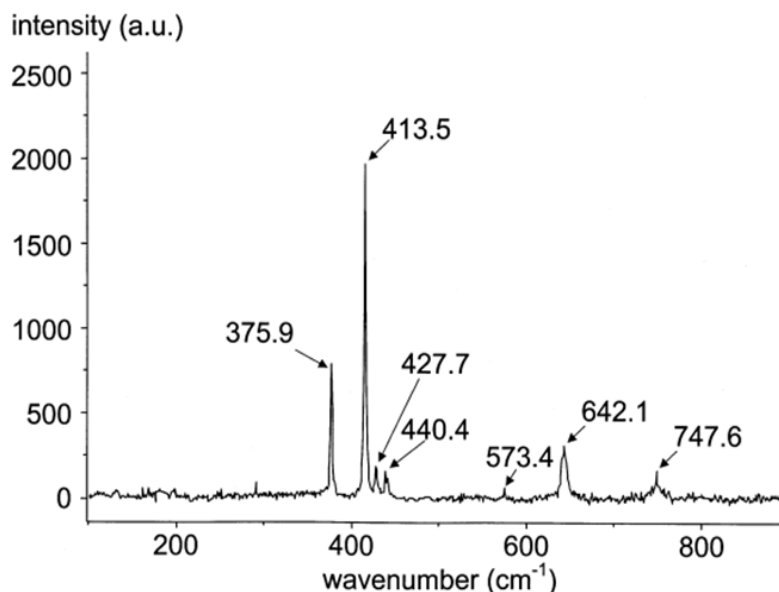
Figure 5.1.1: Raman spectra was collected from the center of a synthetic sapphire at room temperature (Kadleikova et al. 2001).

In this study, the Raman spectra of all samples were collected by using a LabRam con-focal micro-Raman-system HR-800 coupled to an Olympus-BX41 microscope from Horiba Jobin Yvon. The laser source used was a frequency-doubled Nd-YAG laser with an excitation wavelength of 532.21 nm. The Raman-spectrometer was calibrated by using the 520.7 cm^{-1} peak (Kuebler et al. 2006, Frost et al. 2011) of a silicon wafer. The measurements were recorded with the program LabSpec v.4.02 of Horiba Jobin Yvon company in the spectral range from 120 cm^{-1} to 1200 cm^{-1} with 20 seconds exposure time, 2 accumulation scans, a 400 μm con-focal pinhole, 100 μm slit width, 50x magnification, and a grating with 1800 grooves/mm at room temperature.

Table 5.1.1: The Raman peak positions (cm^{-1}) of corundum according to the literature and in this study (the Fe_2O_3 content is "bdl" by EPMA, <0.01 wt% Fe_2O_3).

	$\bar{v}$ (cm^{-1})								
Hibben (1932)						536			728	
Deutschbein (1932)			415							
Bhagavantam, Venkatarayudu (1939)	Seven bands by the group theoretic analysis									
Mani (1942)		376	412							
Krishnan (1947)		375	417	432	450		578	642		751
Porto, Krishnan (1967)		378	418	432	451		578	645		751
Ashkin et al. (1968)		378(±5)	416.7	429.4	448.1		577.1	644.8		746.6
Xu et al. (1968)		377.9	416.6	429.5	451.2		575.9	644.4		749.9
Kadleikova et al. (2001)	176.3	376	414	428	440		573	642	724.6	748
Munisso et al. (2009)		378	418	432	451		578	645		751
This study (<0.01 wt% Fe_2O_3)		379.8	418.3	431.7	446.6		577.7	644.4		750.4

Figure 5.1.2 and Figure 5.1.3 introduce the Raman spectra of a sapphire sample from the north of Vietnam with the Fe_2O_3 content below the detection limit of the EPMA measurements ("bdl", <0.01 wt% Fe_2O_3) with the electric vector E perpendicular and parallel to the c-axis of the sapphire crystal ($E{\perp}c$ and $E//c$). Its Raman spectra have seven peaks similar to the literature given in Table 1 and the peak position values are listed in the Figure 5.1.2 and Figure 5.1.3. In the case of $E{\perp}c$, seven peaks were observed at 379.8, 418.3, 431.7, 446.6, 577.7, 644.4 and 750.4 cm^{-1}. In the case of $E//c$, four Raman peaks at 379.9, 418.3, 431.2, and 644.7 cm^{-1} were observed.
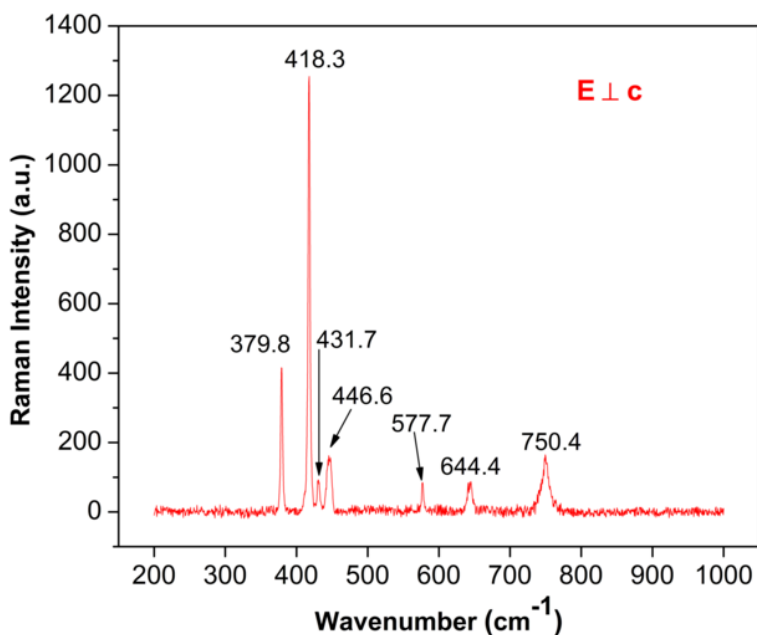
Figure 5.1.2: Raman spectra of a sapphire sample from the north of Vietnam, E⊥c.
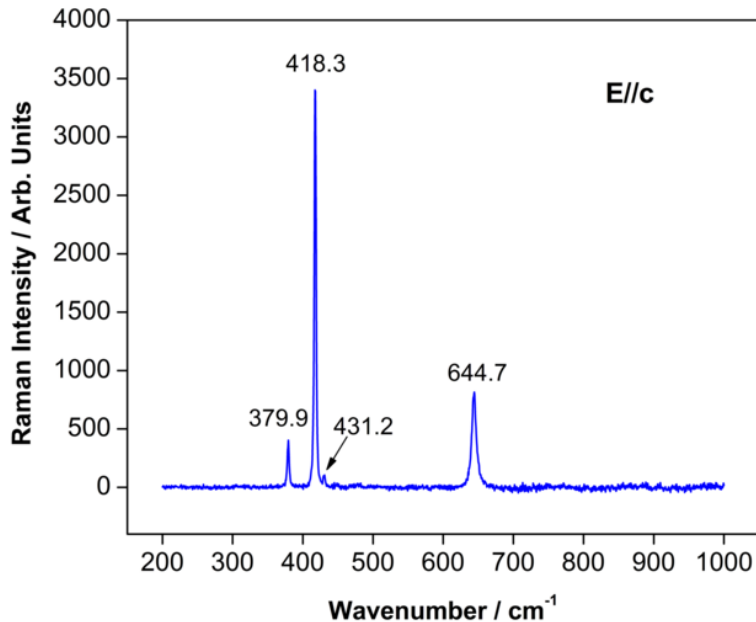
Figure 5.1.3: Raman spectra of a sapphire sample from the north of Vietnam, E//c.

The 418.3 cm^{-1} peak is the strongest peak in both case of $E \perp c$ and $E//c$. Four peaks at 431.7, 446.6, 577.7 and 750.4 cm^{-1} are commonly observed with a relative weak intensity in case of $E \perp c$ and rarely recognized in the case of $E//c$. The peak at 644.7 cm^{-1} is strong in the case of $E//$c, but weak or nearly disappears in the case of $E \perp c$ (644.4 cm^{-1}). These Raman spectra characteristics of this sample are similar to almost all of the others.

Figure 5.1.4 shows the Raman spectra of the samples from some areas. As seen in this figure, the Raman spectra of the sample from Dak Nong or Shandong show additional bands to the seven characteristic peaks. These are two broad bands at about 165-190 cm^{-1} and 230-250 cm^{-1} and two weak peaks at around 475 and 706 cm^{-1}.

These additional bands are assumed to be derived from micro inclusions like hematite or ilmenite which were presented as internal features of sapphires in Chapter 3.
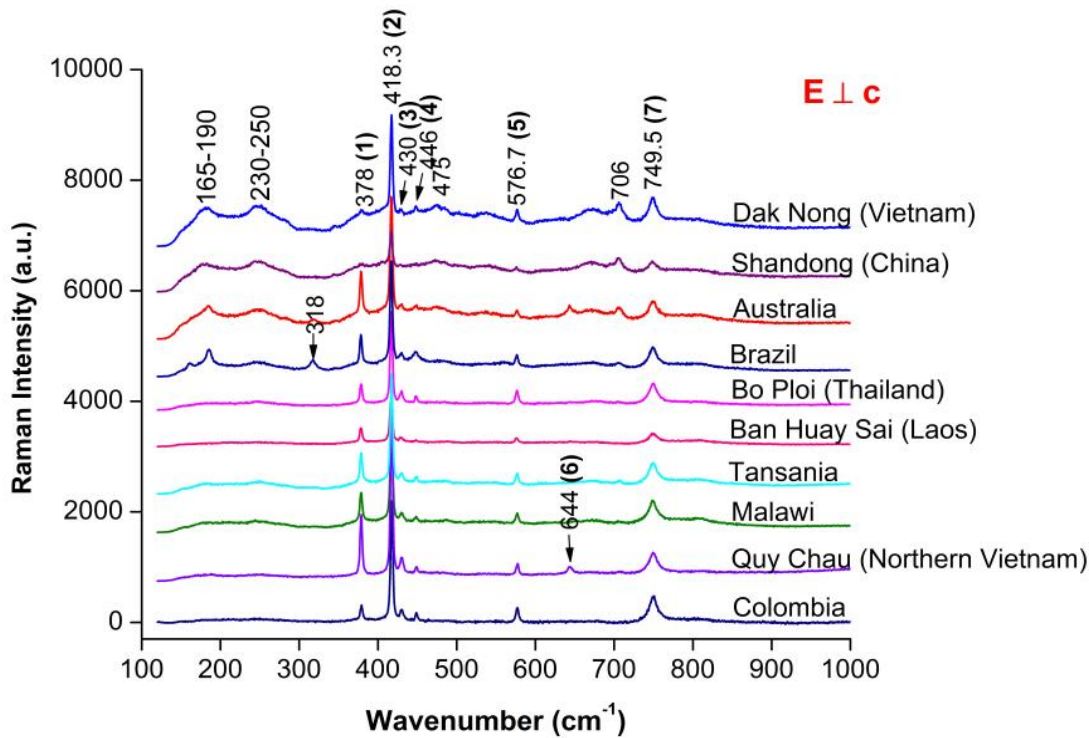
Figure 5.1.4: The Raman spectra of some areas: Dak Nong, Shandong, Australia, Brazil, Bo Ploi, Ban Huay Sai, Tansania, Malawi, Quy Chau and Colombia.

5.2. Relationship between Raman spectra and the Fe_2O_3 content of sapphire

During the last decades, many works conducted investigations on the characteristics of Raman spectra of corundum under certain conditions, such as at high pressure or temperature (Mani 1942) or in different crystal orientations (Xu et al. 1995). However, a correlation between the Raman spectra and chemical elements, such as iron in basaltic corundum has not published yet.

Chemical analyses and Raman spectra measurements presented that the varying of Fe_2O_3 contents in the samples causes the difference of Raman peak positions. The higher Fe_2O_3 content is the smaller wavenumber of the Raman peaks shifts. Figure 5.2.1 shows the Raman spectra with $E \perp c$ of five selected samples with the increasing Fe_2O_3 content: "bdl", 0.40, 0.82, 1.26 and 1.81 wt% Fe_2O_3. A close view shows the Raman shift of the 418.3 cm^{-1} and 577.7 cm^{-1} peak towards smaller wavenumber, 417.1 cm^{-1} and 576.6 cm^{-1} respectively, when the Fe_2O_3 contents increase.
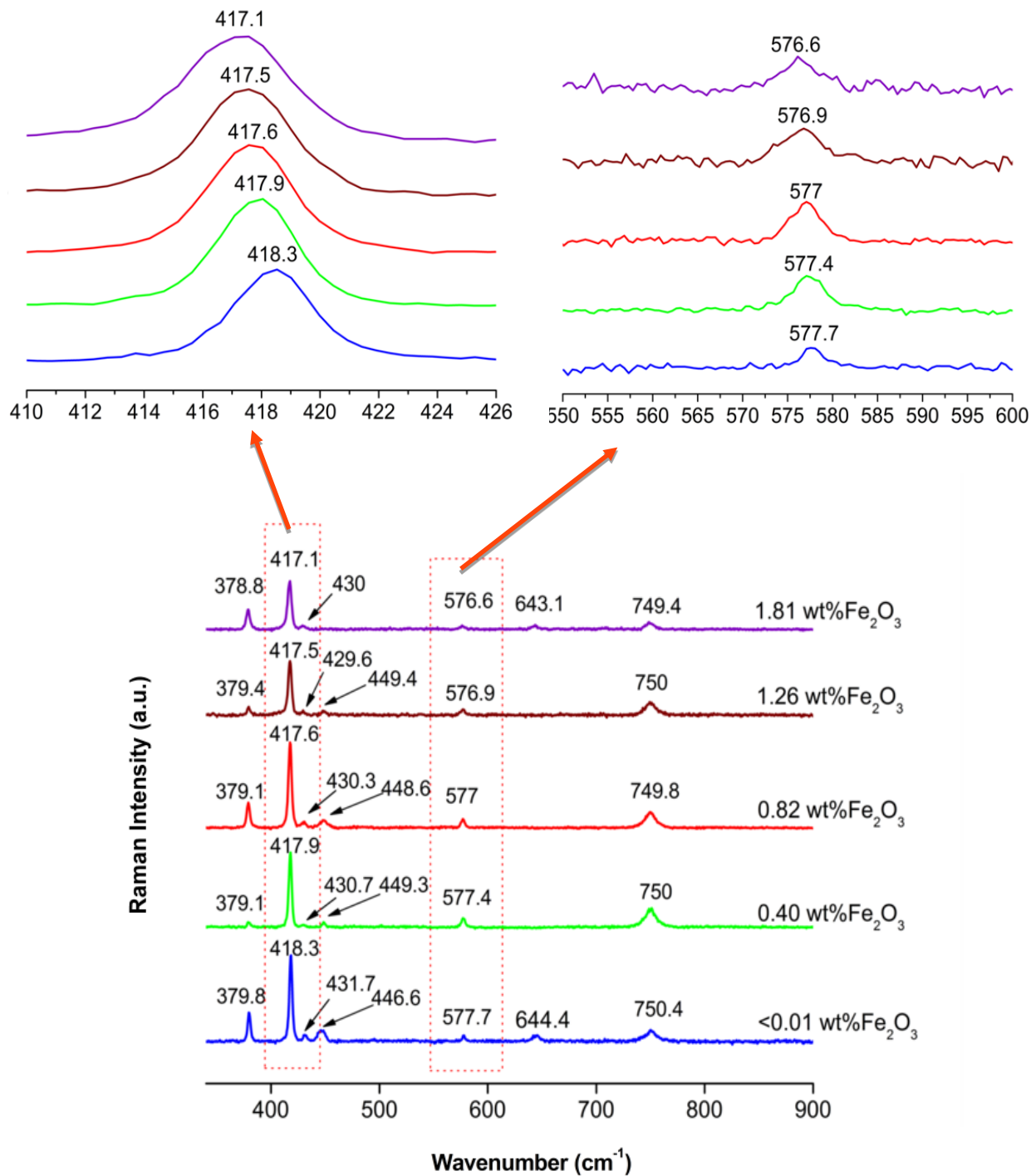
Figure 5.2.1: The Raman spectra of five different samples with increasing Fe₂O₃ contents: "bdl", 0.40, 0.82, 1.26 and 1.81 wt.% Fe₂O₃ showing the shift of the 418.3 cm⁻¹ and 578 cm⁻¹ (E⊥c).

This correlation can be observed with only these two peaks. An explanation is applied for the Raman spectra given in Figure 5.1.2 and Figure 5.1.3. The peak 418.3 cm^{-1} is strongest and sharp, and is easily to get the peak parameters with the Voigt fit functions. The peak 577.7 cm^{-1} has low intensity but it is sharp, standing free and not affected by the others. For the measurements performed with $E \perp c$, the peak 644.4 cm^{-1} is rarely observed because of this strong polarized peak, therefore this peak is not considered in this correlation. The peak at 379.8, 431.7 and 446.6 cm^{-1} often appears with quite low intensity and are also not considered in this relationship. Besides, the peak at 379.8 cm^{-1} is affected by the additional peaks when the sample contains iron micro inclusions of ilmenite or hematite or contains a high iron amount. The peak 750.4 cm^{-1} is broad band and also often affected by the additional peaks with the same above reason.

Figure 5.2.2 and Figure 5.2.3, the Raman peak position of two peaks changing around 418.3 cm^{-1} and 577.7 cm^{-1} are plotted according to the Fe_2O_3 contents. As illustrated, the Raman peak position of these two peaks shift towards smaller wavenumbers corresponding to the increasing of the Fe_2O_3 contents.
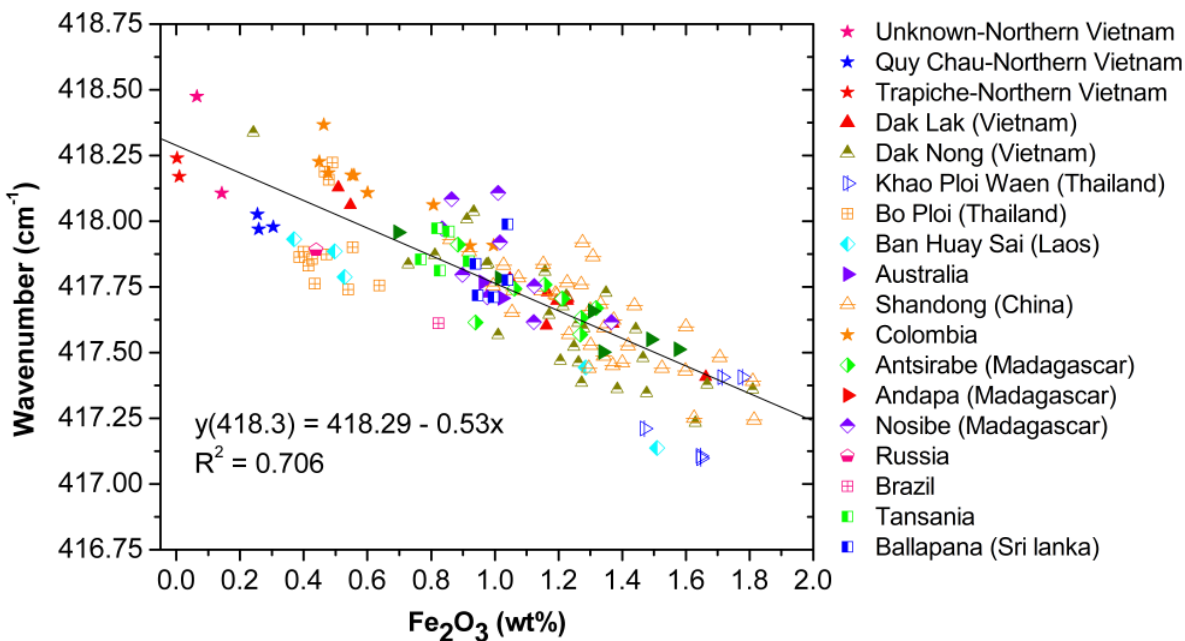
Figure 5.2.2: The Raman peak positions of the peak around 418.3 cm^{-1} shift towards smaller wavenumbers with increasing Fe$_2$O$_3$ contents (wt.%).
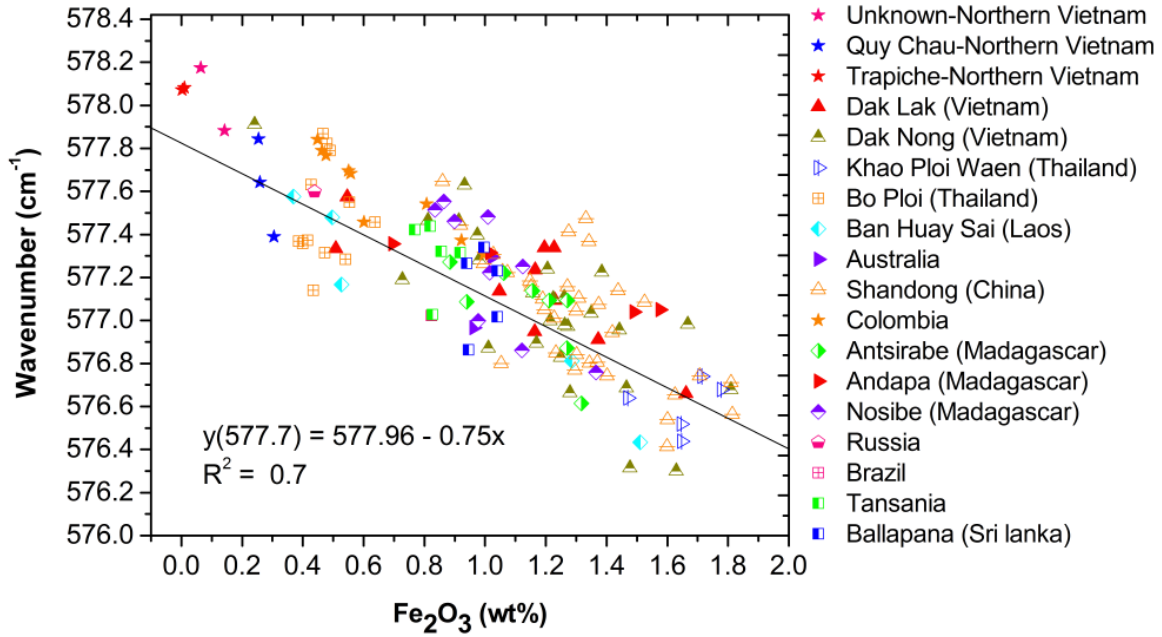
Figure 5.2.3: The Raman peak positions of the peak around 577.7 cm^{-1} shift towards smaller wavenumbers with increasing Fe_2O_3 contents (wt.%).

The scattering of the data points in the two figures could be due to the spectral resolution of approximately 0.5 cm^{-1}, the standard deviation of the chemical analyses, and a small difference between the measured spatial positions of the Raman and EPMA measurements.

The shift of the Raman peak position around 418.3 cm^{-1} and 577.7 cm^{-1} could be explained by the larger ionic radius of Fe^{3+} in comparison to Al^{3+} ($r_{Fe^{3+}} = 0.645$ Å and $r_{Al^{3+}} = 0.535$ Å in an octahedral site, Shannon (1976)) and the electrostatic energy which based on the Coulomb interaction (Crowell 1998, Newman 2008) between two charges given by the formula:

$$E = k \frac{Q_1 Q_2}{r_{1-2}} \qquad (5.1)$$

where k is the Coulomb's constant $k = \frac{1}{4\pi\varepsilon_o} = 8.99 \times 10^9$ Nm^2/C^2 ,

$\varepsilon_o = 8.85 \times 10^{-12} C^2/Nm^2$ is the permittivity of the free space, $Q_1 = z_1 q_e$ is the charge quantities on the charge 1 (in Coulomb), $Q_2 = z_2 q_e$ is the charge quantity on the charge 2 (in

Coulomb), z_1 and z_2 are the quantity of electron in the outermost energy level of the charge 1 and 2, $q_e = 1.602 \: x \: 10^{-19} C$ is the charge of electron, r_{1-2} is the distant between the two charges (in meters). The unit of the electrostatic energy is Nm or Joule (1Nm=1J).

The Q_1 and Q_2 can be positive or negative, therefore E is attractive if both are same charge and is repulsive if both are different charge. However, in mathematical concept they can be used without "+" and "-" signs. The Coulomb's law is an inverse-square law, E decreases with increasing the distance. The larger the magnitude of E, the stronger the ionic bond. Figure 5.2.4 describes the electrostatic energy between two charges and the law of E and r_{1-2}.
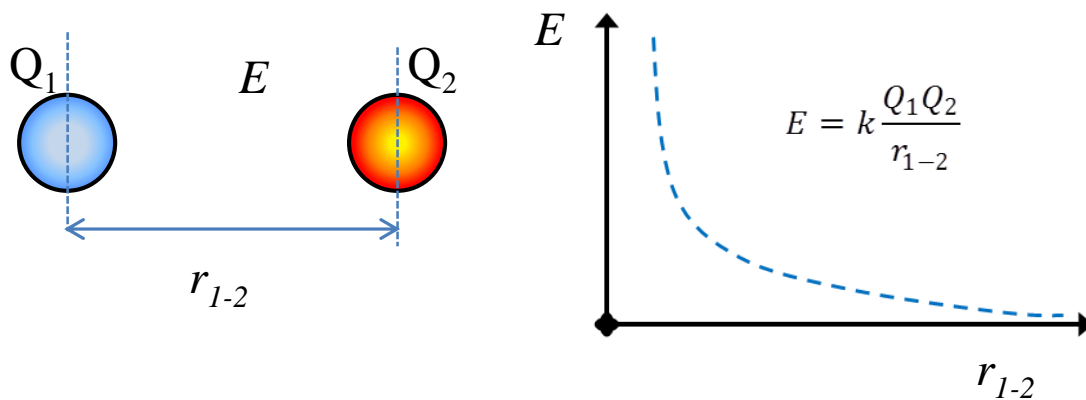
Figure 5.2.4: The electrostatic force or Coulomb interaction between two charges.

In the case of Al_2O_3 or Fe_2O_3, the nature of electrostatic forces of Al^{3+} and O^{2-} or Fe^{3+} and O^{2-} are attractive. The ionic radius of Al^{3+}, Fe^{3+} and O^{2-} ions and the according distances is described in Figure 5. 2.5.
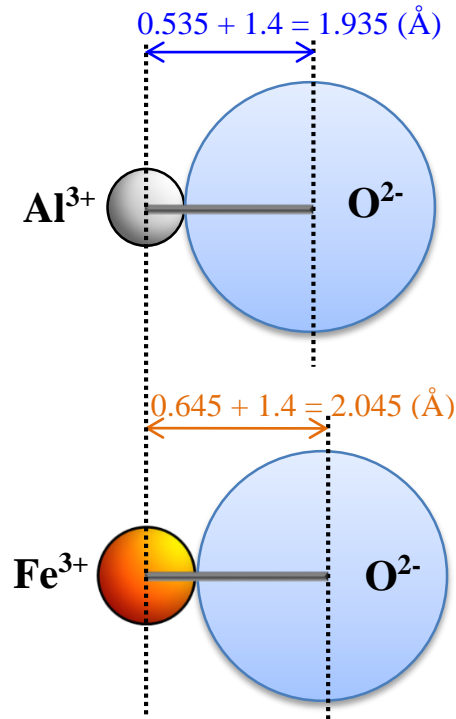
Figure 5.2.5: The ionic radius of Al^{3+}, Fe^{3+} and O^{2-} ions and the according distances. The silver ball: Al^{3+}, the orange ball: Fe^{3+}, the light blue: O^{2-}.

The electrostatic energy E for one Al-O and Fe-O bond are calculated according to the Coulomb interaction.

For one Al-O bond:

$$E_{Al-O} = k\frac{Q_1 Q_2}{r_{Al-O}} = 8.99 \times 10^9 \frac{(3\times 2)(10^{-19})^2}{(0.535+1.4)\times 10^{-10}} = 7.1541 \times 10^{-18} \text{ J} \qquad (5.2)$$

For one Fe-O bond:

$$E_{Fe-O} = k\frac{Q_1 Q_2}{r_{Fe-O}} = 8.99 \times 10^9 \frac{(3\times 2)(10^{-19})^2}{(0.645+1.4)\times 10^{-10}} = 6.7693 \times 10^{-18} \text{ J} \qquad (5.3)$$

As a result, the electrostatic energy of the ionic bond of Fe-O in the octahedral sites is weaker than that of Al-O. Hence, the electrostatic energy of the lattice energy of one mole Al_2O_3 or Fe_2O_3 is given by multiplied with the Avogadro's number N_A. The N_A is the number of atoms or molecules

contained in one mole of substance and $N_A = 6.022 \times 10^{23}$ mol^{-1} (Feynman et al. 1964, Jensen 2010).

Therefore:

$$E_{latt(Al-O)} = E_{Al-O}N_A = (7.1522 \times 10^{-18}) \times (6.022 \times 10^{23}) = 4308.199 \; kJ/mol \qquad (5.4)$$

$$E_{latt(Fe-O)} = E_{Fe-O}N_A = (6.7674 \times 10^{-18}) \times (6.022 \times 10^{23}) = 4076.462 \; kJ/mol \qquad (5.5)$$

As a result, when Fe^{3+} ions substitute Al^{3+} ions in the lattice of α-Al_2O_3, the vibration lattice energy for the Fe-O bond is weaker than that for Al-O bond by an amount of $4308.199 - 4076.462 = 231.737 \; (kJ/mol)$. The lattice vibrates with smaller energy; hence the according Raman spectra occur with the smaller wavenumber. The much more the Fe_2O_3 content in the α-Al_2O_3, the smaller the according Raman spectra.

The observation also show that the full-widths at half-maximums (FWHMs) of the peak around 418.3 cm^{-1} increases corresponding to the decreasing of the wavenumbers as shown in Figure 5.2.6 and therefore this peak increases with the increasing Fe_2O_3 content. However, a correlation between the FWHMs of the peak around 577.7 cm^{-1} cannot be recognized.
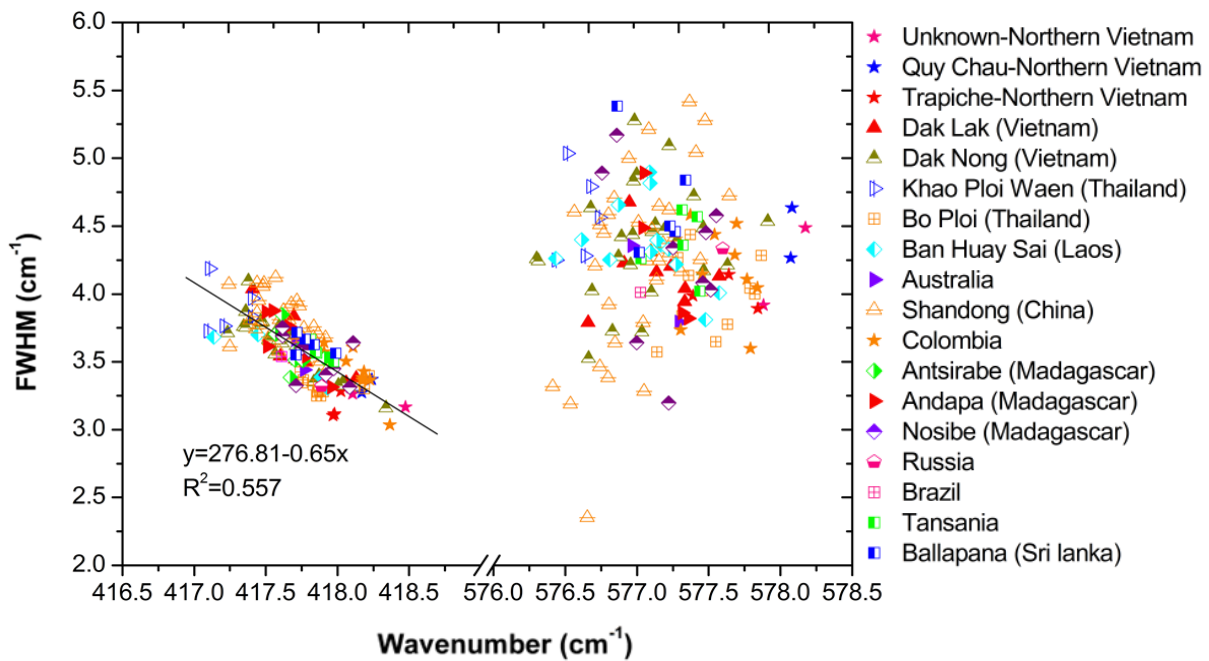
Figure 5.2.6: The correlation between the Raman peak positions and the FWHMs of the two peaks at around 418.3 cm^{-1} and 577.7 cm^{-1}.

The correlation between the Raman peaks and the Fe_2O_3 content give applications by using the two equations $y(418.3) = 418.29 - 0.53x$ and $y(577.7) = 577.96 - 0.75x$. The Fe_2O_3 contents of the sapphire or corundum sample can be easily estimated (is the x factor in these two equations) after collecting the Raman spectra and determining the values $y(418.3)$ and $y(577.7)$ of the peaks around 418.3 cm^{-1} and 577.7 cm^{-1} with the fit functions. This contribution also helps to distinguish sapphires from different origins, for example basaltic from metamorphic origin. Basaltic sapphire has high Fe_2O_3 contents, whereas metamorphic originated sapphire has low Fe_2O_3 contents (Sutherland et al. 1998, Sutherland and Schwarz 2001). Therefore, if the Raman peak position of these two peaks tends to the smaller wavenumbers, the sapphire is basaltic type, in contrary it is metamorphic type. An additional influence on the peak positions of the Raman spectra could occur for the samples which contain other prominent trace elements with a larger ionic radius, such as Cr^{3+}, $Cr^{3+} + Fe^{3+}$ or $Fe^{2+} + Ti^{4+}$.

Chapter 6: Luminescence Spectroscopy of Sapphire and the Influence of Fe_2O_3 Content

6.1. Luminescence spectroscopy of corundum in general

If corundum contains chromium in a certain amount, it becomes rose to red, depending on the chromium content. Most of the natural corundum may contain a very low chromium amount. The red luminescence of corundum is caused by the transition of the ^2E (excited state) to $^4A_2$ (ground state) of the Cr^{3+} (Deutschbein 1932, Krishnan 1947, Pringsheim 1949, Porto and Krishnan 1967). Due to the trigonal distortion and the spin-orbit coupling (Nelson and Sturge 1965, Milos et al. 2008), this transition is split into two levels and leads to two luminescence lines, the so-called R_2 (about 692.8 nm) and R_1 (about 694.2 nm) lines as given in Figure 6.1.1 and 6.1.2.
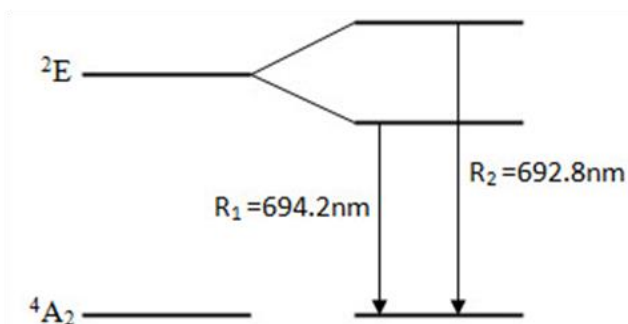
Figure 6.1.1: Two luminescence lines R_1 and R_2 due to the splitting into two level of the ^2E-level (Nelson and Sturge 1965).

Since the intensity of luminescence is affected by the orientation of the crystal (He and Clarke 1997, Häger and Dung 2000, 2003), all the samples in this study were measured with the electric vector E of the laser beam perpendicular to the c-axis of the sapphire crystal. A typical Cr^{3+} induced luminescence spectra of a sample from Colombia (247 ppm Cr by LA-ICP-MS and 0.015 wt.% Cr_2O_3 by EMPA) at room temperature is shown in Figure 6.1.2. The luminescence spectra were fitted with Voigt functions after subtracting a linear background. The luminescence spectra of this

sample are strong and sharp with two R lines: R_1=694.3 nm and R_2=692.8 nm. In Figure 6.1.2, the red discrete points represent the experimental data, the two grey lines represent the fitted R_1 and R_2 lines and the solid black line is the sum of the fitted R_1 and R_2 lines. Because of the low Cr^{3+} content (<0.01 wt.%) and the high intensity of the R lines, the n-lines at 701.6 nm and 704.3 nm which originate from the emission of Cr^{3+}-pairs (Powell et al. 1967, Häger and Dung 2000, 2003) and sidebands at 714.3 nm (Rothamel et al. 1983) cannot be observed in all of samples of this study. The luminescence spectra with n-lines and sidebands was observed from a synthetic ruby containing a high chromium amount, 0.622 mol % Cr_2O_3 (Häger and Dung 2000, 2003). In this study, the chromium content in all samples is low, and almost below the detection limit of the EMPA (<0.01 wt.%) and varying in a large range from 1.8 ppm to 247 ppm.
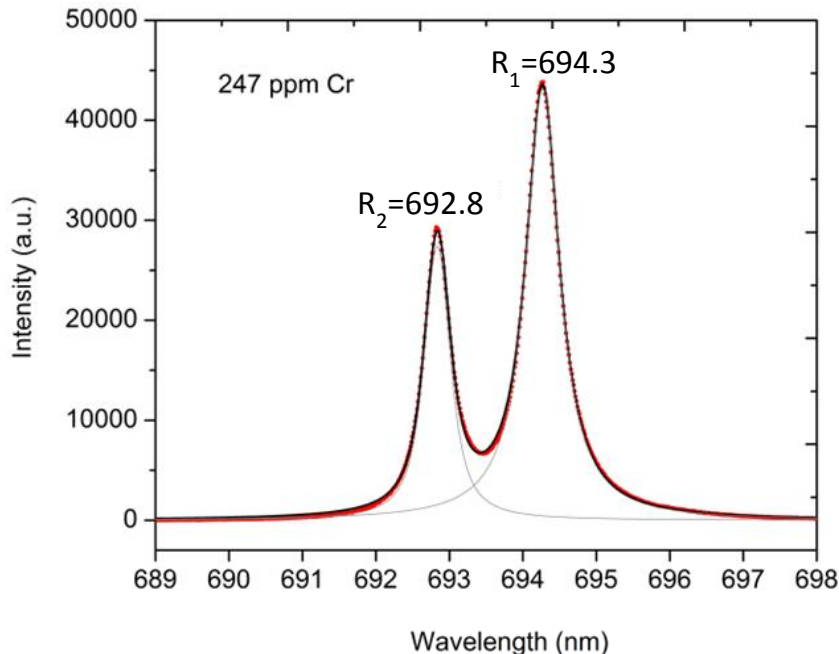
Figure 6.1.2: Typical luminescence spectra of a Cr^{3+}-containing sample from Colombia (E⊥c).

For this study, luminescence spectra of 150 sapphire samples were collected by confocal micro Raman spectroscopy, and the according chemistry were measured by LA-ICP-MS to determine the chromium content and with the EPMA the Fe_2O_3-content. The luminescence spectra were observed in almost all of the samples with strong intensity, except in the dark brown core and arm zones of trapiche type sapphires from Dak Nong (Vietnam) and Shandong (China). Although

chromium is major trace element causing the luminescence in corundum, the intensity of luminescence also depends on other factors like defect centers or it is affected by quenching, when corundum is rich in iron (Fritsch and Waychunas 1993, O'Donoghue 1997, Häger and Dung 2000, 2003, Nasdala et al. 2004).

Figure 6.1.3 shows nine luminescence spectra which were measured with the same acquisition condition, with the increasing of the luminescence intensity while the chromium content does not increase in the same way. This can be explained that the intensity of luminescence spectra depends not only on chromium but also on other effects like quenching by iron.
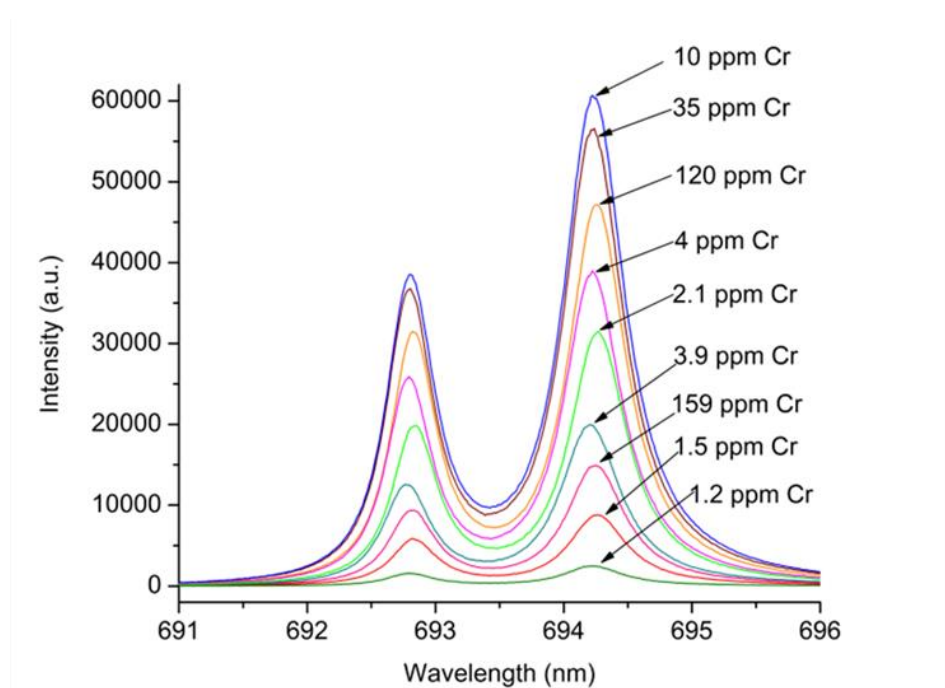
Figure 6.1.3: Luminescence spectra of nine samples with increasing intensities.

6.2. Effect of Fe_2O_3 content on the R-line position of sapphires

Similar to Raman spectra, the Fe_2O_3 content also influences the luminescence spectra of sapphires. When the Fe_2O_3 content increases, the peak position of the R lines shifts towards smaller wavelength.
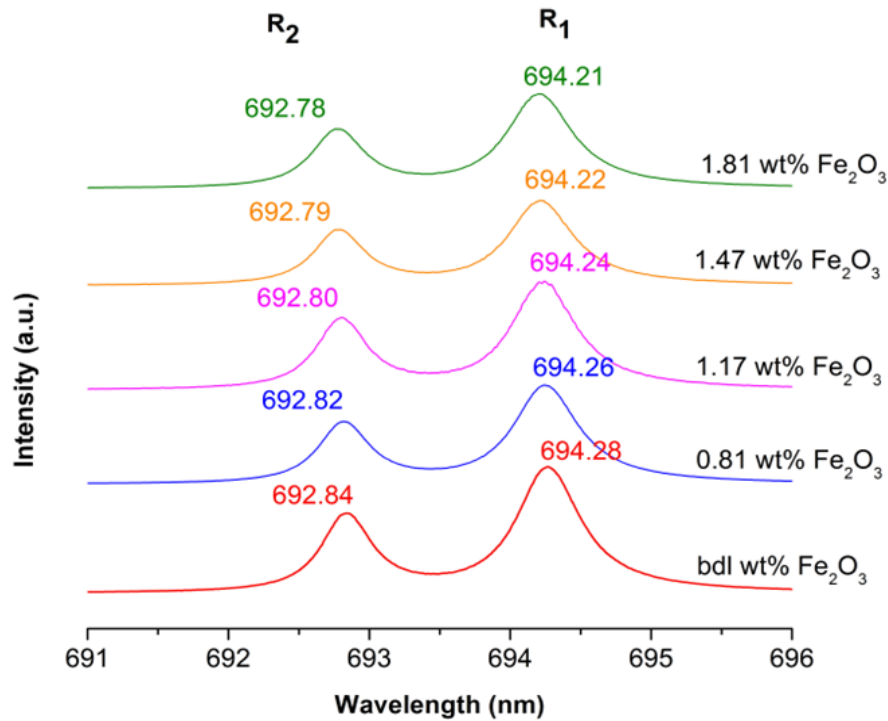
Figure 6.2.1: Luminescence spectra of five samples with the increasing iron content "bdl", 0.81, 1.17, 1.47 and 1.81 wt.% Fe_2O_3.

Figure 6.2.1 presents the luminescence spectra of five samples with the increasing iron content: "bdl" (<0.01 wt.% Fe_2O_3), 0.81, 1.17, 1.47 and 1.81 wt.% Fe_2O_3. The spectra show that the peak positions of the R line shift towards smaller wavelength when the Fe_2O_3 contents increase. This correlation is plotted in Figure 6.2.2 and Figure 6.2.3, and is expressed by the equations:

$$y(R_2) = 692.86 - 0.049x \qquad (6.1)$$

$$y(R_1) = 694.29 - 0.047x \qquad (6.2)$$

in which x is Fe_2O_3 content in wt.% and y is R line peak position (in nm). The scattering of the luminescence data points can be explained similar as Raman data points above, but with the spectral resolution of 0.01 nm. Two of these equations can be used to determine the Fe_2O_3 content in the sample with a quite good regression R^2, respectively 0.754 for R_2 and 0.748 for R_1. This can be performed quickly since luminescence spectra are sensitive with too low chromium content.
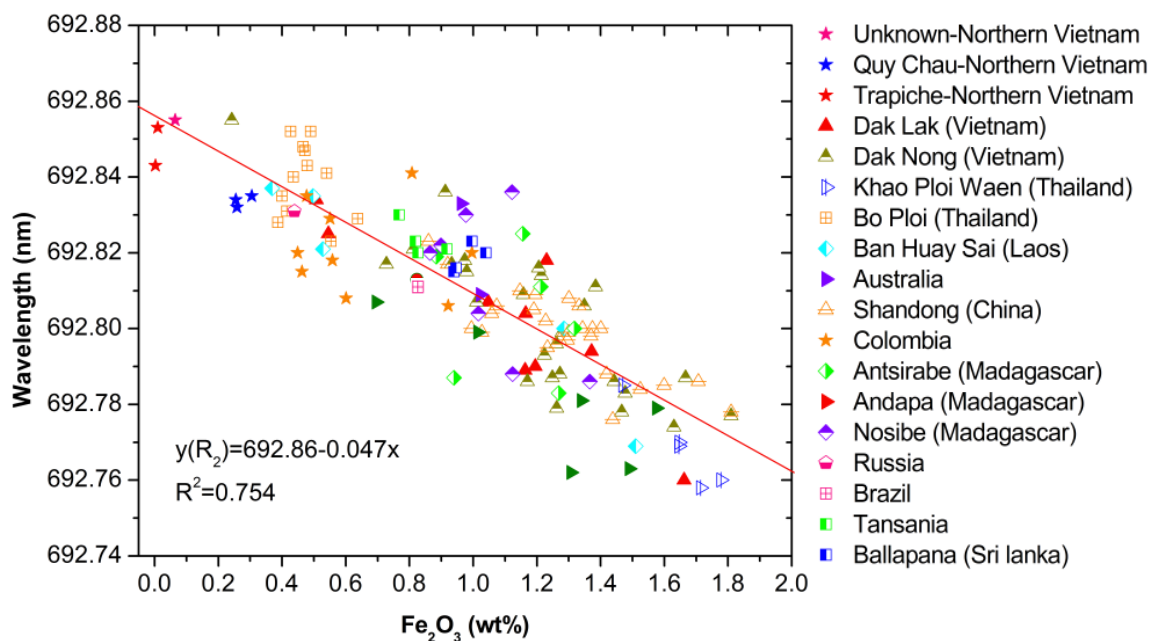
Figure 6.2.2: The shift of R₂ line around 692.84 nm corresponding to the Fe₂O₃ content.
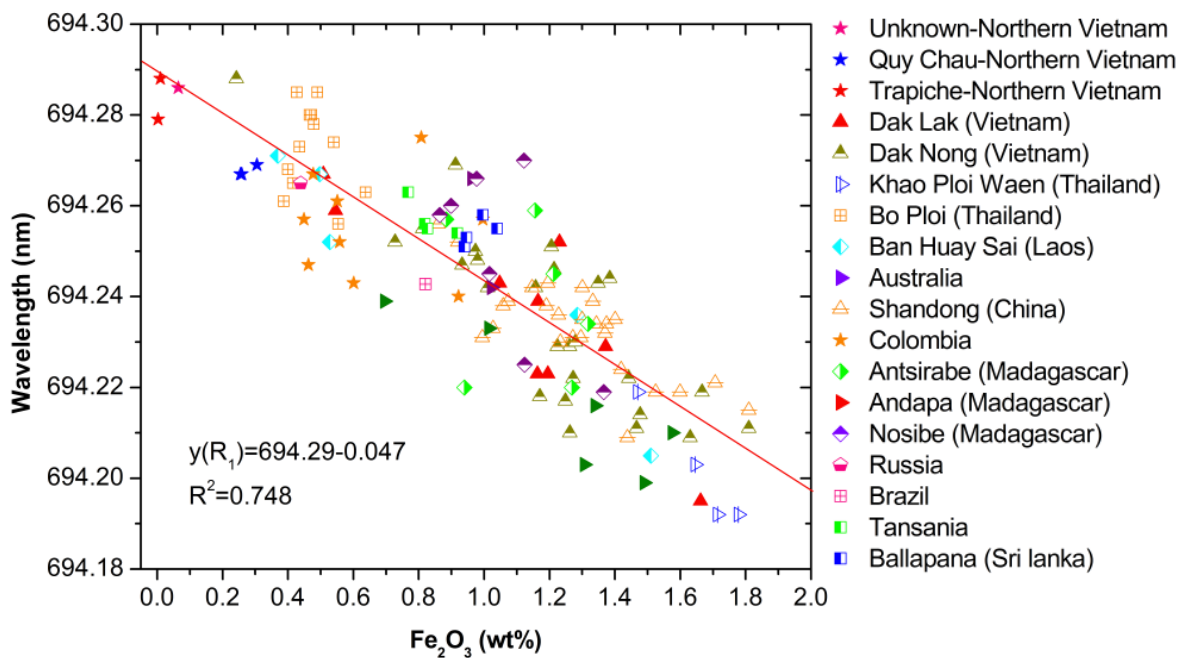
Figure 6.2.3: The shift of R₁ line around 694.28 nm corresponding to the Fe₂O₃ content.

The R lines are used for determining the internal pressure in Cr^{3+}-containing corundum because of the shift of the R lines towards longer wavelength with increasing pressure (Collins et al. 1960, Mao and Bell 1978, Munro et al. 1985, Mao et al. 1986, Horn and Gupta 1989, Gupta and Shen 1991, Shen and Gupta 1993, Chai and Brown 1996, Banini et al. 2001, Gaft et al. 2005). Häger et al. (2010) and later Noguchi et al. 2013 used this effect to determine the remnant pressure around inclusions in Cr^{3+} containing corundum. When the octahedral oxygen coordination is exposed to a high pressure, it gets locally compressed. Confirmation for the result of the Raman spectra, the octahedral gets expanded when the Fe_2O_3 content increases. This illustration is given in Figure 6.2.4. Consequently, the R lines shift towards smaller wavelength when the Fe_2O_3 content increases. An additional influence on the peak positions of the luminescence spectra could occur for the samples which contain other prominent chemical elements with a larger ionic radius, such as Cr^{3+}, $Cr^{3+} + Fe^{3+}$ or $Fe^{2+} + Ti^{4+}$.
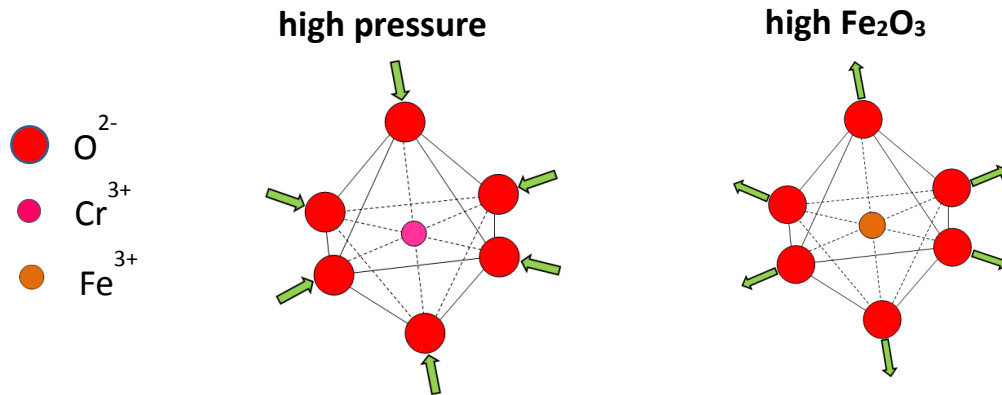
Figure 6.2.4: The compression and expansion of the octahedral coordination.

Figure 6.2.5 shows an equal shift of two R line. The relation is described by the equation:

$$y(R_1) = 10.14 + 0.99x(R_2) \qquad (6.3)$$

with a high regression $R^2=0.993$. Few data points are slightly scattered around the linear line and can be explained by the spectral resolution or the deviation of fitting values of R_1 and R_2 lines. The equal shift of the two lines shows that the R_1-R_2 splitting is in this case nearly a constant. The experimental data revealed the value of this constant varying from 1.43 nm to 1.44 nm.
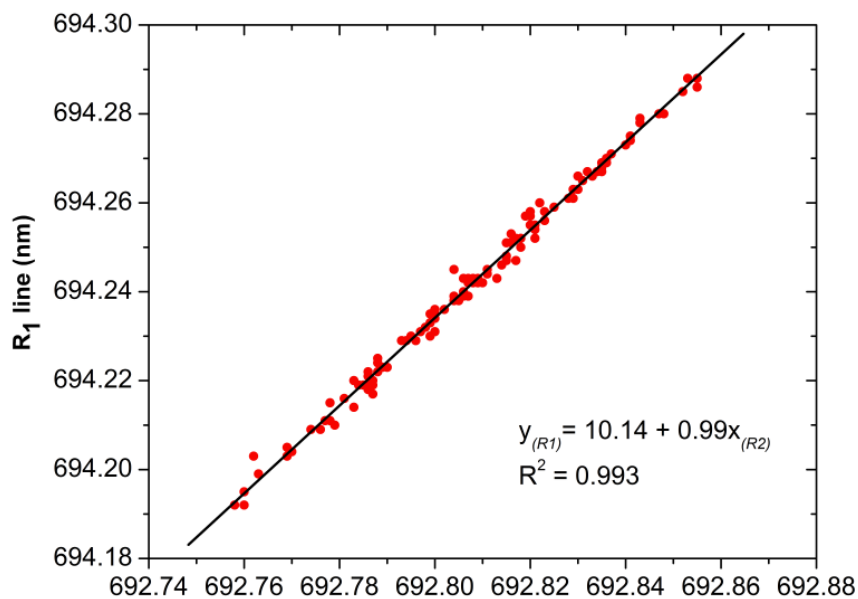
Figure 6.2.5: The R_1 and R_2 lines shift.

Similar to the correlation of Raman peak position and the Fe_2O_3 content, this correlation can be applied to estimate the Fe_2O_3 content in sapphires or corundum. This relationship can help to distinguish sapphires from different origins, for example, basaltic sapphires from metamorphic sapphires. Sapphires from basaltic origins usually have a high Fe_2O_3 content, therefore the peak position of R lines of sapphires tend to centre at smaller wavelength. On the other hand, sapphires from metamorphic origins have low Fe_2O_3 contents and the peak positions of R lines tend to centre at longer wavenumbers.

The shift of the R lines has been used for high pressure experiments or determine the remnant pressure around inclusions (Collins et al. 1960, Mao and Bell 1978, Munro et al. 1985, Mao et al. 1986, Horn and Gupta 1989, Gupta and Shen 1991, Shen and Gupta 1993, Chai and Brown 1996, Banini et al. 2001, Gaft et al. 2005, Häger et al. 2010, Noguchi et al. 2013). However the effect of the Fe_2O_3 content for the shift has been not taken into. This study recommends a 0-pressure position calibration as follows:

1. Determine the pressure at the positions which are far from an inclusion to ensure that these positions are not affected by the inclusion. Such positions could be A, B and C in Figure 6.2.5 Due to the effect of Fe_2O_3, the pressure values at position A, B or C are unequal 0.

2. Set the pressure values at A, B or C positions to 0-pressure. One requirement is that the measured area and the area around the inclusion must be transparent and free of fissures or cracks so that they cannot be taken into the real pressure values.
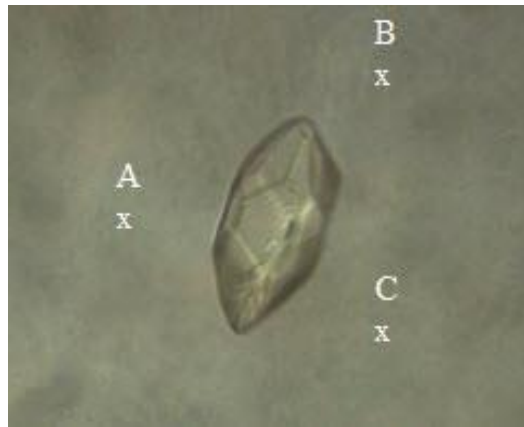
Figure 6.2.5. Zircon inclusion in a sapphire sample from Andapa, Madagascar. The A, B, C positions represent 0-pressure positions.

Subsequent to the pressure calibration and the collection of the luminescence measurements or luminescence mapping, the pressure can be calculated according to the following two equations (Schawlaw 1961, Kaplyanskii and Przhevuskii 1962, Ostertag 1991):

$$R_1 \text{ line: } \Delta v(R_1) = 7.590P - 1.5S \qquad (6.4)$$

$$R_2 \text{ line: } \Delta v(R_2) = 7.615P - 0.6S \qquad (6.5)$$

where $\Delta v(R_1)$ and $\Delta v(R_2)$ are the respective shifts of the R_1 and R_2 lines (in cm^{-1}) and P and S are the hydrostatic and non-hydrostatic components of the stress or pressure (in GPa), respectively. If the stress is purely hydrostatic (S=0), the R_1 and R_2 lines shift equally with the applied hydrostatic stress P.

Chapter 7: FTIR Spectroscopy of Sapphire and the Influence of Fe_2O_3 Content on the Spectra

7.1. FTIR spectroscopy of sapphire

OH-groups in corundum have been reported both on synthetic and natural corundum. Previous researchers investigated OH-groups on Verneuil-growth synthetic of different trace elements like Ti, Fe, or V and colors (Eigenmann and Günthard 1971, 1972, Eigenmann et al. 1972, Volynets et al. 1969, 1972, Moon and Philips 1991, 1994, Beran 1991). Study on OH-groups was also carried out on hydrothermally growth synthetic rubies (Belt 1967, Peretti and Smith 1993). Besides, many works have been performed on natural corundums, like rubies from Mong Hsu (Smith 1995), an unknown and non-heat treated natural sapphire (Häger and Greiff 1994, Häger 1996), blue basaltic sapphires from Phan Thiet and Di Linh in the southern Vietnam (Smith et al. 1995), sapphire from Vietnam (Emmett et al. 2003), corundum for many localities (Beran and Rossman, 2006), corundums from Marosely, Madagascar (Catier 2009). Figure 7.1.1 shows IR absorption spectra of a Fe,Ti:α-Al_2O_3 Verneuil-grown sapphire from Moon and Philips (1994). Table 7.1 summarizes absorption bands of OH-groups from the literature as mentioned.
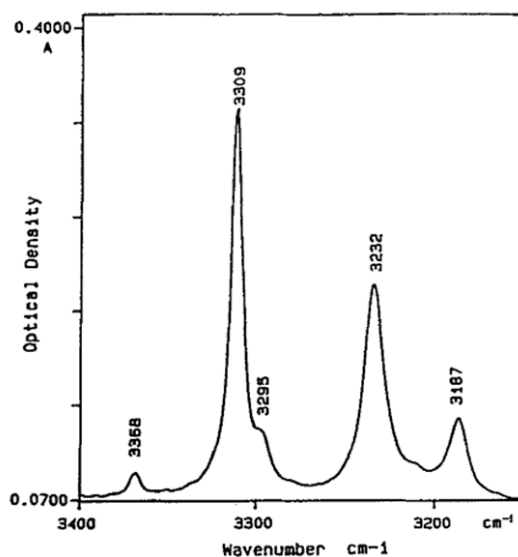
Figure 7.1.1: FTIR absorption spectra of a Verneuil-growth sapphire with Fe,Ti:α-Al_2O_3 (Moon and Philips 1994).

Table 7.1: The peak positions of the absorption bands of OH-groups from the literature.

Authors	Absorption bands (cm^{-1})											The kind of samples
Belt, 1967			3180	3230									Hydrothermally growth ruby
Eigenmann & Günthard, 1971			3180	3230			3310						Verneuil-growth sapphire
Eigenmann et al., 1972			3180	3230			3310						Verneuil-growth sapphires
Volynets et al. 1972	3000	3160		3225	3275		3310			3420			Verneuil-growth corundum
Beran, 1991		3160	3185	3230	3280	3290	3310						Verneuil-growth corundum
Moon & Philips, 1991, 1994			3187	3232		3295	3309	3368					Verneuil-growth sapphire
Peretti & Smith, 1993				3238			3310	3389		3498	3575		Hydrothermally growth ruby
Smith, 1995			3187	3232		3292	3310	3368					Ruby from Mong Hsu
Smith et al. 1995			3189	3232	3269	3293	3309	3367					Sapphires from southern Vietnam
Häger & Greiff, 1994			3187			3295	3310						Unknown and non-heat treated natural sapphire
Häger, 1996			3187			3295	3310						Unknown and non-heat treated natural sapphire
Emmett et al., 2003			3185	3233			3310	3367					Sapphire from Vietnam
Beran & Rossman, 2006			3185	3233			3310	3367	3395				Corundum for many localities
Cartier, 2009		3160					3309						Corundum from Marosely, Madagascar

In this study, the structural bonding of OH-groups in natural sapphire samples was examined by FTIR spectroscopy in the region of 3100-3600 cm^{-1}. Besides, the FTIR spectra also show the presence of hydrous mineral inclusions occurring in the tested samples.

Figure 7.1.2 presents a FTIR absorption spectra with the beam condenser method and transmission mode of a light purplish blue Dak Nong (Vietnam) sample with the thickness t=0.082cm. The spectra shows the distinctive spectral bands. The strong absorption below 1500 cm^{-1} is caused by Al-O bonding (Wefers and Bell, 1972). The band around 2400 cm^{-1} with two peaks centered at 2342 and 2362 cm^{-1} can originate from CO_2 gas in the environment and CO_2 gas in negative crystals. The peaks around 2853 and 2924 cm^{-1} correspond to oils or fats, which were probably due to the contaminations from handling or the substance for polishing the samples (Catier 2009). The distinct peaks in the range of 3100-3400 cm^{-1} characterize the OH functional group vibrations.
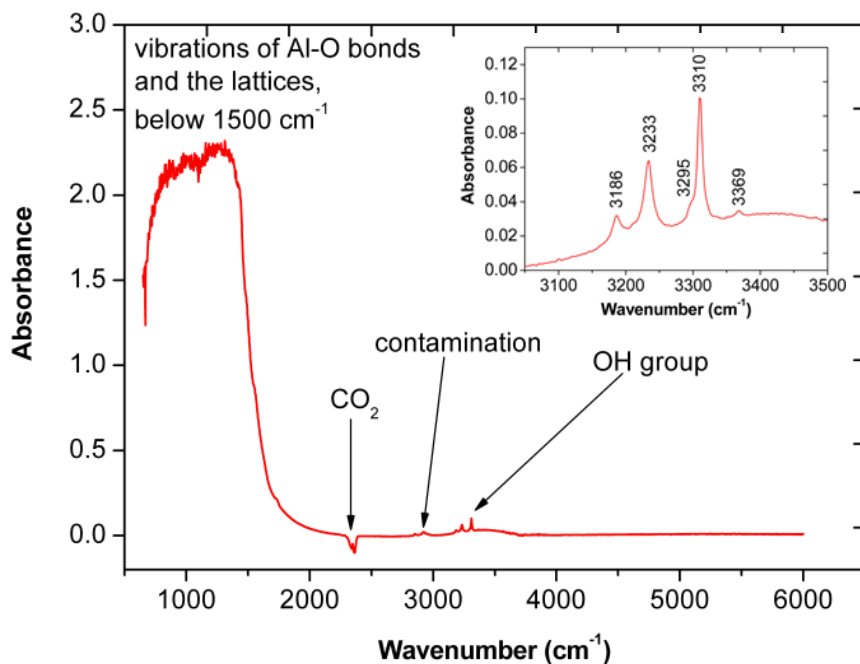
Figure 7.1.2: FTIR spectra of a sample from Dak Nong (Vietnam) recorded in the spectral region from 600 to 6000 cm^{-1}, t=0.081 cm.

Figure 7.1.3 shows a polarized absorption spectra of these OH-groups in the (linear) absorption coefficient (cm^{-1}) in the region of 3150-3400 cm^{-1}. The (linear) absorption coefficient (cm^{-1}), which is defined by $\alpha = A/t$ with $A = \log (I_o/I)$ is the absorbance and t (cm) is the thickness of the plane-parallel sample. For $E \perp c$, the OH-groups include three distinct sharp and strong peaks centered at 3186, 3233, and 3310 cm^{-1}, a small shoulder at 3295 cm^{-1} and an additional peak at 3367 cm^{-1}. For the case of $E//c$ the absorption of OH-groups are very weak or absolutely not to be observed. The intensity of absorption bands for $E//c$ is always contributed by the portion of $E \perp c$ due to the condenser lens.
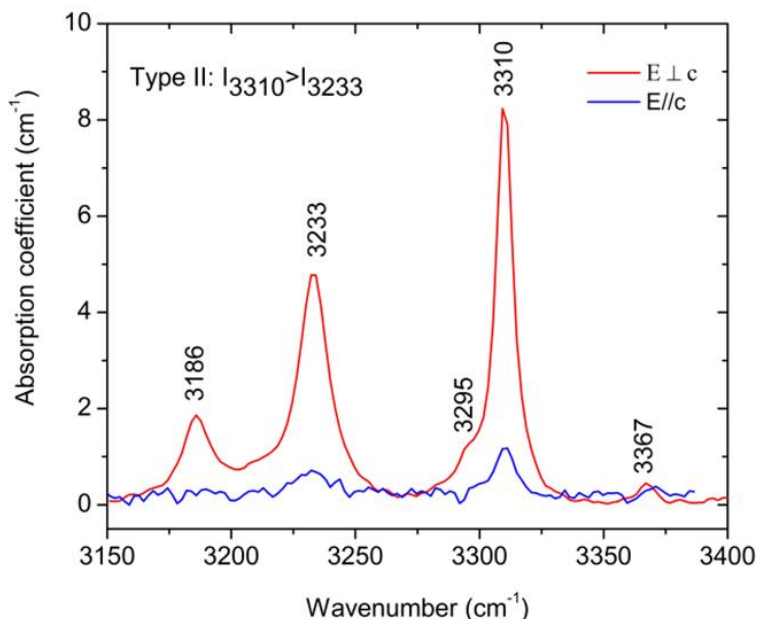
Figure 7.1.3: Polarized FTIR spectra of OH-groups in a Dak Nong (Vietnam) sample in a close-up view, t=0.081. It is type II spectra with I$_{3310>3233}$ according to Beran (1991).

For almost all of samples, the 3310 cm^{-1} peak was reported to be the strongest. According to Beran (1991), spectra characterized by the dominance of 3310 cm^{-1} peak defined as type II spectra, while type I spectra are defined by the dominance of 3233 cm^{-1} peak. The type II spectra of OH-groups are normally observed in almost all of the samples. There are few cases showing type I spectra with the dominance of the peak at 3233 cm^{-1}. Figure 7.1.4 shows polarized type I spectra of OH-

103

groups from a sample from Antsirabe (Madagascar). Similarly with type II, the OH-groups in type I are strong and sharp in $E \perp c$ and too weak in $E //c$.
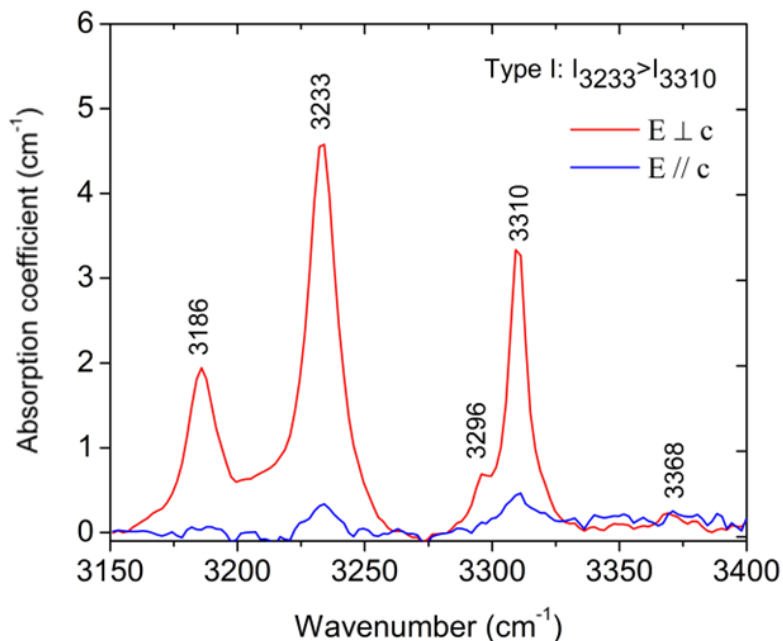
Figure 7.1.4: Polarized FTIR spectra of OH-groups in an Antsirabe sample, t=0.0089cm. It is type I with $I_{3233>3310}$ according to Beran (1991).

For a general view, Figure 7.1.5 shows the FTIR spectra with the presence of OH-groups in the region of 3100 - 3500 cm^{-1} of sapphires from several localities. All sapphires from blue to light blue and very light blue sapphires, except samples from Quy Chau (Vietnam) and a trapiche sample from an unknown source from the north of Vietnam, showing these structurally bonded OH-groups. The highest absorption coefficient of the 3310 cm^{-1} peak has been found in a blue sapphire from Dak Nong (Vietnam) with 28.038 cm^{-1}. High absorption coefficients were also found for blue sapphires from Nosibe and Andapa (Madagascar), Ban Huay Sai (Laos), Dak Lak (Vietnam), respectively 18.615, 18.471, 14.675 and 10.743 cm^{-1}. Almost light blue to very light blue sapphires show absorption coefficient lower than these medium blue sapphires. For example, the 3310 cm^{-1} peak of the samples from Dak Nong (light blue), Shandong (light blue), Antsirabe (light blue), and

Nosibe (light greenish blue) has absorption coefficient were 6.806, 4.481, 3.494, and 2.25 cm^{-1} respectively.
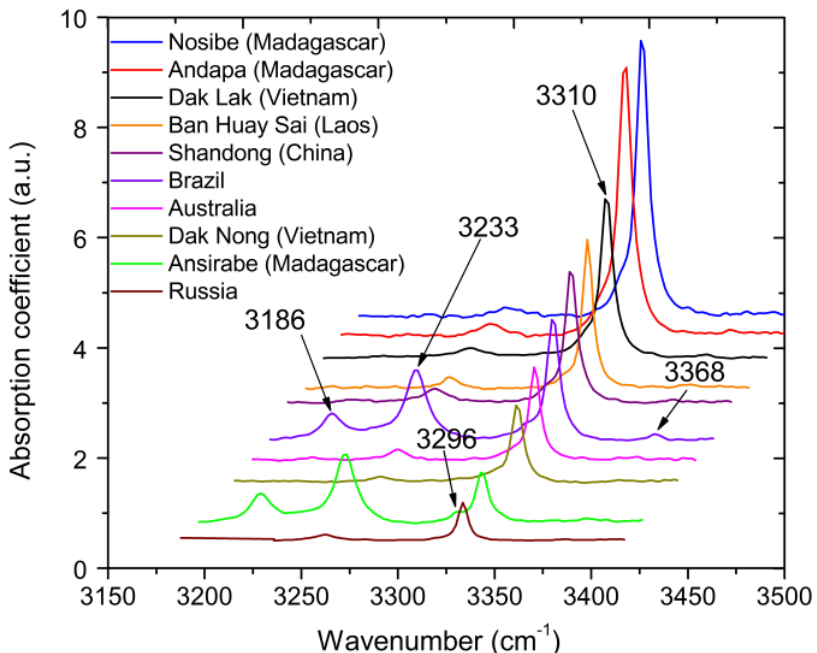
Figure 7.1.5: FTIR spectra from 3100 to 3500 cm^{-1} of sapphires from different localities.

Colorless, light pink, light yellow, opaque light blue, opaque white, yellow-brown, violet-brown, brown, dark brown, light green and green sapphires show a weak absorption of this peak. The trapiche Dak Nong sapphire (in the brown core), Shandong (in the brown core), Bo Ploi (violet-brown), Dak Lak (very light yellow), and Khao Ploi Waen (light grayish green) show absorption coefficient of OH-groups with the values of 1.205, 0.947, 0.823, 0.625, and 0.229 cm^{-1} respectively. No OH-groups were detected in most sapphires from Colombia (colorless, light pink, pale), Bo Ploi (colorless, violet-brown), Russia (colorless), and in some brown samples from Shandong, Ban Huay Sai and Dak Nong.

Furthermore, none of the OH-groups signal was detected in all samples from Tansania, Malawi and the north of Vietnam, but diaspore, boehmite or kaolinite mineral inclusions were observed in the range from around 1750 to 3800 cm^{-1}, and water was sometimes observed with a broad band

from 3000 to 3500 cm^{-1}. This water can be due to fluid inclusions as determined by Raman spectroscopy or absorptive humidity in the environment. These hydrous inclusions distribute in the whole sample similar to diaspore inclusions which are detected by micro Raman. Sapphires from Tansania and unknown-source samples from the north of Vietnam are opaque white or colorless. Malawi samples are mostly colorless and combined with brown stains healed by diaspore.

Beside the OH-groups including three main peaks at 3186, 3233 and 3310 cm^{-1}, Balmer et al. (2006) reported the 3160 cm^{-1} band in yellow sapphires and probably associated with two peaks at 3242 and 3353 cm^{-1}. However they could not confirm whether this group is related to goethite or to a silanol (SiH$_3$OH) group where an OH-groups is attached to Si^{4+}. Smith and Bogert (2006) reported the 3162-series having six bands approximately at 2420, 2459, 3075, 3161, 3242 and 3355 cm^{-1} in natural sapphires from Sri Lanka as shown in Figure 7.1.6. The 3161-series occurs normally in yellow-to-orange and padparadscha sapphires from low-iron metamorphic environments. The authors suggested that the 3161-series is due to Mg^{2+} bonding to OH-groups by LA-ICP-MS measurements and the heat treatments. However the chemcial analyses were not provided and the affect of trace elements to the 3161-series is assumed to originate from more trace elements, not onlly Mg^{2+} because of natural sapphires. This 3160-series also reported by GIT Gem Testing Lab (2008) for a Winza ruby, Schwarz et al. (2008) for rubies and sapphires from Winza, central Tanzania, and Cartier (2009) for rubies and sapphires from Marosely, Madagascar. However these authors did not evaluate which trace elements affect this series.

Although this 3160-series were reported in the literarure, this series was not observed in any samples of this study.
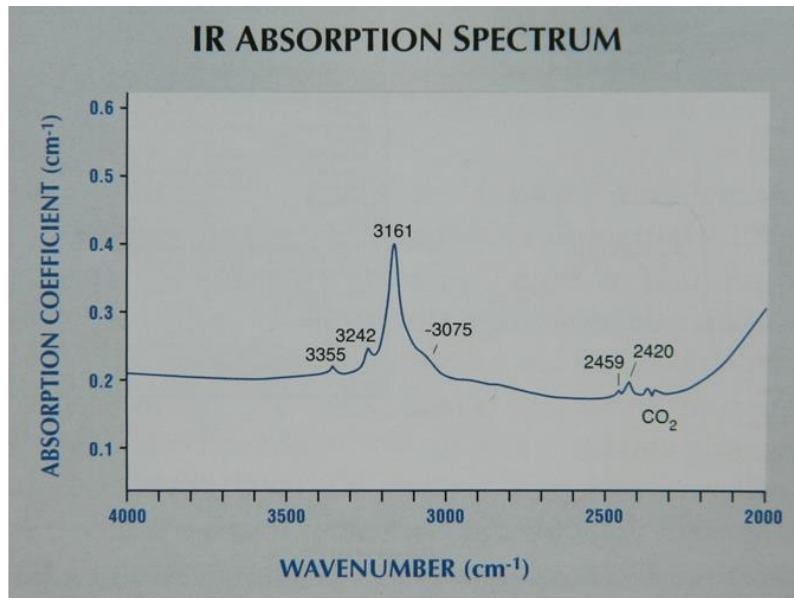
Figure 7.1.6: The 3161-series due to Mg^{2+} bonding to OH-groups in the natural sapphire from Sri Lanka from Smith and Bogert (2006).

7.2. OH bond angles in sapphire

Moon and Philips (1991) calculated the angle of OH bond to the *c*-axis in synthetic sapphire containing Ti impurities by rotation experiments of the *c*-axis to the electric vector *E*. The dipole bond angle is calculated by using the following expression:

$$\frac{\alpha \perp c}{\alpha //c} = \frac{1}{2} tan^2 \theta \qquad (7.2)$$

where θ is the angle of OH dipole bond to the c-axis, $\alpha \perp c$ and $\alpha //c$ are the absorption coefficients of OH band with $E \perp c$ and *E//c*, respectively. The absorption coefficient intensity was reported as a function of the angle of vector E and the *c*-axis $\wedge(E,c)$. According to the results of these authors, the intensity of the absorption coefficient increase when $\wedge(E,c)$ varies from 0 to 80-90° and the OH dipole bond angle to the *c*-axis for three main bands at 3309, 3132 and 3187 cm^{-1} are 75.4 ($\Delta\theta^o =$ ±1.1), 79.0 ($\Delta\theta^o$ = ±3.6), and 79.9° ($\Delta\theta^o$ = ±11.8), respectively.

In this study, to determine the intensity absorption of the OH bond, the angle between the *c*-axis and the *E* was changed by rotating the samples. The peak positions of OH-groups were fitted with the Voigt functions. The results of rotation experiments are presented in Figure 7.2.1.
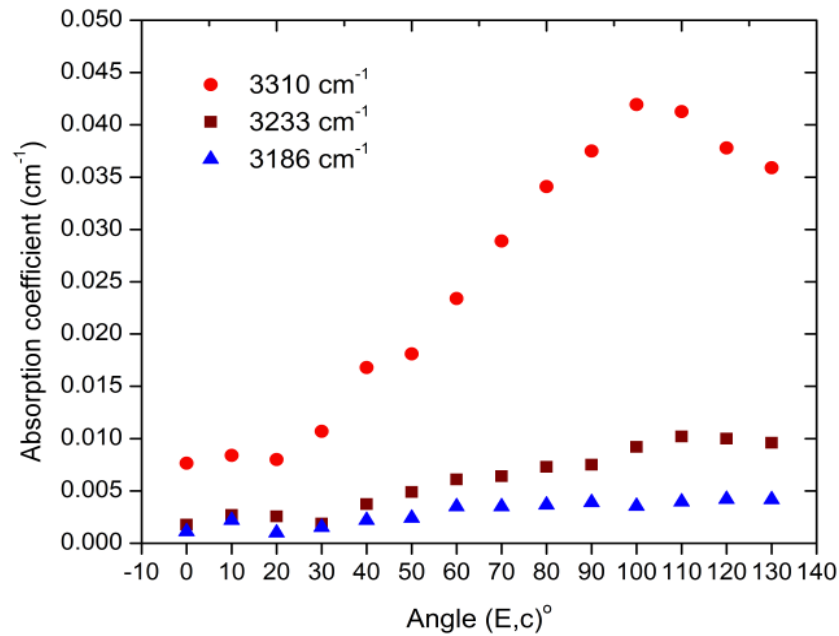
Figure 7.2.1: Absorption coefficient (cm⁻¹) as a function of the angle of vector e and the c-axis the crystal sapphire.

As shown in Figure 7.2.1, the intensity of the absorption coefficient of OH bands increase with the $\wedge$(E,c) in the region from 0 to 90-100º.

The OH bond angles to the *c*-axis were calculated according to the expression (7.2).

For the 3310 cm⁻¹ mode:

$$\frac{\alpha\perp c}{\alpha//c} = \frac{0.0375}{0.0077} = \frac{1}{2} tan^2\theta \Rightarrow \theta = 72.29^o$$

For the 3233 cm⁻¹ mode:

$$\frac{\alpha\perp c}{\alpha//c} = \frac{0.0075}{0.0018} = \frac{1}{2} tan^2\theta \Rightarrow \theta = 70.99^o$$

For the 3186 cm⁻¹ mode:

$$\frac{\alpha\perp c}{\alpha//c} = \frac{0.039}{0.0011} = \frac{1}{2} tan^2\theta \Rightarrow \theta = 69.25^o$$

The angle of OH bond to the c-axis of the tested crystal sapphires may be affected much on the impurities in the samples like Ti, Fe, or V because the tested samples are natural sapphires. It has difference with synthetic sapphire which contains only Ti impurity as in the results of Moon and Philips (1991).   This calculation can be applied to determine the angle of the OH bond to the c-axis even the weak intensity of absorption coefficient.

7.3. The correlation of 3310 cm^{-1} peak and the Fe$_2$O$_3$ contents of sapphires

The OH-groups in natural and synthetic corundum can be attached with various trace elements, such as Ti, Fe or V and these trace elements affect the intensity as well as position of OH bands (Eigenmann and Günthard 1971, 1972, Eigenmann et al. 1972, Volynets et al. 1972, Beran 1991, Moon and Phillips 1994, Häger and Greiff 1994, Häger 1996). For example, Volynets et al. (1972) reported that when Mg increases, the absorption coefficient of a broad band around 3000 cm^{-1} increase. The absorption coefficient of the peaks at 3160, 3233 and 3310 cm^{-1} increase when Si, V, Ti increases correspondingly. Häger (1996) reported also a broad band of OH-groups around 3000 cm^{-1} in a Verneuil-grown sapphire doped with Mg or (Mg+Fe).

Moon and Phillips (1994) investigated the absorption spectra of the Fe,Ti:α-Al$_2$O$_3$ system with natural and synthetic sapphires containing only Fe, only Ti and a range of Fe and Ti solute and incorporated with hydrogen. These authors proved that iron and titanium affect the full width at half maximum (FWHM) of OH-groups. In both (H,Ti)-Al$_2$O$_3$ and (H,Ti,Fe)-Al$_2$O$_3$ the peak of OH-groups center at the same position but the FWHM of (H,Ti)-Al$_2$O$_3$ smaller than the FWHM of (H,Ti,Fe)-Al$_2$O$_3$. Other evidences supported that hydrogen enters the structure of corundums by an oxidation-reduction reaction which is expressed by Fe^{3+} + O^{2-} + ½ H$_2$ = Fe^{2+} + OH$^-$(Eigenmann and Günthard 1972, Eigenmann et al. 1972, Moon and Phillips 1994). In this process, Fe^{3+} is reduced corresponding to the producing an OH-groups in its immediate neighbor We can see that the absorption spectra depend not only on one trace element, but also a combination of trace elements. However, there is no expression revealing the real relationship between these trace elements and OH-groups proposed in the literature so far. In this study, a relationship between the iron content and the OH-groups was found. One remarkable thing is that most of the studied sapphire samples contain high iron content due to basaltic origins. This iron content affects the

presence of the 3310 cm^{-1} peak in OH-groups. The 3233 cm^{-1} occurs normally in much weaker absorption intensity compared with the 3310 cm^{-1}, and in few cases its intensity is approximately a half compared of the 3310 cm^{-1} peak. The 3186 cm^{-1} peak is weaker than the 3233 cm^{-1} peak. For these reasons, there was only the 3310 cm^{-1} peak was investigated for $E \perp c$.

Chemical analysis and FTIR measurements show that if the iron content increases, the 3310 cm^{-1} peak shifts forward to longer wavenumber. This shift could be explained that the charge substitution of Fe^{3+} for Al^{3+} changes electronegativity of ions at octahedral sites surrounding OH-groups (Wilkins and Ito 1967, Strens (1974), Velde 1983). Another reason could be, that due to the larger ionic radius of Fe^{3+} (0.645 Å) in comparison to Al^{3+} (0.535 Å) in the octahedral sites the crystal structure locally widen. This changes the vibration frequencies of the OH bonds. In this study, the 3310 cm^{-1} peak shift from 3309 cm^{-1} to 3311 cm^{-1} if the iron content increases from 0.4 to 1.78 wt% Fe_2O_3. The peak position of the 3310 cm^{-1} of OH-groups as a function of wt.% Fe_2O_3 is shown in Figure 7.3.1. The relationship between other trace elements and the shift of OH-groups, like Ti was not found. The Ti content is too low to influence OH bond.
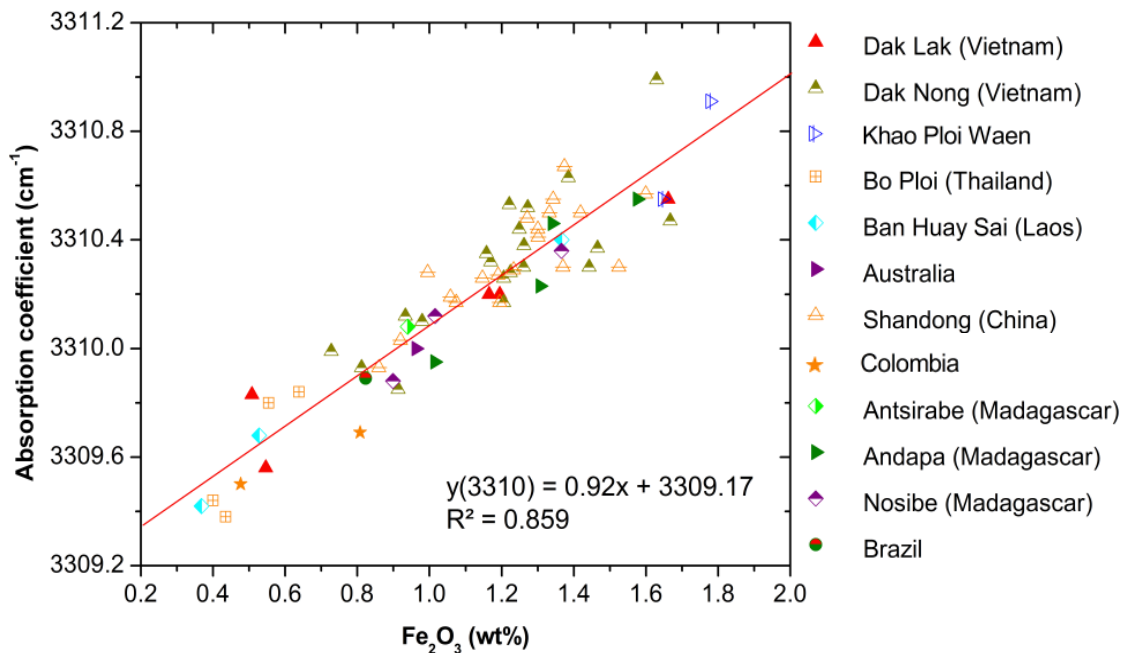
Figure 7.3: The shift of the 3310 cm^{-1} peak as a function of Fe_2O_3 content.

As seen from Figure 7.2.2, the relationship between the peak position of 3310 cm^{-1} is expressed by the equation $y(3310) = 0.92x + 3309.17$, in which x is wt.% Fe_2O_3 and y is peak position of the 3310 cm^{-1}. This equation can be applied to determine the Fe_2O_3 content in the samples and from here can distinguish sapphires from different origins.

Chapter 8: UV-Vis-NIR Spectroscopy of Sapphire

Corundum appears colored due to selective absorption of visible light. This is caused by trace elements of transition metal which replace for Al^{3+} ions in the corundum structure e.g. Fe, Ti, Cr, and V in the octahedral sites (Fritsch and Rossman 1987, 1988 (Part 2 and Part 3), Volynets et al. 1972, Ferguson and Fielding 1972). The color of corundum are resulted from different mechanisms such as single ion, ion pair transitions, intervalence charge transfer, color centers, or a combination among these reason (Ferguson and Fielding 1972, Fritsch and Rossman 1987, 1988 (Part 2 and Part 3), Schmetzer 1987, Nassau 1983, Emmentt and Douthit 1993, Burns 1993, Häger 1992, 1993).

The red color of ruby results from electronic transitions on Cr^{3+} ions in octahedral sites of the corundum structure (Nassau 1983, Fritsch and Rossman 1987, Garcia-Lastra et al. 2005). The UV-Vis-NIR spectra of dark red ruby from Winza, Central Tansania show two broad absorption bands with maximum at 405 and 560 nm, and a narrow small band at 694 nm (Schwarz et al. 2008). Besides, the UV-Vis spectra of ruby from Colombia also show two additional absorption peaks at 468 nm and 475-477 nm (Duroc-Danner 2002). The blue color of sapphire originates from intervalence charger transfer (IVCT) of Fe^{2+}/Ti^{4+} with maximum absorption band at around 570 nm or IVCT of Fe^{2+}/Fe^{3+} with a maximum absorption at around 880 nm (Schmetzer 1987, Fritsch and Rossman 1987, 1988 (Part 2 and Part 3), Ferguson and Fielding 1971, 1972, Moon and Philips 1991, 1994, Smith el al. 1995, Schwarz et al. 2000). Yellow sapphire is resulted from single Fe^{3+} and ion pair transition of Fe^{3+}/Fe^{3+} (Ferguson and Fielding 1971, 1972) or color centers (Schmetzer et al. 1982, 1983, Emmentt and Douthit 1993, Häger 1993). The absorption spectra relative to Fe^{3+} are characterized by bands at around 376, 388 and 450 nm (Ferguson and Fielding 1971, 1972, Smith el al. 1995, Schwarz et al. 2000, Häger 2001, Schwarz et al. 2008).

The sapphire samples in this study can be separated into three groups according to the color:

- Group 1: Blue, green or bluish green sapphires. Most of the samples belonging to this group and coming from Dak Nong, Dak Lak, Quy Chau (Vietnam), Shandong (China), Khao Ploi Waen (Thailand), Australia, Ban Huay Sai (Laos), Russia, Brazil, and Andapa, Antsirabe and Nosibe (Madagascar).

- Group 2: The light pink sapphires from Colombia.
- Group 3: Brown to grey, or almost colorless sapphire. This group includes samples from Dak Nong (Vietnam), Shandong (China), Bo Ploi (Thailand), Ballapana (Sri Lanka), Colombia, Tansania, Dak Nong (Vietnam) and Bo Ploi (Thailand).

8.1. Group 1: The blue, green or bluish green sapphire
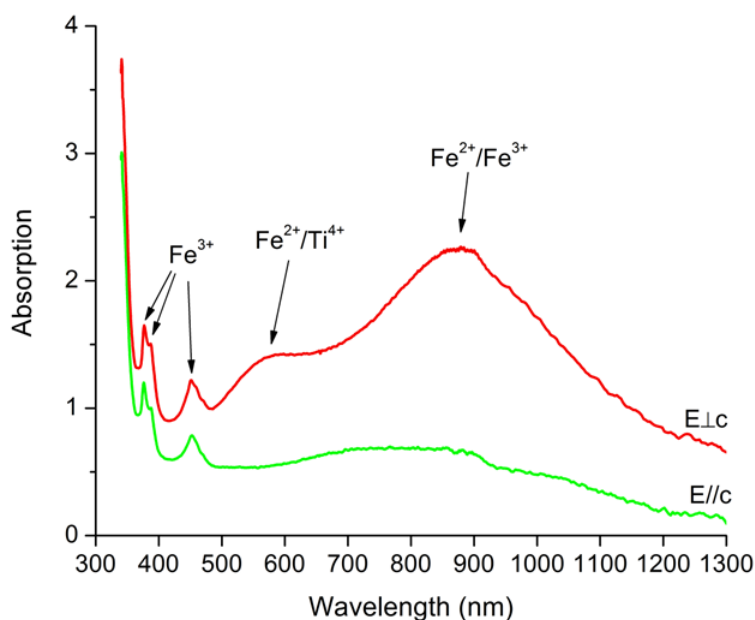
Figure 8.1.1: The polarized UV-Vis-NIR absorption spectra of a bluish green sample from Dak Lak (Vietnam).

The UV-Vis-NIR absorption spectra in this study are typically contributed by Fe^{3+}-affects with two strong and sharp bands in the visible region at about 377, 387 nm, and as well as in the invisible region a group od at about 451, 460 and 471 nm (Figure 8.1.1). Charge transfer of Fe^{2+}/Ti^{4+} show the absorption between 520 and 610 nm. Strong broad band by Fe^{2+}/Fe^{3+} charge transfer appears in the region approximately 800-920 nm. Typical polarized UV-Vis-NIR absorption spectra of a bluish green sapphire which show all transition mechanisms is given in Figure 8.1.1 for a Dak Lak

113

sample. The UV-Vis-NIR absorption spectra for this sample were measured with E perpendicular and parallel to the c axis. For $E\perp c$, sharp bands of Fe^{3+} have maxima position at 377, 387 and 451 nm. The intervalence charge transfer by Fe^{2+}/Ti^{4+} show maximum absorption at about 570nm when $E\perp c$, and 650-800nm when $E//c$. The charge transfer absorption by Fe^{2+}/Fe^{3+} is responsible for a broad band toward the near infrared from 800-950 nm. Moreover, gem sapphires from Krong Nang, Dak Lak were grouped by a color investigation by UV-Vis-NIR spectroscopy (Phan et al. 2014).

The measurements and chemical analyses show that the absorption coefficient intensity is more dominant when the iron content in the samples is higher. Figure 8.1.2 shows the UV-Vis-NIR spectra of four samples with different content of Fe_2O_3 and more or less the titanium content. The titanium content was detected by LA-ICP-MS technique. The UV-Vis-NIR spectra of a light green sample (from Shandong) with 1.707 wt.% Fe_2O_3 has very high Fe^{3+}-absorption. The absorption coefficient of the two charge transfer mechanisms of Fe^{2+}/Ti^{4+} and Fe^{2+}/Fe^{3+} of this light green sample are also more dominant than in the remaining others.
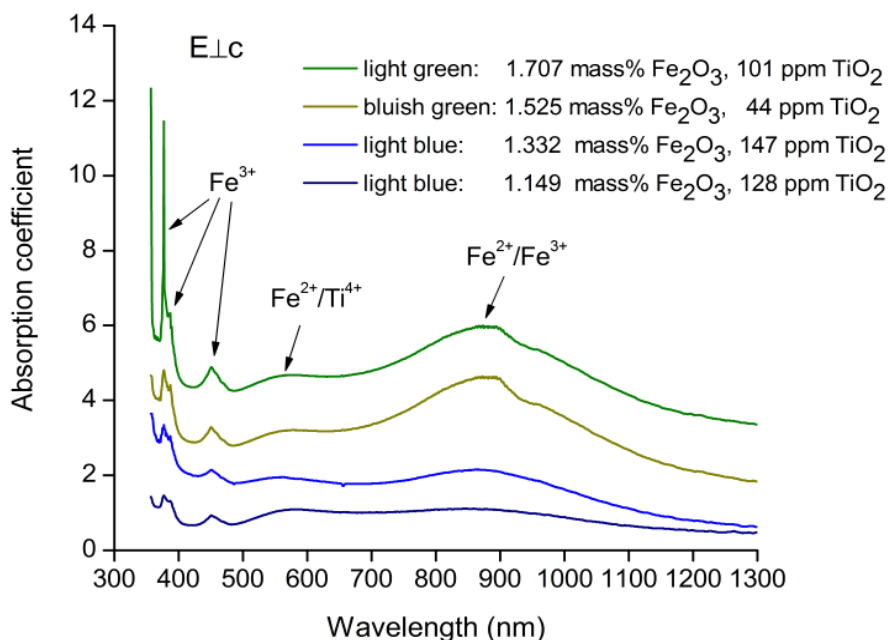
Figure 8.1.2: Absorption coefficient of four samples with different content of Fe₂O₃ and more or less the titanium content.

The UV-Vis-NIR spectra introduced in Figure 8.1 and absorption coefficient in Figure 8.2 are observed commonly in the samples with hue of blue and green like in Dak Nong, Dak Lak, Shandong or Khao Ploi Waen. There is no absorption band by Cr^{3+} ions observed in these samples. The Chromium content in these samples varies from few ppm to 35.12 ppm (see again in Chapter 4).

8.2. Group 2: The light pink sapphire
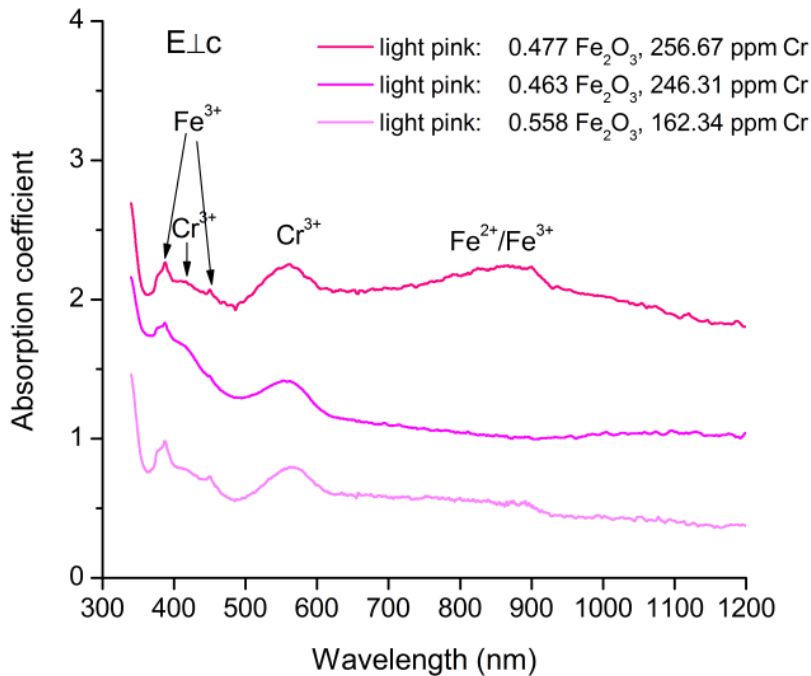
Figure 8.2: Absorption coefficient of light pink Colombia sapphire with the strong broad band by Cr³⁺ ions.

Besides absorption by Fe^{3+} ions, the samples from very light pink to light pink of Colombia show absorption by Cr^{3+} ions, as shown in Figure 8.3. The absorption contributed by Cr^{3+} shows a broad band with maxima at 560 nm and a weak band at about 405-415 nm.

8.3. Group 3: The brown to grey, or nearly colorless sapphire

In the group of grey to brown or brownish yellow samples, the absorption is mostly caused by Fe^{3+} ions at 377, 387 and 451 nm (Figure 8.3.1). The intervalence charge transfer absorption by Fe^{2+}/Ti^{4+} at about 570 nm and Fe^{2+}/Fe^{3+} at about 875 nm are also observed but with weak intensity. Note that, two peaks at 486 and 656 nm are due to artifact from the background.
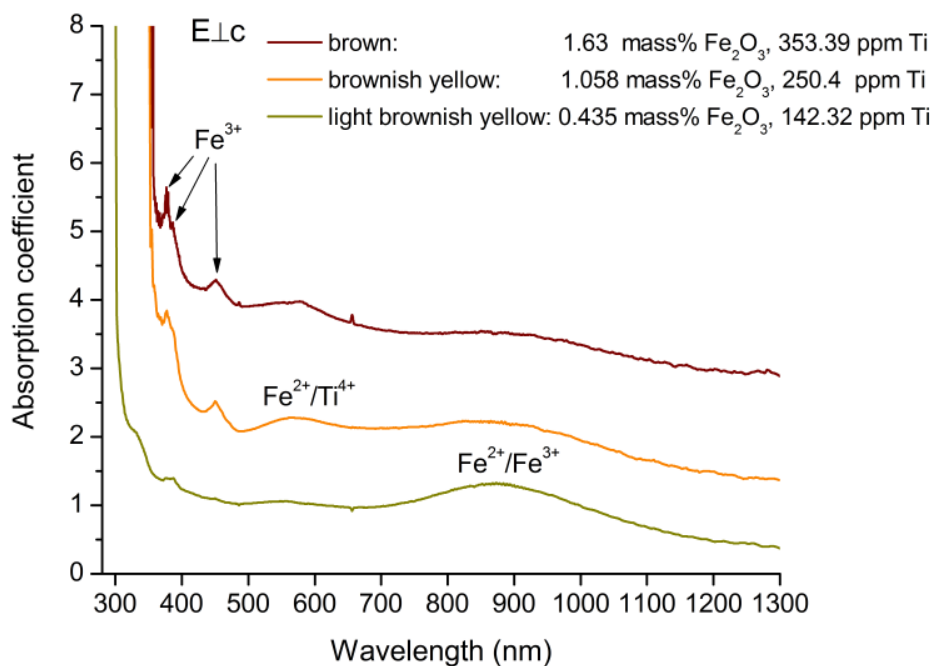
Figure 8.3.1: Absorption coefficient of three samples with hue of brown and yellow.

There are some grey samples with the weak absorption in the region from 400-500 nm, and almost none of absorption by intervalence charge transfer Fe^{2+}/Ti^{4+} and Fe^{2+}/Fe^{3+} as shown in Figure 8.3.2. Also in this figure, two peaks at 486 and 656 nm are due to artifact from the background.
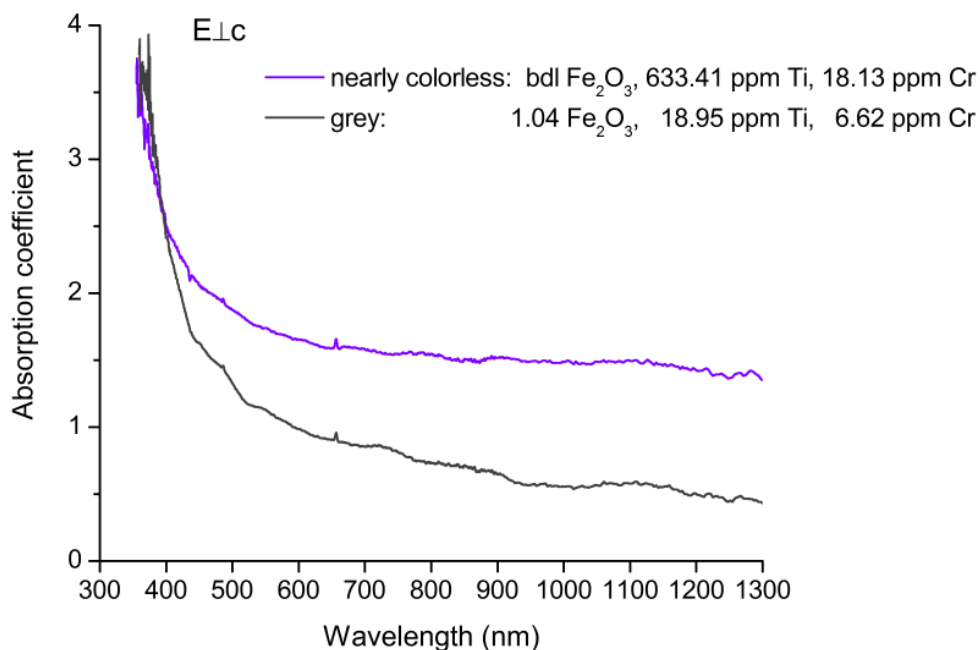
Figure 8.3.2: Absorption coefficient of two colorless samples shows no absorption.

Generally, the UV-Vis-NIR absorption spectra of sapphires in this study normally show the absorption bands by Fe^{3+} at 377, 387 and 451 nm, IVCT by Fe^{2+}/Ti^{4+} at 570nm ($E\perp c$), and IVCT by Fe^{2+}/Fe^{3+} in the NIR region of 800-950 nm. These absorption bands are corresponding to blue, greenish blue sapphire, or brown or yellowish brown sapphires. The absorption bands contributed by Cr^{3+} are observed in very light pink Colombia sapphires with a strong broad band with maximum at 560 nm and a weak band at about 404-415 nm.

Chapter 9: Conclusions

This thesis contributes to the internal features, chemical compositions and spectroscopic properties of natural sapphires, mainly sapphires from 18 areas in the world.

The internal features of sapphires observed in this study include color zoning, twinning, trapiche patterns, fingerprint, fluid-, gas-, and solid inclusions and hydrous mineral inclusions. Sapphires from Dak Nong, Dak Lak in the south of Vietnam, Shandong in China, Ban Huay Sai in Laos, Bo Ploi and Khao Ploi Waen in Thailand, Australia typically show iron-containing inclusions like goethite, ilmenite, hematite, or magnetite. Sapphires from these areas reveal cracks healed by brown or yellowish brown micro goethite or ilmenite. Furthermore these sapphires contain many silicate inclusions, typically feldspar. Sapphires from Andapa, Antsirabe and Nosibe in Madagascar show more feldspar inclusions. Zircon inclusions are observed in many areas in single crystals, and especially as clusters in sapphires from Colombia, Tansania and Malawi. Sapphires from Tansania, Malawi and northern Vietnam reveal a large number of diaspore inclusions.

Chemical analyses show that iron is a dominant trace element in sapphires, up to 1.947 wt.% Fe_2O_3. Sapphires from northern Vietnam show a low iron content, from "bdl" to 0.3 wt.% Fe_2O_3. Sapphires with high Fe_2O_3 content normally show the ratio of Cr_2O_3/Ga_2O_3 lower than 1, as a characteristic relative to basaltic origin, while Quy Chau sapphires show this ratio higher than 1. The iron content in Colombia sapphires is high, 0.4-1.0 wt.% Fe_2O_3 but the Cr_2O_3/Ga_2O_3 typically higher than 1. The trapiche like sapphires and unknown sapphires from northern Vietnam show this ratio from 0-2.

The iron element influences the spectroscopic characteristics of sapphires. The strongest peak at around 418.3 cm^{-1} and the peak at around 577.7 cm^{-1} shift towards smaller wavenumber when the Fe_2O_3 content increases. Furthermore, the FWHMs of the 418.3 cm^{-1} peak decreases when the Fe_2O_3 content increases. Two equations $y(418.3) = 418.29 - 0.53x$ and $y(577.7) = 577.96 - 0.75x$, in which x is the Fe_2O_3 content in wt.% and y is the Raman peak position (cm^{-1}) of the according peak can be used to determine the iron content in sapphire or corundum in general, and help to distinguish basaltic from metamorphic sapphires. Sapphires from basaltic origins have high iron contents, whereas sapphires from metamorphic origins have low iron contents. Therefore, the

Raman peak positions of these two peaks tend to locate at smaller wavenumbers for basaltic sapphires and longer wavenumbers for metamorphic sapphires.

The luminescence spectra of sapphire are characterized by R_1 at around 694.3nm and R_2 at about 692.8 nm (with the sample containing 247ppm Cr). The peak position of these two lines is also affected by the iron element. The R lines shift towards smaller wavelength when iron content in sapphire increases. The two equations $y(R_2) = 692.86 - 0.049x$ and $y(R_1) = 694.29 - 0.047x$ in which x is wt.% Fe_2O_3 and y is R line peak positions can be applied to estimate the iron content in sapphires or corundum, and may distinguish basaltic sapphire from metamorphic sapphire. This influence has to be taken into account for determining the internal pressure around inclusion in corundum. The formula to calculate the pressure has to be modified for corundum with high iron content.

The FTIR absorption spectra show the presence of OH-groups in the region 3100-3500 cm^{-1}. The FTIR spectra also show the presence of hydrous mineral inclusions: kaolinite, diaspore, boehmite. The iron content also affects the strongest peak, 3310 cm^{-1} of the OH-groups. This peak shifts towards longer wavenumber when the Fe_2O_3 content increases. This relationship is expressed by the equation $y = 0.92x + 3309.17$, in which x is wt.% Fe_2O_3 and y presents the peak positions of the 3310 cm^{-1}. Similar to application of the Raman and luminescence spectra, this equation can be also applied to determine the iron content in corundum, and may distinguish sapphire from different origins.

The UV-Vis-NIR absorption spectra explain the cause of the sapphire color. The UV-Vis-NIR absorption spectra normally show the absorption bands by Fe^{3+} at 377, 387 and 451 nm, IVCT by Fe^{2+}/Ti^{4+} at 570nm ($E \perp c$), and IVCT by Fe^{2+}/Fe^{3+} in the region of 800-950 nm. This is the cause to sapphire color like blue, greenish blue, or brown or yellowish brown. The absorption bands contributed by Cr^{3+} are only observed in several very light pink sapphires from Colombia with maxima at 560 nm and a weak band at about 405-415 nm.

This contribution may be considered as a complete study for natural sapphires with the internal features, chemical analyses and spectroscopic characteristics. The results can be applied in evaluating sapphire or corundum in general.

Bibliography

Arnond, V. P., Intasopa, S., Wathanakul, P., Griffin, W. L., Atichat, W. and Sutthirat, C. (2005). Corundum xenocrysts in basalt from the Bo Ploi gem field, Kanchanaburi, Western Thailand, *GEOINDO 2005*, Khon Kaen, Thailand.

Ashkin, M., Parker, J. H. Jr. and Feldman, D. W. (1968). Temperature dependence of the Raman lines of α-Al_2O_3, *Solid State Communication,* 6, 343-346.

Balmer, W. A., Leelawatanasuk, T., Atichat, W., Wathanakul, P., and Somboon, C. (2006). Update on characteristics of heated yellow sapphires, *GIT2006: 1st International Gem and Jewelry Conference*, Bangkok, 91.

Banini, G. K., Chaudhri, M. M., Smith, T. and Hayward, I. P. (2001). Measurement of residual stresses around Vickers indentations in a ruby crystal using a Raman luminescence microscope, *Journal of Applied Physics D*, 34(22), 122-124.

Belt, R. F. (1967). Hydrothermal ruby: Infrared spectra and X-ray topography, *Journal of Applied Physics*, 38(6), 2688-2689.

Belyaev, L. M. (1980). (Ed.) *Ruby and Sapphire*. Amerind Publishing, New Delhi, India.

Beran, A. (1991). Trace hydrogen in Verneuil-grown corundum and its color varieties - an IR spectroscopic study, *European Journal of Mineralogy,* 3, 971-975.

Beran, A. and Rossman, G. R. (2006). OH in naturally occurring corundum, *European Journal of Mineralogy,* 18(4), 441-447.

Bermanec, V., Cobic, A., Zigovecki, G. Z., Skoda, R., Zebec, V. and Wegner, R. (2009). Non-metamict microlite subgroup mineral and manganotantalite from Alto do Giz pegmatite, Equador, Rio Grande do Norte, Brazil, *Estudos Geológicos,* 19 (2), 57-61.

Bhagavantam, S. and Venkataryudu, T. (1939). Raman effect in relation to crystal structure, *Proceedings of the Indian Academy of Science A*, 9, 224-258.

Bristow, J. K., Tiana, D., Parker, S. C. and Walsh, A. (2014). Defect chemistry of Ti and Fe impurities and aggregates in Al_2O_3, *Journal of Materials Chemistry A*, 2, 6198-6208.

Burns, R. G. (1993). *Mineralogical applications of crystal field theory.* 2nd Edition, Cambridge University Press, Cambridge.

Buschow, K. H. J., Cahn R., Flemings, M., Ilschner, B., Kramer, E., Mahajan, S. and Veyssiere, P. (2001). *Encyclopedia of Materials: Science and Technology.* Elsevier, Amsterdam.

Cartier, L. E. (2009). Ruby and sapphire from Marosely, Madagascar, *The Journal of Gemmology,* 31(5-8), 171-179.

Chai, M. and Brown, J. M. (1996). Effects of static non-hydrostatic stress on the R lines of ruby single crystals, *Geophysical Research Letters,* 23, 3539-3542.

Chitty, W. (2009): *A study of sapphires and rubies from Tanzania's Tunduru district.* Bsc. Thesis, Kingston University, London.

Coenraads, R. R., Vichit, P. and Sutherlnad, F. L. (1995). An unusual sapphire-zircon-magnetite xenolith from the Chanthaburi Gem Province, Thailand, *Mineralogical Magazine*, 59, 465-479.

Collins, R. J., Nelson, D. F., Schawlow, A. L., Bond, W., Garrett, C. G. B. and Kaiser, W. (1960). Coherence, narrowing, directionality, and relaxation oscillations in the light emission from ruby, *Physical Review Letters,* 5(7), 303-305.

Crowell, B. (1998). *Light and Matter.* Fullerton, California, USA.

Dana J. D. and Dana E. S. (1962). *The system of mineralogy of James Dwight Dana and Edward Salisbury Dana.* 6th Edition, Yale University, 1837-1892, Volume 3, J. Wiley and Sons, inc.

De Maesschalck, A. A. and Oen, I. S. (1989). Fluid and mineral inclusions in corundum from gem gravels in Sri Lanka, *Mineralogical Magazine*, 53, 539-545.

Deutschbein, O. (1932). Die linienhafte Emission und Absorption der Chromphosphore II, *Annals of Physics,* 406, 729-754.

Dharmaratne, P. G. R., Premasiri, H. M. R., and Dillimuni, D. (2012). Sapphires from Thammannawa, Kataragama area, Sri Lanka, *Gems & Gemology*, 48(2), 98-107.

Duroc-Danner (2002). *A study of Colombian corundum.* Diploma thesis, Geneva, Switzerland.

Ehrmann, M. L. (1957). Burma, the Mineral Utopia, A reprint from *The Lapidary Journal*, 9(1), *https://www.palagems.com/burma_mineral_utopia.htm.*

Eigenmann, K. and Günthard, H. (1971). Hydrogen incorporation in doped a-Al_2O_3 by high temperature redox reactions, *Chemical Physics Letters*, 12(1), 12-15.

Eigenmann, K. and Günthard, H. (1972). Valence states, redox reactions and biparticle formation of Fe and Ti doped sapphire, *Chemical Physics Letters,* 13, 58-61.

Eigenmann, K., Kurtz, K. and Günthard, H. H. (1972). Solid state reactions and defects in doped Verneuil sapphire, *Helvet Physica Acta,* 45, 452-480.

Emmett, L. J., Scarratt, K., McClure, S. F., Moses, T., Douthit, T. R., Hughes, R., Novak, S., Shigley, J. E., Wang, W., Bordelon, O. and Kane, R. E. (2003). Beryllium diffusion of ruby and sapphire, *Gems & Gemology*, 3(2), 84-135.

Emmett, J. L. and Douthit, T. R. *(*1993*).* Heat treating the sapphires of Rock Creek, Montana, *Gems & Gemology*, 29(4), 250-272.

Epstein, D. S., Brennan, W. and Mendes J. C. (1994). The Indaia sapphires deposits of Minas Gerais, Brazil, *Gems & Gemology*, 30(1), 24-32.

Ferguson, J. and Fielding, P. E. (1971). The origin of the colours of yellow, green and blue sapphires, *Chemical Physics Letters*, 10(3), 262-265.

Ferguson, J. and Fielding, P. E. (1972). The origins of the colours of natural yellow, blue, and green sapphires, *Australian Journal of Chemistry*, 25, 1371-1385.

Feynman, R. P., Leighton, R. B. and Sands, M. (1964). *The Feynman lectures on Physics, Vol. 2: Mainly electromagnetism and matter*. Addison-Wesley, New York, USA.

Fritsch, E. and Rossman, G. R. (1987). An update on color in gems. Part I. Introduction and colors caused by dispersed metal ions, *Gems & Gemology,* 23, 126-139.

Fritsch, E. and Rossman, G. R. (1988). An update on color in gems. Part III. Colors caused by physical optics, *Gems & Gemology,* 24, 81-103.

Fritsch, E. and Rossman. G. R. (1988). An update on color in gems. Part II. Colors caused by charge transfers and color centers, *Gems & Gemology,* 24, 3-15.

Fritsch, E. and Waychunas, G. (1993). The fluorescence of gemstones. In Robbins M., editor, *Fluorescence: gems and minerals under ultraviolet light.* Geoscience Press, 149–174. Phoenix, AZ.

Gaft, M., Reisfeld, R., and Panczer, G. (2005). *Modern luminescence spectroscopy of minerals and materials*, Springer.

Garcia-Lastra, J. M., Barriuso, M. T., Aramburu, J. A. and Moreno, M. (2005). Origin of the different colour of ruby and emerald, *Physical Review B,* 72, 113104.

Garnier, V., D. Ohnenstetter, G. Giuliani, A. Fallick, T. Phan Trong, D. Schwarz, V. Hoang Quang and L. Pham Van (2005). Basalt petrology, zircon ages and sapphire genesis from Dak Nong, SouthernVietnam, *Mineralogical Magazine,* 69(1), 21-38.

Graham, I., Sutherland, L., Zaw, K., Nechaev, V. and Khanchuk, A. (2008). Advances in our understanding of the gem corundum deposits of the West Pacific continental margins intraplate basaltic fields, *Ore Geology Reviews*, 34(1), 200-215.

Grice, J. D., Ferguson, R. B. and Hawthorne, F. C. (1976). The crystal structures of tantalite, ixiolite and wodginite from Bernic Lake, Manitoba I. Tantalite and ixiolite, *The Canadian Mineralogist*, 14, 540-549.

Gübelin, E. J. and Koivula J. I. (2008). *Photoatlas of inclusions in gemstones.* Vol 3. Opinio Publishers.

Gübelin, E. J. and Koivula, J. I. (1986). *Photoatlas of inclusions in gemstones*. ABC Edition, Zurich.

Guo, J., O'Reilly, S.Y., and Griffin, W.L. (1996), Corundum from basaltic terrains: a mineral inclusion approach to the enigma, *Contributions to Mineralogy and Petrology*, 122, 368-386.

Guo, J., Wang, F. and Yakounielos, G. (1992), Sapphires from Changle in Shandong Province, China. *Gems & Gemology*, 28(4), 255-260.

Gupta, Y. M. and Shen, X. A. (1991), Potential use of the ruby R_2 line shift for static high pressure calibration, *Applied Physics Letters*, 58(6), 583-585.

Häger, T. (1992). Farbgebende und "farbhemmende" Spurenelemente in blauen Saphiren, *Berichte der Deutschen Mineralogischen Gesellschaft -Beihefte zum European Journal of Mineralogy,* 4, 109.

Häger, T. (1993). Stabilisierung der Farbzentren von gelben natürlichen Saphiren, *Berichte der Deutschen Mineralogischen Gesellschaft -Beihefte zum European Journal of Mineralogy,* 5, 188.

Häger, T. (1996). *Farbrelevante Wechselwirkungen von Spurenelementen in Korund.* Dissertation, University of Mainz.

Häger, T. (2001). High temperature treatment of natural corundum, *Proceedings of International workshop on Material Characterization by Solid State Spectroscopy: Gems and Minerals of Vietnam*, Hanoi, Vietnam, 24-37.

Häger, T. and Dung, P. T. (2000). Quantative Fluoeszenz-Spektroskopie an natürlichen und sznthetischen Rubinen, Ber. Dt. Mineral. Ges. Beih., *European Journal of Mineralogy* 12, 72.

Häger, T. and Dung, P. T. (2003). Quantitative laser-induced photoluminescence and cathodoluminescence spectroscopy of natural and synthetic rubies, *Proceedings of International Workshop on Geo-and Material-Science on Gem-Minerals of Vietnam*, Hanoi Vietnam, 122-128.

Häger, T. and Greiff, S. K. (1994). A study of hydrous components in corundum, *European Journal of Mineralogy*, 6, 89.

Häger, T., Dung, P. T., Tuyen, V. P., Wanthanachaisaeng, B. and Hofmeister, W. (2010). Cr^{+3}-luminescence: a powerful tool in gemology and in gemstone research, *Proceedings of the 5th International Workshop on Provenance and Properties of Gem and Geo-Materials*, Hanoi, Vietnam, 1-5.

He, J. and Clarke, D. R. (1997). Polarization dependence of the Cr^{3+} R-line fluorescence from sapphire and its application to crystal orientation and piezospectroscopic measurement, *Journal of the American Ceramic Society,* 80(1), 69-78.

Henn, U., Bank H. (1996). Trapicheartige Korunde aus Myanmar. Gemmologie. *Zeitschrift der Deutschen Gemmologischen Gesellschaft*, 45(1), 23-24.

Hibben, J. H. (1932). An investigation of intermediate compound formation by means of the Raman effect, *Proceedings of National Academy of Sciences*, 18, 532-538.

Horn, P. D. and Gupta, Y. M. (1989). Luminescence R-line spectrum of ruby crystals shocked to 125 kbar along the crystal c axis, *Physical Review B*, 39(2), 973-979.

Hu, W. X, Song, Y. C., Chen, X. M., Tao, M. X. and Zhang, L. P. (2007). Noble gases in corundum megacrysts from the basalts in Changle, Shandong Province, Eastern China, *Chinese Science Bulletin*, 52(3), 380-387.

Hughes, R. W. (1997). *Ruby & Sapphire*. RWH Publishing, Boulder, CO.

Hurlbut, C. S., Sharp, W. E., and Dana, E.S. (1998). *Dana's Minerals and How to Study Them*. 4th Edition, Wiley, New York, 81.

Jensen, W. B. (2010). Why has the value of Avogadro's Constant changed over time? *Journal of Chemical Education*, 87(12), 1302.

Joseph, D., Lal, M., Shine, P. S. and Padalia, B. D. (2000). Characterization of gem stones (rubies and sapphires) by energy-dispersed X-ray fluorescence spectrometry, *X-ray Spectrometry*, 29, 147-150.

Kadleikova, M., Breza, J. and Vesely, M. (2001). Raman spectra of synthetic sapphire, *Microelectronics Journal* 32, 955-958.

Kanyarat, K., Panjawan, T. and Theerapongs, T. (2010). Characteristics of trapiche blue sapphires from Southern Vietnam, *Chiang Mai Journal* of *Science* 37(1), 64-73.

Kaplyanskii, A. A. and Przhevuskii, A. K. (1962).The piezospectroscopic effect in ruby crystals*, Soviet Physics- Doklady*, 142(2), 313-316.

Keller, P. C. (1982). The Chanthaburi-Trat gem field, Thailand, *Gem & Gemology*, 18(4), 186-196.

Keller, P. C., Koivula, J. I. and Jara, G. (1985). Sapphire from the Mercaderes-Rio Mayo area, Cauca, Colombia, *Gems & Gemology*, 21(1), 20-25.

Khanchuk, A., Zalishchak, B., Pakhomova, V., Odarichenko, E. and Sapin, V. (2003). Genesis and gemology of sapphires from the Nezametnoye deposit, Primorye region, Russia, *Australian Gemmologist,* 21, 329-335.

Kiefert, L., Schmetzer, K., Krzemnicki, M. S., Bernhardt, H.-J. and Hänni, H. A. (1996). Sapphires from the Andranondambo area, Madagascar, *Journal of Gemmology*, 25(3), 185–209.

Koivula, J. I., Kammerling, R. C. and Fritsch, E. (1994). Gem news:"Trapiche" purple-pink sapphire, *Gems & Gemology*, 30(3), 197.

Krishna, R. S. (1947). Raman spectrum of alumina and the luminescence of ruby, *Proceedings of the Indian Academy* o*f Science* A, 26, 450.

Krishnan, R. S. (1947). Raman spectrum of alumina and the luminescence and absorption spectra of ruby, *Nature* 160, 26-26.

Levinson, A. A. and Cook, F. A. (1994). Gem corundum in alkali basalt: Origin and occurrence, *Gems & Gemology*, 30(4), 253-262.

Libowitzky, E. and Beran, A. (2006). The structure of hydrous species in normally anhydrous minerals: Information from polarized IR spectroscopy, *Reviews in Mineralogy & Geochemistry*, 62, 29-52.

Long, V. P., Giulian, G., Garnier, V. and Ohnenstetter, D. (2004). Gemstones in Vietnam: A review, *The Australian Gemologist*, 22(4), 162-168.

Mani, A. (1942). Fluorescence, absorption and scattering of light in ruby, *Proceedings of the Indian Academy* of *Science A*, 15, 52.

Mao, H. K. and Bell, P. M. (1978). High-Pressure Physics: Sustained Static Generation of 1.36 to 1.72 Megabars, *Science*, 200(4346), 1145-1147.

Mao, H. K., Xu, J., and Bell, P. M. (1986). Calibration of the ruby pressure to 800 kbar under quasi-hydrostatic conditions, *Journal of Geophysical Research*, 91, 4673-4676.

McKague, H. L. (1964). Trapiche emeralds from Colombia, part I, *Gems & Gemology*, 11(7), 210-213.

Milos, M., Kairouani, S., Rabaste, S. and Hauser, A. (2008). Energy migration within the 2E state of Cr^{3+}, *Coordination Chemistry Reviews,* 252(23-24), 2540-2551.

Moon, A. R. and Phillips, M. R. (1991). Defect clustering in $H,Ti:\alpha-Al_2O_3$, *Journal of Physics and Chemistry of Solids,* 52, 1087-1099.

Moon, A. R. and Philips, M. R. (1994). Defect clustering and color in $Fe,Ti: \alpha-Al_2O_3$, *Journal of The American Ceramic Society,* 77(2), 356-367.

Muhlmeister, S., Fritsch, E., Shigley, E. J., Devouard, B. and Laurs, M. B. (1998). Separating natural and synthetic rubies on the basis of trace-element chemistry, *Gems & Gemology*, 34(2), 80-101.

Munisso, M. C., Zhu, W. and Pezzotti, G. (2009). Raman tensor analysis of sapphire single crystal and its application to define crystallographic orientation in polycrystalline alumina, *Phys. Status Solidi B*, 246(8), 1893-1900.

Munro, R. G., Piermarini, G. J., Block, S. and Holzapfel, W. B. (1985). Model line shape analysis for the ruby R lines used for pressure Measurement, *Journal of Applied Physics*. 57(2), 165-169.

Nasdala, L., Götze, J., Hanchar, J. M., Gaft, M., and Krbetschek, M. R. (2004). Luminescence techniques in Earth sciences, In Beran A. and Libowitzky E., Editors, *Spectroscopic methods in mineralogy,* 43-91.

Nassau, K. (1983). *The physics and chemistry of color: The fifteen causes of color*. Wiley, New York.

Nassau, K. and Jackson, K. A. (1970). Trapiche emeralds from Chivor and Muzo, Colombia. *American Mineralogist*, 55(3-4), 416-427.

Nelson, D. F. and Sturge, M. D. (1965). Relation between absorption and emission in the region of the R lines of ruby, *Physical Review A*, 137(4), 1117-1130.

Newman, J. (2008). *Physics of the Life Sciences*. Springer, New York, USA.

Nguyen, N. K., Hauzenberger, C., Duong, A. T., Nguyen, T. D., Nguyen, T. M. T., Phan, T. M. D. (2014). Some characteristics of newly discovered corundum deposits in Krong Nang district, Dak Lak Province (Vietnam) and problems of sustainable and environment-friendly

mining, *13th International Symposium on Mineral Exploration, Toward Sustainable Society with Natural Resources - Frontiers in Earth Resources Technologies and Environmental Conservation,* Hanoi, Vietnam.

Noguchi, N., Abduriyim, A., Shimizu, I., Kamegata, N., Odakea, S. and Kagi, H. (2012). Imaging of internal stress around a mineral inclusion in a sapphire crystal: application of micro-Raman and photoluminescence spectroscopy, *Journal of Raman spectroscopy,* 44(1), 147-154.

O'Donoghue, M. J. (1971). Trapiche emerald, *Journal of Gemmology*, 12(8), 329-332.

O'Donoghue, M. (1997). *Synthetic, Imitation and Treated Gemstones*. Butterworth-Heinemann, Oxford, 70.

Ostertag, C. P., Robins, L. H. and Cook, L. P. (1991). Cathodoluminescence measurement of strained alumina single crystals, *Journal of the European Ceramic Society,* 7, 109-116.

Palmer D. (1995). *CrystalMaker: Interactive crystallography for Macintosh.* User Manual Software, Cambridge, England.

Peretti, A. and Smith, C.P. (1993). A new type of synthetic ruby on the market, offered as hydrothermal rubies form Novosibirsk, *Australian Gemmologist*, 18, 149-156.

Porto, S. P. S. and Krishnan, R. S. (1967). Raman effect of corundum, *The Journal of Chemical Physics*, 47(3), 1009-1012.

Powell, R. C., Dibartolo, B., Birang, B. and Naiman, C. S. (1967). Fluorescence studies of energy transfer between single and pair Cr^{3+} systems in Al_2O_3, *Physical Review*, 155(2), 296-308.

Pratt, J. H. (1906). *Corundum and its occurrence and distribution in the United States*. U. S. Geological Survey Bulletin 180, 269.

Pringsheim, P. (1949). *Fluorescence and Phosphorescence*. Interscience Publishers, Inc., New York, 637-645.

Rakotondrazafy, A. F. M., Giuliani, G., Ohnenstetter, D., Fallick, A. E., Rakotosamizanany, S., Andriamamonjy, A., Ralantoarison, T., Razanatseheno, M., Offant, Y., Garnier, V., Maluski, H., Dunaigre, C., Schwarz, D. and Ratrimo, V. (2008). Gem corundum deposits of Madagascar: A review, *Ore Geology Review,* 34, 134-154.

Rankin, A. H. (2002). Natural and heat-treated corundum from Chimwadzulu Hill, Malawi: genetic significance of zircon clusters and diaspore-bearing inclusions, *The Journal of Gemmology*, 28(2), 65-75.

Rhamdhor, R. and Milisenda, C. C. (2004), Neue Vorkommen von Saphir-Seifenlagerstätten auf Nosy-Bé, Madagaskar, *Zeitschrift der Deutschen Gemmologischen Gesellschaft,* 53(4), 142-158.

Rothamel, U., Heber, J. and Grill, W. (1983). Vibronic sidebands in ruby, *Journal of Physics: Condensed Matter*, 50(4), 297-304.

Saminpanya, S., Manning, D. A. C., Droop, G. T. R. and Henderson, C. M. B. (2003). Trace elements in Thai gem corundums, *Journal of Gemmology*, 28(7), 392-398.

Schawlaw, A. L. (1961). *Advances in quantum electronic.* In Singer J. R., Editors, Columbia University Press, New York.

Schmetzer, K. (1987). Zur deutung der farbursache blauer Saphir-Eine diskution, *Neues Jahrbuch für Mineralogie*, Monatshefte, 8, 337-343.

Schmetzer, K., Bosshard, G. and Hänni, H. A. (1982). Naturfarbene und behandelte gelbe und orange-braune Sapphire, *Zeitschrift der Deutschen Gemmologischen Gesellschaft*, 31(4), 265-279.

Schmetzer, K., Bosshard, G. and Hänni, H. A. (1983). Naturally coloured and treated yellow and orange-brown sapphires, *Journal of Gemmology,* 18, 607-622.

Schmetzer, K., Hänni, H. A., Bernhardt, H.-J. and Schwarz, D. (1996). Trapiche rubies, *Gems & Gemology*, 32(4), 242-250.

Schwarz, D., Kanis, J. and Schmetzer, K. (2000). Sapphires from Antsiranana Province, Northern Madagascar, *Gems & Gemology*, 36(3), 216-233.

Schwarz, D., Pardieu, V., Saul, J. M., Schmetzer, K., Laus, B. M., Giuliani, G., Klemm, L., Malsy, A., Erel, E., Hauzenberger, C., Toit, G. D., Fallick, A. E. and Ohnenstetter, D. (2008). Rubies and Sapphires from Winza, Central Tanzania, *Gems & Gemology*, 44(4), 322-347.

Shannon, R. D. (1976). Revised effective ionic radii and systematic studies of interatomie distances in Halides and Chaleogenides, *Acta Crystallographica A*, 32, 751-767.

Shen, X. A. and Gupta, Y. M. (1993). Effect of crystal orientation on ruby line shifts under shock compression and tension, *Physical Review B*, 48, 2929-2940.

Skogby, H. and Rossman, G. R. (1989). OH in pyroxenes: An experimental study of incorporation mechanisms and stability, *American Mineralogist,* 74, 1059-1069.

Smith, C. P. (1995). A contribution to understanding the infrared spectra of rubies from Mong Hsu, Myanma*, Journal of Gemmology,* 24, 5.

Smith, C. P., Kammerling, R. C., Keller, A. S., Peretti A., Scarratt, K.V., Khoa, N.D. and Repetto, S. (1995). Sapphires from southern Vietnam, *Gems & Gemology*, 31(3), 168-186.

Smith, C.P. and Van der Bogert, C. (2006). Infrared spectra of gem corundum, *Gems & Gemology,* 42(3), 92-93.

Stern, W. B. and Hänni, H. A. (1982). Energy dispersive X-ray spectrometry: A non-destructive tool in gemology, *Journal of Gemmology*, 18(4), 285-296.

Strens, R. G. J. (1974). The common chain, ribbon and ring silicates. In Farmer V. C, editor, *The infrared spectra of Minerals*, Mineralogical Society, London.

Sutherland, F. L. and Schwarz, D. (2001). Origin of gem corundums from basaltic fields, *Australian Gemmologist*, 21, 30-33.

Sutherland, F. L., Schwarz, D., Jobbins, E. A., Coenraads, R. R. and Webb, G. (1998b). Distinctive gem corundum suites from discrete basalt fields: a comparative study of Barrington, Australia, and West Pailin, Campodia, gemfields, *Journal of Gemmology*, 26(2), 65-85.

Sutherland, F.L., Bosshart, G., Fanning, C.M., Hoskind, P.W.O., and Coenraads, R.R. (2002). Sapphire crystallization, age and origin, Ban Huai Sai, Laos: age based on zircon inclusions, *Journal of Asian Earth Sciences,* 20(7), 841-849.

Tang, S. M., Tang, S. H., Mok, K. F., Retty, A. T. and Tay, T.S. (1989). A study of natural and synthetic rubies by PIXE, *Applied Spectroscopy*, 43(2), 219-222.

Tang, S. M., Tang, S. H., Tay, T. S. and Retty, A. T. (1988). Analysis of Burmese and Thai rubies by PIXE, *Applied Spectroscopy*, 42(10), 44-48.

Velde, B. (1983). Infrared OH-stretch bands in potassic micas, talcs and saponites; influence of electronic configuration and site of charge compensation, *American Mineralogist*, 68, 1169-1173.

Vichit, P. (1975). *Origin of corundum in basalt*. Master of Science in Geology, Institute of Mining and Technology, Socorro, New Mexico.

Villars, P. (1991). *Pearson's Handbook of Crystallographic Data for Intermetallic Phases*. 2nd Edition, ASM International.

Volynets, F. K., Vorob′ev, V. G., and Sidorova, E. A. (1969). Infrared absorption bands in corundum crystals, *Journal of Applied Spectroscopy*, 10(6), 665-667.

Volynets, F. K., Sidorova, E. A. and Stsepuro, N. A. (1972). OH-groups in corundum crystals which were grown with the Verneille technique, *Journal of Applied Spectroscopy*, 17(6), 1626-1628.

Waltham, T. (2011), Sapphires from Sri Lanka, *Geology Today*, Blackwell Publishing Ltd, The Geologists' Association & The Geological Society of London, 27(1), 20-24.

Wanthanachaisaeng, B., Häger, T., Hofmeister, W. and Nasdala, L. (2006). Raman- und fluoreszenzspektroskopische Eigenschaften von Zirkon-Einschlüssen in chrom-haltigen Korunden aus Ilakaka und deren Veränderung durch Hitzebehandlung, *Zeitschrift der Deutschen Gemmologischen Gesellschaft,* 55, 123-136.

Webster, R. (1983). *Gems: Their Sources, Descriptions and Identification*. 4th Edition, revised by Anderson, Butterworths, London.

Wefers, K. and Bell, G. M. (1972). Oxides and Hydroxides of Alumina, *Alcoa Research Laboratories Technical Paper*, Alcoa Research Laboratories, St. Louis, Missouri, 19.

Wilkins, R. W. T. and Ito, J. (1967). Infrared spectra of some synthetic talcs, *American Mineralogist*, 52, l649-1661.

Woodhead, A. J., Rossman, G. R. and Silver, T. L. (1991). The metamictization of zircon: Radiation dose-dependent structural characteristics, *American Mineralogist*, 76, 74-82.

Xu, J., Huang, E., Lin, J. and Xu, L. Y. (1995). Raman study at high pressure and the hermodynamic properties of corundum: Application of Kieffer's model, *American Mineralogist*, 80, 1157-1165.

Zhang, A. C., Wang, R. C., Hu, H., Zhang, H., Zhu, J. C. and Chen, X. M. (2004). Chemical evolution of Nb-Ta oxides and zircon from the Koktokay No. 3 granitic pegmatite, Altai, northwestern China, *Mineralogical Magazine,* 68(5), 739-756.

Zhang, M., Salje, K. H. E., Farnan, I., Graeme-Barber, A., Daniel, P., Ewing, C. R., Clark, M. A. and Leroux, H. (2000). Metamictization of zircon: Raman spectroscopic study, *Journal of Physics*: *Condensed Matter,* 12, 1915-1925.

Programs

CrystalMaker version 2.5

Origin Lab version 7.5

LabSpec version 5

Mercury version 2.3

Acknowledgements

Mainz, May 12, 2015

Phan Thi Minh Diep

List of publication

Curriculum Vitae

Mainz, May 12, 2015

....

Phan Thi Minh Diep